

RGD-CONTAINING LIGANDS FOR TARGETING LIPOSOMAL NANOPARTICLES

by

Sonya Cressman

B.Sc., The University of Victoria, 2000

A THESIS SUBMITTED IN PARTIAL FULFILLMENT OF THE REQUIREMENTS
FOR THE DEGREE OF
DOCTOR OF PHILOSOPHY
in

THE FACULTY OF GRADUATE STUDIES

(Biochemistry and Molecular Biology)

THE UNIVERSITY OF BRITISH COLUMBIA

Vancouver, Canada

September 2007

© Sonya Cressman, 2007

ABSTRACT

The use of a targeting ligand to enhance the delivery of liposomal nanoparticles (LNs) to specific cells in diseased tissue is an attractive strategy that has progressed very slowly since the idea originated over 25 years ago. The slow progress can be attributed, in part, to the difficulties involved in producing well-defined targeted LN systems. This work concerns the development of peptide-based ligands for targeting LNs to cells that overexpress the $\alpha_v\beta_3$ integrin, which is considered a unique marker of the tumor-associated endothelium.

Initial work focused on using Fab' fragments of monoclonal antibodies as targeting ligands and employing literature techniques for coupling these proteins to lipids that can then be inserted in preformed LNs. However, it was found that the coupling procedures resulted in low yields of poorly defined lipid-ligand conjugates that were difficult to quantitate when incorporated into LN.

Attention was then given to the development of a peptide-targeting agent that could be incorporated into an LN at the time that the LN is made. The RGD-containing cyclic peptide, cRGDfK, was employed as the targeting ligand. In order to characterize its binding to the $\alpha_v\beta_3$ integrin, a fluorescently labeled analogue, cRGDfK-488, was synthesized and capillary electrophoresis was employed for analysis. This procedure proved advantageous for studying receptor ligand interactions, since it allowed for the binding to be characterized in solution without the need for covalent modification of receptor or ligand. A 2:1 RGD ligand to integrin specific binding stoichiometry was revealed with the second binding event having a similar affinity as the first binding event.

The next phase of these studies investigated the ability of cRGDfK-488 to bind to integrins on human umbilical vascular endothelial cells (HUVEC) and subsequently undergo endocytosis. This was compared to the binding and uptake properties of a fluorescently labeled monoclonal antibody, LM609X, which specifically binds $\alpha_v\beta_3$ integrin. Using flow cytometry and fluorescence microscopy, it is shown that the RGD ligand exhibited considerably greater uptake following incubation at endocytosis permitting temperatures (37°C) as compared to endocytosis inhibiting temperatures (4°C). A 7.4-fold increase in uptake of the RGD-lipid was observed following a one-hour incubation with HUVEC at 37°C, as compared to 4°C. In contrast, only a 1.9 fold increase in cell-associated fluorescence was observed on incubation with LM609X at 37°C as compared to 4°C. It is suggested that this ability of RGD ligands to stimulate endocytosis may be of utility for achieving enhanced intracellular delivery of ligand-associated drugs in anti-angiogenic applications.

The cyclic peptide was then used to construct a fluorescently labeled RGD-spacer-lipid construct of defined molecular weight that could be incorporated into LN at the time of manufacture. It is shown that the resulting RGD-LNs bind to HUVEC with increasing avidity as the amount of RGD-spacer-lipid incorporated is increased. Further, these RGD-LNs are straightforward to make and can load and retain anti-cancer drugs such as doxorubicin. It is shown that RGD-LNs loaded with doxorubicin and incubated with HUVEC selectively deliver the drug to the cytosol while non-targeted LNs are not internalized by the cell, suggesting potential utility as targeted drug delivery systems *in vivo*.

TABLE OF CONTENTS

ABSTRACT	ii
TABLE OF CONTENTS	iv
LIST OF TABLES	vii
LIST OF FIGURES	viii
ABBREVIATIONS	ix
ACKNOWLEDGEMENTS	xi
CO-AUTHORSHIP STATEMENT	xiii
1 Introduction to Targeted Liposomal Nanoparticles	1
1.1 Liposomal Nanoparticles	1
1.2 Liposomal Nanoparticles and Drug Delivery	2
1.3 LNs with Extended <i>in vivo</i> Circulation Lifetimes	4
1.4 Immunoliposomes (ILNs)	5
1.4.1 Targeting LNs to the Disease Site	5
1.5 Contemporary ILNs and ILN Production	8
1.5.1 ILNs <i>in vivo</i>	9
1.5.2 ILNs in the Clinic	10
1.6 Small Molecule Targeting Ligands	11
1.6.1 Peptides with Disease Site Affinity	12
1.6.2 Arginine-Glycine-Aspartic Acid (RGD)	13
1.7 RGD-Targeting Ligands and Affinity Analyses	14
1.8 Objectives, Evolution and Structure of this Thesis	16
2 Preliminary Experiments	20
2.1 Introduction	20
2.2 Methods	22
2.2.1 Materials	22
2.2.2 Fab' Formation	22
2.2.3 Maleimide-PEG ₂₀₀₀ -DSPE Analysis	23
2.2.4 Fab'-PEG ₂₀₀₀ -DSPE Conjugation	23
2.2.5 Fab'-PEG ₂₀₀₀ -DSPE Purification	24
2.3 Results	25
2.3.1 Quality of Mal-PEG-DSPE	25
2.3.2 Fab'-Maleimide-PEG-DSPE Conjugation	26
2.3.3 Pure Fab'-PEG-DSPE Preparations are Inherently Difficult to Achieve	27
2.4 Discussion	29
3 RGD-ligand Synthesis and Binding to the Isolated $\alpha_v\beta_3$ Integrin	32
3.1 Introduction	32
3.1.1 Targeting Angiogenesis	32
3.1.2 The CE-FA Method for Measuring Binding to the $\alpha_v\beta_3$ Integrins	35
3.2 Methods	40
3.2.1 Materials	40
3.2.2 Peptide Synthesis, Cyclization and Labeling	40
3.2.3 Capillary Electrophoresis (CE) Analysis	43
3.2.4 Capillary Electrophoresis Frontal Analysis Method	44
3.3 Results and Discussion	45

3.3.1	Peptide Synthesis, Labeling and Analysis.....	45
3.3.2	cRGDfK-488 Peptide Purity.....	46
3.3.3	Binding to Isolated $\alpha_v\beta_3$ Integrin as Measured by the CE-FA Method	47
4	Cellular Binding and Endocytosis of RGD-Containing Targeting Ligands	51
4.1	Introduction	51
4.2	Methods.....	54
4.2.1	Materials	54
4.2.2	Cell Culture.....	54
4.2.3	Cell Binding.....	55
4.2.4	Cellular Uptake	55
4.2.5	Receptor Quantitation	56
4.2.6	Fluorescence Microscopy	57
4.3	Results	59
4.3.1	HUVEC Express 2.63×10^5 Integrins Per Cell	59
4.3.2	cRGDfK-488 Undergoes Extensive Endocytosis Following Binding to HUVEC at 37°C	61
4.3.3	Time Dependent Uptake of cRGDfK-488 by HUVEC.....	63
4.3.4	$\alpha_v\beta_3$ Expression Decreases Upon RGD Binding	65
4.3.5	Endocytosis as Visualized by Fluorescence Microscopy	66
4.4	Discussion	69
5	Targeted Drug Delivery	72
5.1	Introduction	72
5.2	Methods.....	76
5.2.1	Materials and Reagents	78
5.2.2	Peptide Synthesis	78
5.2.3	cRGDfK-SUCC-DSPE (Compound I) Synthesis.....	79
5.2.4	cRGDfK-(SUCC-343) ₃ -DSPE (Compound II) Synthesis.....	80
5.2.5	cR(Pbf)GD(t-Bu)fK-PEG ₂ -COOH and cR(Pbf)GD(t-Bu)fK-PEG ₂ -K(MCA)-PEG ₂ -COOH Synthesis (preceding compounds III and IV, respectively)	81
5.2.6	Synthesis of cR(Pbf)GD(t-Bu)fK-PEG ₂ -DSPE (Compound III) and cRGDfK-PEG ₂ -K(MCA)-PEG ₂ -DSPE (Compound IV).....	83
5.2.7	cRGDfK-PEG ₂ -K(MCA)-PEG ₂ -DSPE Formulation into LNs	84
5.2.8	Post-Insertion of cRGDfK-PEG ₂ -K(MCA)-PEG ₂ -DSPE into Pre-Formed LNs	86
5.2.9	HPTS Loading	86
5.2.10	Doxorubicin Loading	87
5.2.11	Doxorubicin Leakage Assay	87
5.2.12	Cell Culture and LN Binding Assays.....	88
5.2.13	Cellular HPTS Uptake.....	89
5.2.14	Doxorubicin Uptake into Cells as Determined by Flow Cytometry	89
5.2.15	LN Uptake into Cells as Observed by Microscopy.....	90
5.3	Results and Discussion.....	91
5.3.1	Synthesis of Targeting Lipids.....	91
5.3.2	RGD-LN Characterisation.....	92
5.3.3	Methods for Producing RGD-LNs.....	95
5.3.4	Drug Retention in RGD-Targeted LNs.....	96

5.3.5 Cellular Uptake and Processing of RGD-LNs.....	97
5.3.6 <i>In vitro</i> Drug Delivery by RGD-LNs.....	99
5.3.7 Relation to Existing RGD-LN Data.....	101
6 Future Work.....	104
6.1 Pharmacokinetics of RGD-LNs.....	104
6.2 Anti-tumor Efficacy of RGD-Targeted Therapeutics.....	105
6.3 Choice of Drug to be Delivered.....	107
6.4 Bimodal and Multifaceted Chemotherapy Regimes.....	108
References.....	109
APPENDIX.....	122

LIST OF TABLES

Table 1.1 Summary of <i>in vitro</i> binding characterisations for RGD-containing ligands targeting the $\alpha_v\beta_3$ integrin	15
Table 5.1 Summary of RGD-lipids used to study RGD-LNs <i>in vivo</i>	73
Table 5.2 Summary of RGD-lipids synthesized	91
Table 5.3 Characterization of RGD-LNs	93

LIST OF FIGURES

Figure 1.1 Types of LN employed for drug delivery	2
Figure 1.2 Antibody engineering.....	7
Figure 2.1 Comparison of Mal-PEG-DSPE reagents obtained from different suppliers	25
Figure 2.2 Addition of Mal-PEG-DSPE to Fab' to form Fab'-PEG-DSPE	26
Figure 2.3 Size exclusion purification of Fab'-PEG-DSPE	27
Figure 2.4 Ion-exchange chromatography of Fab'-PEG-DSPE conjugates	28
Figure 2.5 Two methods of incorporating targeting ligands for ILN manufacture	29
Figure 3.1 The angiogenic transition.....	32
Figure 3.2 Schematic of the Capillary Electrophoresis Frontal Analysis Method	38
Figure 3.3 Synthesis of fluorescently labeled cRGDfK peptides	45
Figure 3.4 Electrophoregram demonstrating the purity of cRGDfK-488	46
Figure 3.5 Electrophoregrams produced for CE-FA experiments.....	48
Figure 3.6 cRGDfK-488: $\alpha_v\beta_3$ integrin binding isotherms generated from the CE-FA method	49
Figure 4.1 Binding and Endocytosis of cRGDfK-488 via the $\alpha_v\beta_3$ integrin	51
Figure 4.2 Quantitation of the $\alpha_v\beta_3$ receptor on cultured cells	59
Figure 4.3 Binding of fluorescently labeled peptides to HUVEC or M21L cells.....	61
Figure 4.4 Specific Binding and Endocytosis of cRGDfK-488 and LM609 to HUVEC and M21L cells.....	62
Figure 4.5 Competition of cRGDfK-488:HUVEC binding with free cRGDfK	63
Figure 4.6 Time-dependent uptake of cRGDfK-488 and cRADfK-488 by HUVEC	65
Figure 4.7 $\alpha_v\beta_3$ integrin surface receptor expression after exposure to cRGDfK	66
Figure 4.8 Binding at 37°C as seen by fluorescence microscopy.....	67
Figure 4.9 Binding at 4°C as seen by fluorescence microcopy	68
Figure 5.2 RGD-lipids synthesized	76
Figure 5.3 Steps in the synthesis of cRGDfK-PEG ₂ -K(MCA)-PEG ₂ -DSPE.....	77
Figure 5.4 RGD-LN binding by HUVECs at 4°C and 37°C.....	94
Figure 5.6 Comparison of formulation and post-insertion methods for incorporating RGD-lipids into LNs.....	95
Figure 5.7 Doxorubicin is retained equally well in RGD-LNs and non-targeted LNs.....	96
Figure 5.8 RGD-LNs are internalized and acidified by HUVEC.....	98
Figure 5.9 Uptake of doxorubicin presented in the free form, in non-targeted LN or RGD-LN by cells expressing various levels of the $\alpha_v\beta_3$ integrin	100

ABBREVIATIONS

^1H NMR NOE	Proton nuclear magnetic resonance nuclear overhauser effect
ABC	Antibody binding capacity
aqACN	Aqueous acetonitrile
bFGF	Basic fibroblast growth factor
B_{max}	Binding maximum
CE	Capillary electrophoresis
CHCl_3	Chloroform
Chol	Cholesterol
DAPI	4',6-diamidino-2-phenylindole
DCM	Dichloromethane
DLS	Dynamic light scattering
DMF	Dimethylformamide
DNA	Deoxyribonucleic acid
Doxil	PEGylated Liposomal doxorubicin
DSPC	Distearylphosphatidyl choline
EC	Endothelial cell
ECM	Extracellular matrix
EDTA	Ethylenediamine tetraacetic acid
EPR	Enhanced permeability and retention
ESI-MS	Electrospray mass spectrometry
Fab'	Monomeric antibody fragment, variable region
Fab ₂	Dimeric antibody fragment, variable region
FBS	Fetal bovine serum
Fc	Antibody fragment, constant region
FMOC	9-fluorenylmethyloxycarbonyl
FPLC	Fast protein liquid chromatography
Fv	Antibody variable fragment
HBS	HEPES buffered saline
HBTU	O-Benzotriazole-N,N,N',N'-tetramethyl-uronium-hexafluorophosphate
HEPES	4-(2-hydroxyethyl)-1-piperazineethanesulfonic acid
HOBt	N-hydroxybenzotriazole
HPTS	8-hydroxypyrene-1, 3, 6-trisulfonic acid
HUVEC	Human umbilical vein endothelial cells
IC_{50}	Half maximal inhibitory concentration
IgG	Immunoglobulin G
ILN	Immunoliposomal nanoparticle
kD	Kilodalton
K_d	Dissociation constant
k_{obs}	Observed rate constant
LIF	Laser induced fluorescence
LM609X	Fluorescently labeled anti- $\alpha_v\beta_3$ antibody
LN	Liposomal nanoparticle

mAb	Monoclonal antibody
MALDI-TOF	Matrix-assisted laser desorptive ionization time of flight spectroscopy
Mal-PEG-DSPE	Maleimide polyethylene glycol ₂₀₀₀ distearoylphosphatidylethanolamine
MCA	7-methyl coumarin
ME	Molar Equivalents
MeOH	Methanol
MFI	Mean fluorescence intensity
MLV	Multilamellar vesicle
MW	Molecular weight
NGR	Asparagine-Glycine-Arginine
NME	N-mercaptoethylamine
Pa	Pascal
Pbf	2,2,4,6,7-pentamethyldihydrobenzofuran-5-sulfonyl side chain protecting group
PBS	Phosphate buffered saline
PBS/FBS	10% (v/v) fetal bovine serum in phosphate buffered saline
PEG	Polyethylene glycol
PK	Pharmacokinetic
Psi	Pounds per square inch
PyBop	Benzotriazol-1-yl-oxytripyrrolidinophosphonium hexafluorophosphate
RES	Reticuloendothelial system
Rf	Retention factor
RGD	Arginine-Glycine-Aspartic Acid
RGD-LNs	Arginine-Glycine-Aspartic Acid Liposomal Nanoparticles
Rhod:PE	Rhodamine phosphatidyl ethanolamine
RP-HPLC	Reversed phase-high pressure liquid chromatography
SAR	Structure activity relationship
SDS-PAGE	Sodium dodecyl sulphate polyacrylamide gel electrophoresis
siRNA	Small interfering RNA
SPPS	Solid phase peptide synthesis
$t_{1/2}$	Half time (s)
TAMRA	5-carboxy-tetramethylrhodamine
t-Bu	t-butyl side chain protecting group
TEA	Triethylamine
TFA	Trifluoroacetic acid
TIS	Triisopropyl silane
TLC	Thin layer chromatography
UV	Ultraviolet
VEGF	Vascular endothelial growth factor
Z	Benzyl side chain protecting group

ACKNOWLEDGEMENTS

I would like to thank my parents, Carol and Tim Cressman, who have inspired me to enjoy life and nature. From delivering those first lessons in basic reasoning to providing ongoing financial support, they have made this thesis possible.

Secondly, I would like to thank Professor Cullis, a gifted leader, scientist, businessman and colleague. His mentorship has significantly changed my life and taught me the importance of clear communication, focus and prioritization in research.

Exceptional guidance is duly acknowledged from Dr. Theresa Allen, a close mentor for this project. Kind thanks are likewise given to my supervisory committee, Dr. Roger Brownsey, and Dr. David Chen for their insightful and intellectually stimulating feedback, which has greatly enriched the quality of this thesis.

I am forever indebted to my family and friends. First, a heartfelt thanks to those of which have stood by me for many years; Desirae Rovere, Michael Guiterrez, Jean Cressman, Maxine Williams, Fred Newhouse and Maxwell Newhouse. Secondly, thanks to friends from UBC; Barbara Lej-Garolla Di Bard, Nicole Quenneville, Kaley Wilson, Lianne McHardy, Chantal Levesque, Sue De Jong, Ian Dobson and Dr. Scott Covey. Likewise, the members of the Cullis lab have been supportive of this project, and I thank each person for their friendship and collaboration.

I extend my thanks to the UBC Biochemistry Department for providing a first class PhD program and the infrastructure for communication within the department and the scientific community. Likewise, thanks to several members of the UBC Chemistry Department who have facilitated this project, in particular; Dr. David Chen and members

of the Chen lab, Dr. John Sherman and members of the Sherman lab, Dr. Lawrence McIntosh, Dr. Mark Okon and the Bioservices facility.

I would like also to acknowledge my mentors from Gryphon Therapeutics, Dr. Gerd Kochendoerfer, Dr. Shiah-Yun Chen, and Dr. Stephen Kent for sharing their expertise in peptide chemistry. A kind thank you is also extended to Mr. Don Moslin, my high school Biology teacher. Along with the basics of life sciences, he taught me the importance of surrounding yourself with positive people.

Finally, financial support from the National Science and Engineering Research Council (NSERC), and Canadian Institute for Health Research (CIHR) in the form of PhD studentships, the American Peptide Society for travel grants to attend international symposia and research operating grants provided by NSERC, CIHR and Tekmira Pharmaceuticals Inc. is acknowledged.

CO-AUTHORSHIP STATEMENT

¹H-NMR-based confirmation of the cyclic structure of cRGDfK was acquired by Dr. Mark Okon, who also aided in the interpretation of the spectra.

Chapters 3 and 4 describe work that is submitted for publication in the journal, *Biochemistry*. The cell-based binding characterization has been summarized in a manuscript written by myself and revised by Dr. Pieter Cullis. Dr. David Chen, Ms. Jane Maxwell and Ms. Yin Sun are listed as co-authors for their help with interpretation of the cell-binding kinetics and characterization of the cRGDfK-488 peptide conjugates.

Likewise, all CE experiments have been conducted in collaboration with either Dr. Ning Fang or Ms. Yin Sun in Dr. Chen's lab. The application of capillary electrophoresis frontal analysis (CE-FA) to describe $\alpha_v\beta_3$:integrin binding as presented in this thesis constitutes part of a manuscript written by Ms. Sun and revised by Dr. Chen. I am responsible for initiating the project, experimental design, interpretation of results and co-authorship of this manuscript. A substantial part of the manuscript and interpretation of the data obtained by the CE-FA method is rationalized by new equations for determining multi-site binding parameters, which were developed by Ms. Sun and Dr. Chen. These equations have been included as an appendix (written entirely by Ms. Sun and Dr. Chen) to this work since they are applied to the results obtained in this thesis. The full manuscript has been submitted to the journal, *Analytical Chemistry* in July of this year.

Acquisition of the M21 and M21L melanoma cell lines was made possible through a material transfer agreement between Dr. David Cheresch and Dr. Pieter Cullis, established in July of 2006.

Work done under my direction by Mr. Ian Dobson, a undergraduate student in Dr. Cullis' lab, contributed to the synthetic procedures that were developed in Chapter 5, and constitute a significant portion of the results compiled in a manuscript in preparation for submission, co-authored by Dr. Cullis, Mr. Dobson and myself.

1 Introduction to Targeted Liposomal Nanoparticles

1.1 Liposomal Nanoparticles

The use of liposomal nanoparticles as drug delivery agents has evolved from a line of research originating over 40 years ago, based on the ability of these unilamellar vesicles to entrap material in an aqueous compartment (Bangham et al., 1965). It was then known that most amphipathic membrane lipids form multilamellar vesicles (MLV) consisting of concentric bilayers when they are dispersed in aqueous media. MLV are relatively large (micron) sized structures, however they can be extruded through 100 nm pore size polycarbonate filters to produce unilamellar vesicles with a homogeneous size distribution (Olson et al., 1979; Szoka et al., 1980). Typically, the resulting liposomal nanoparticles (LNs) are 100 nm in diameter and each particle contains approximately 1.25×10^5 lipid molecules (Winterhalter and Lasic, 1993).

LNs have been widely used as models of biological membranes to study membrane permeability and transport across the bilayer (Madden et al, 1987). In addition to their utility as model membranes, drugs may be encapsulated within the particle's aqueous interior compartment. The ability of LNs to deliver drugs preferentially to disease sites, such as solid tumors, can result in considerable improvements in efficacy; therefore, LNs are widely studied for use in therapeutic applications (Figure 1.1).

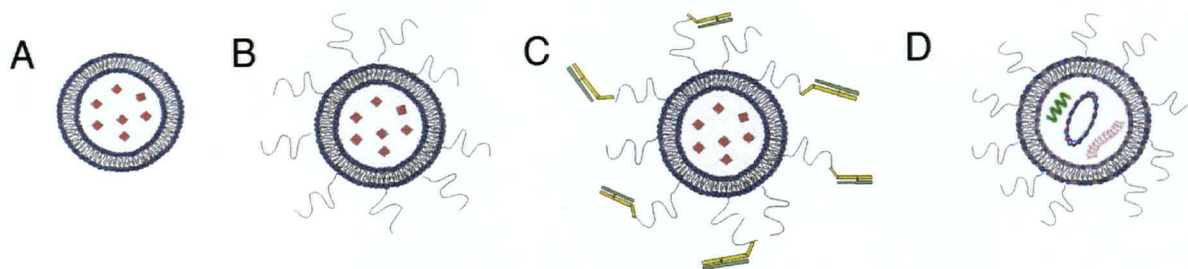


Figure 1.1 Types of LN employed for drug delivery

A) LNs that encapsulate small molecule drugs B) “Stealth®” LNs have a hydrophilic surface coating (typically polyethylene glycol (PEG)) that enables them to survive in the circulatory system for extended periods of time C) Targeted LNs are surface-modified with a targeting ligand to increase the accumulation of the particle in target cells D) LNs that encapsulate nucleic acid-based drugs such a plasmid, antisense oligonucleotides or siRNA.

1.2 Liposomal Nanoparticles and Drug Delivery

The first preparation of a liposome with entrapped solute was characterized in 1965 by A. D. Bangham in Cambridge, UK (Bangham et al., 1965). The evolution of liposomes as drug delivery systems was subsequently accelerated in the 1980’s by the development of techniques to rapidly generate well defined nanoparticulate liposomal systems and to efficiently load them with drugs (Gabizon et al., 1985; Mayer et al., 1985; Szoka et al., 1980). The observation that long-circulating LN preferentially accumulate at sites of disease, including sites of infection, inflammation and tumors, due to the leaky nature of the vasculature in these regions (Segal et al., 1975; Jain, 1987), gave a solid rationale for delivering drugs in LN systems.

LNs have several features that have contributed to their success as a drug delivery system. Encapsulation within the aqueous cavity of an LN can enhance the *in vivo* activity of drugs by protecting them from breakdown in the body and can reduce the toxic effects

of drugs, such as anti-cancer drugs, by reducing delivery to sensitive tissue (Forsen et al., 1981). In addition, LNs are biocompatible, so that they may be used *in vivo*, and their physical properties can be readily manipulated. LN production and drug-loading techniques have been optimized and standardized such that LNs can be manufactured on a large scale. LN technology also offers flexibility such that the lipid composition may be varied to match the desired characteristics of the drug that is being delivered, and can be used to optimize the halftime of release of the drug from the LN. These features are summarized by Maurer et al., 2001, and more recently by Allen and Martin, 2004, noting examples where LN encapsulation gave the associated drug long circulation lifetimes, enhanced accumulation at disease sites and increased efficacy for a variety of drugs.

The range of material that may be encapsulated within the LN is diverse. LNs have been used for the encapsulation of small molecule drugs including anti-cancer (Olson et al., 1982) and antifungal drugs (Mehta et al., 1984), and nucleic acid-based drugs such as plasmids for gene therapy (Ambegia et al., 2005; Choi et al., 2003), immunogenic DNA oligonucleotides (Mui et al., 2001) and siRNA oligonucleotides (Zimmermann et al., 2006) (Figure 1.1). A review of the current status of modern drug delivery systems and their *in vivo* application has been published, noting six LN formulations that are clinically approved drugs and many others in advanced clinical trials (Allen and Cullis, 2004).

The application of LNs as carriers of nucleic acids has required the development of a sophisticated class of nanoparticles for *in vivo* LN delivery. These particles must entrap high amounts of nucleic acid (Jeffs et al., 2005), survive for prolonged amounts of time in the circulatory system (Fenske et al., 2002) and release their contents in the cytoplasm of cells that internalize the particle (Kale and Torchilin, 2007; Li et al., 2005).

1.3 LNs with Extended *in vivo* Circulation Lifetimes

Despite the advantages of encapsulating drugs within an LN, 25 years passed after the discovery of liposomes, before the first LN drug formulation, Ambisome®, achieved regulatory approval for clinical use (Adler-Moore, 1994). This can be explained in part by the complexity of LN behavior when administered *in vivo*. A particularly important issue emerged from early *in vivo* experiments that showed that LNs were rapidly removed from the circulation by uptake of the particle by fixed and free macrophages of the reticuloendothelial system (RES) that reside in the liver and spleen (Allen and Everest, 1983).

A major breakthrough came from the observation that modification of the LN surface could prevent the cells of the RES from recognizing and subsequently clearing the foreign particle. It was originally shown that the inclusion of sialic acid (Allen and Chonn, 1987) or polyethylene glycol (PEG)-containing lipids, (Klibanov et al., 1990; Papahadjopoulos et al., 1991) in the LN formulation could significantly extend the circulation lifetime. The term “Stealth® liposome” describes LNs that can survive in the blood stream for prolonged amounts of time. PEG-containing LN formulations have shown the greatest life-time enhancement, and some optimized formulations, such as Doxil®, have reported circulation half-times of up to 45 h in humans (Gabizon et al., 1994). A long circulation half-life is a major advantage because the accumulation of LNs at the site of a tumor has been shown to increase with the amount of time that the particles remain circulating in the body (Huang et al., 1992).

In 1995, a doxorubicin-containing LN (DOXIL®) became the first major anti-cancer LN to be approved. It was initially approved for use against Aids-related Kaposi's

sarcoma (Northfelt et al., 1996), and subsequently for the treatment of refractory ovarian cancer in 1999 (Muggia and Hamilton, 2001).

1.4 Immunoliposomes (ILNs)

1.4.1 Targeting LNs to the Disease Site

LNs containing anti-cancer drugs that accumulate at the tumor site without the aid of a targeting molecule (defined as “passive” targeting) take advantage of the enhanced permeability and retention (EPR) effect, caused by the leaky nature of the neovasculature that supplies blood to the tumor (Maeda et al., 2000). In addition, the tumor microenvironment does not have effective lymphatic drainage to remove particles from the tumor after they accumulate there. The EPR effect thus facilitates extravasation of LNs from the circulation into tumor tissue and their subsequent retention there.

Since the early days of LN drug development, it has been hoped that LNs could be designed to deliver their contents to specific cells *via* a molecular targeting mechanism (Torchilin, 1985). In this concept, a targeting ligand on the surface of an LN could aid in the binding of the LN-encapsulated drug specifically to the target cells at the disease site. It is hypothesized that the targeted LN should further improve the therapeutic index of the drug over that of non-targeted LNs. Commonly used anti-cancer drugs are often delivered below their effective dose due to their toxic side effects. Thus, if a targeted LN can deliver drug to the tumour at concentrations greater than the effective dose, the anti-cancer effect should also increase.

Initiatives to covalently tether antibodies to liposomes began with work done in the early 1980's by Heath and colleagues who demonstrated that the attachment of anti-human erythrocyte antibodies to an LN surface could promote adherence of the particle to human red blood cells in a mixed cell population (Heath et al., 1981, Leserman et al, 1981). Shortly after, researchers began to investigate antibody-targeted liposomes, or immunoliposomal nanoparticles (ILNs) to deliver a variety of drugs targeting diseases of viral, oncologic and malarial origin (reviewed in Sapra and Allen, 2003).

One of the first *in vivo* studies with ILNs was conducted using an IgG antibody against the gp80 antigen present on the avian myeloblastosis virus coat protein (Dhananjaya and Antony, 1988). The resulting ILNs showed promising efficacy against the viral infection, with higher accumulation of the particles in target tissues, long circulation lifetimes and no immune response from the host. The last finding was surprising, since the IgG antibody used for targeting was produced in a rabbit while the experiment was done in a mouse. The authors do not acknowledge any response by the host's immune system to the foreign antibody. Recent *in vivo* studies report the opposite effect, that the ILNs are rapidly cleared. These findings have been attributed to recognition of foreign antibodies on the ILN's surface by the host's immune system, (Harding et al., 1997).

Advancements, such as the somatic cell hybridization technique (Kohler and Milstein, 1975), and improvements in antibody engineering (Padlan, 1991) have had a tremendous impact on the progression of antibody-based therapeutics. Improved formulation techniques have further enabled several antibody-based therapeutics to come to market with great success (Daugherty and Mersny, 2006). The approval status and anti-

cancer effect of the dozen or so approved antibody-based drugs has recently been reviewed (Imai and Takaoka, 2006). In 1997, a chimeric (part human and part mouse (Fig. 1.2A)) antibody, Rituxan[®], used to treat B-cell lymphomas, became the first antibody to receive United States Federal Drug Advisory (FDA) approval. This was followed by Herceptin[®], a humanized antibody (Figure 1.2B), approved in 1998 for the treatment of Her-2/neu positive breast cancers. Humanized antibody scaffolds are favored since their design enables long circulation lifetimes of the antibody with a circulation half-time of 13 days (Stephens et al. 1995). A current review of FDA approved and antibody-based drug candidates can be found in Nayeem and Khan, 2006.

Clinicians are now trying to optimize the combination of antibodies with conventional anti-cancer drugs. In this regard it has been shown that the administration of an LN-encapsulated drug in combination with Rituxan[®] improves the clinical outcome for patients with non-Hodgkin's lymphoma (Zaja et al. 2006).

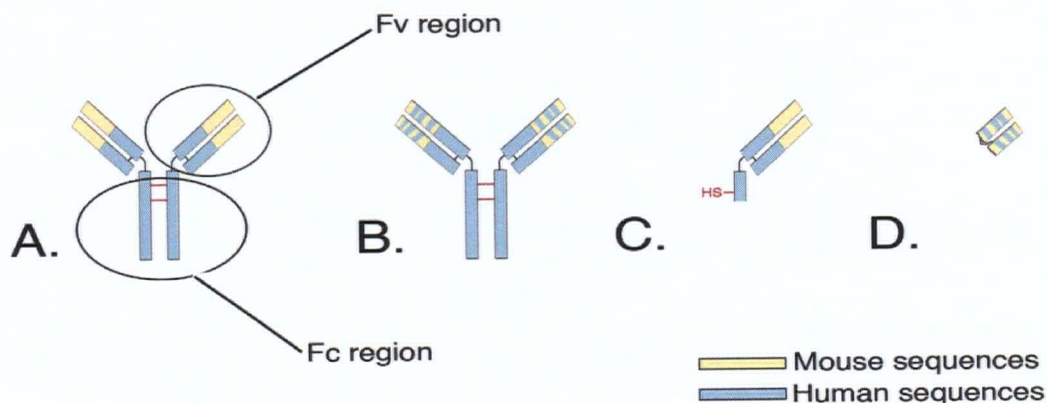


Figure 1.2 Antibody engineering

A) Chimeric monoclonal antibody (mAb). B) Humanized mAb. C) Fab' fragments. Fab' fragments are typically made by enzymatic digestion of the Fc region and subsequent reduction of the disulphide between the antibody dimers D) Single chain variable fragment (scFv) antibodies, a recombinant antibody that contains the minimal protein sequences required for antigen binding.

The use of antibody fragments for LN targeting such as Fab' (the antibodies variable region including the complementarity determining region (CDR)), or scFv (a recombinant protein made from the CDR) is preferential to using whole antibodies for targeting since they are less prone to rapid clearance from the circulation (Maruyama et al., 1997). This is largely attributable to a reduction in the immune response to the species-specific sequences that exist in the Fc region of the antibody when it is removed from the whole mAb (Gagne et al., 2002).

1.5 Contemporary ILNs and ILN Production

Our understanding of the desired *in vivo* characteristics of ILNs has progressed together with the increased availability of antibodies. In the past decade, important concepts such as the need to target receptors that internalize the particle (Sapra and Allen, 2002) and new approaches to formulation and ILN production methods (Ishida et al., 1999) have also brought the technology closer to the clinic.

A significant breakthrough in the advancement of ILN production has been the use of the "post-insertion" method (Ishida et al., 1999; Moreira et al., 2002). In this method, a targeting ligand, such as an antibody, is first coupled to a lipid anchor, and then co-incubated with pre-formed LNs. The advantage that this approach holds over conventional ILN production methods is that the targeting construct can be made, analyzed and purified before it is incorporated into the LN formulation, resulting in a well-characterized system.

1.5.1 ILNs *in vivo*

Unlike passive targeting, which relies on the EPR effect to enhance accumulation of LN at disease sites due to the leaky nature of the vasculature in these regions, active targeting implies the direct binding of the LN to surface receptors on target cells followed by endocytosis of the ligand that binds to these receptors. This can also result in internalization of the LN into the target cells, thereby enhancing efficacy (Allen et al., 2002; Moreira et al., 2002).

The importance of ILN internalization was established through a series of experiments using ILNs targeted with anti-CD19 (internalizing) or anti-CD20 (non-internalizing) antibodies in a B-cell lymphoma mouse model (Sapra and Allen, 2002). Since both antibodies bind to antigens present on malignant B-cells, the effect of targeting with an internalizing versus non-internalizing antibody could be demonstrated. This study showed that the internalized ILN could increase the life span of the mouse by 65.2% as opposed to 24.3% for non-internalized ILN.

In another encouraging contribution by Park and colleagues, ILNs were made with scFv antibody fragments against the HER2/neu growth factor that is over-expressed on some breast cancer cells. The results reported cures of up to 50 % in tumor-bearing mice when the target cells expressed high antigen densities (Park et al., 2002).

This work has resulted in many pre-clinical demonstrations of improved efficacy in animal models yet none have progressed to demonstrate efficacy in humans. This is evidenced by a series of recent publications that describe the gram-scale and GMP-compliant production of anti-HER2 scFv-PEG₂₀₀₀-distearoylphosphatidylethanolamine (DSPE) for post-insertion into LNs (Nellis et al., 2005a; Nellis et al., 2005b). This is

perhaps the best characterized of the ILN pre-clinical formulations, however, no clinical trial on this system has been initiated.

1.5.2 ILNs in the Clinic

Despite encouraging pre-clinical results, only one clinical study of an ILN doxorubicin formulation has been reported. It describes a Phase I clinical trial of a targeted ILN, made with Fab₂ antibody fragments directed against stomach cancer antigens (Matsumura et al., 2004). The authors found that their ILNs showed the same *in vivo* circulation kinetics as non-targeted LNs and established a recommended dosing regime for phase II clinical trials. Further detail on this formulation is limited, as the supporting pre-clinical studies have not been reported.

The major challenges that must be overcome before targeted LNs can be used in the clinic include the accurate characterization of these particles and the reproducible and cost-effective manufacture of these particles. With almost a hundred pre-clinical studies on targeted ILNs published, only one well-documented and convincing method for ILN production and characterization has been presented. This uses chemically defined scFV-PEG₂₀₀₀-DSPE lipids that are post-inserted into pre-formed LNs. Further work is needed to achieve well-characterized ILN systems that can be readily manufactured and where efficacy is well correlated with the composition, size and contents of the ILN. As shown in Chapter 2 of this thesis, techniques that involve the coupling of targeting proteins to LN to produce ILN result in systems that are inherently difficult to characterize, manufacture and reproduce, and are also extremely expensive. For these reasons the bulk of this thesis

concerns the development of smaller molecule peptide targeted systems that allow more rigorous analysis and that can be incorporated into LN in a quantitative manner at the time of LN manufacture.

1.6 Small Molecule Targeting Ligands

From many perspectives, the use of smaller molecules with well-defined analytical characteristics is attractive for LN targeting. Although they have lower affinities for target molecules than antibodies, small molecules such as peptides and peptidomimetics are more straightforward to develop clinically than macromolecular drugs (Cho and Juliano, 1996; Livnah et al., 1996). For example, small molecule ligands can be made to be chemoselective during conjugation to lipid anchors by the use of protecting groups that shield other sites until after the conjugation reaction is complete. Peptides may also be confined in space by conformational restrictions to mimic biological interactions between proteins and may also protect the peptide against enzymatic degradation in the body (Cho and Juliano, 1996; Livnah et al., 1996). These, along with several other advancements in the field of peptide science, have facilitated the development of many new pharmaceuticals over the past 20 years.

Over a hundred peptide-based drugs are now approved and generating substantial revenue. Some hallmark examples of successful peptide drugs on the market include Fuzeon[®], an anti-entry HIV inhibitor, Exubera[®], an inhalable version of insulin and Forteo[®], an analogue of the human parathyroid hormone used for treatment of osteoporosis (reviewed in Watt, 2006).

1.6.1 Peptides with Disease Site Affinity

The search for peptides that might serve as affinity agents for targeting has been facilitated by work from Ruoslahti's group in the early 1990's using a method known as *in vivo* phage display. In these experiments, a library of phage expressing different peptides on their surface were injected into a mouse and subsequently isolated from specific organs. The peptides that were associated with the recovered phage particles were then identified. Using this method, Ruoslahti and colleagues have identified peptides that will specifically home to the brain (Pasqualini and Ruoslahti, 1996), heart (Zhang et al., 2005), prostate (Arap et al., 2002), and bladder (Lee et al., 2007; Pasqualini et al., 2000).

Ruoslahti's *in vivo* phage display technology has also led to the identification of peptides that bind to tumor vasculature (Ruoslahti, 2000). The asparagine-glycine-arginine (NGR) and arginine-glycine-aspartic acid (RGD) tri-peptide motifs were identified in several different phages that selectively bind to the tumor-associated endothelium, but not to the vasculature of healthy tissues. Both the NGR and the RGD motifs have thus been pursued as tumor targeting agents. The NGR motif was later found to home to aminopeptidase N, a cell surface protein expressed on the vascular endothelium (Pasqualini et al., 2000). Peptides containing NGR have been shown to guide both high molecular weight proteins and LN to the site of a tumor (Pastorino et al., 2006; Pastorino et al., 2004).

The tumor targeting properties of the RGD motif were consistent with targeting to the $\alpha_v\beta_3$ integrin expressed during angiogenesis as established by Cheresh and Ruoslahti

(Brooks et al., 1994c; Cheresh, 1987; Cheresh et al., 1987). Subsequently, the use of RGD as an anti-angiogenesis agent has been heavily pursued, resulting in drugs now in late phase II clinical trials (Friess et al., 2006).

1.6.2 Arginine-Glycine-Aspartic Acid (RGD)

Originally identified in Ruoslahti's group as a component of fibronectin (Pierschbacher and Ruoslahti, 1984), the RGD sequence is present in several other proteins of the extracellular matrix that interact with the cell through the integrin receptors. This will be discussed in more detail in Chapter 3 regarding the involvement of RGD-containing proteins in angiogenesis. Members of Kessler's laboratory have produced detailed studies to relate structure to activity to optimize the pharmacophoric contacts between an $\alpha_v\beta_3$ -selective RGD peptide and the $\alpha_v\beta_3$ integrin (Dechantsreiter et al., 1999). The resulting compound has the cyclic amino acid sequence: Arginine-Glycine-Aspartic acid-n-methyl-d-Phenylalanine-Valine, (cRGD(nme)fV) and features an n-methylated amide bond between the D and f residues. Merck has developed this compound as an anti-angiogenesis drug candidate with the trade name Cilengitide®. In phase I clinical results, Cilengitide® is effective without toxic side effects and has achieved complete and partial responses in patients with glioblastoma multiforme (Nabors et al., 2007). Cilengitide® is also currently employed in several phase II clinical trials and has orphan drug status in Europe against pediatric glioma.

1.7 RGD-Targeting Ligands and Affinity Analyses

The RGD sequence has also been pursued as an affinity agent for targeting to the tumor vasculature. A range of RGD-based constructs have been used in attempts to increase the concentration of drugs (Kim and Lee, 2004), imaging agents (Chen et al., 2004b; Li et al., 2007a; Wu et al., 2005), antibodies (Schraa et al., 2002) and LNs (using methods of surface coupling) (Dubey et al., 2004; Janssen et al., 2003; Schiffelers et al., 2003) at the site of solid tumors. While these studies have reported some encouraging results, many aspects of the basic ability of RGD-based targeting ligands to target to the $\alpha_v\beta_3$ integrin remain uncharacterized. This is because the characterization of most anti-angiogenic RGD-ligands is done by an inhibition or competition assay, which reports a half maximal inhibitory concentration, or IC_{50} value. In this case, the IC_{50} value describes the half-maximal concentration of RGD-drug that is required to compete with a naturally occurring ligand that binds to the $\alpha_v\beta_3$ integrin. A low IC_{50} value indicates that only a small amount of the competitor is required in order to disrupt the integrin:ligand interaction. Many researchers use purified vitronectin as the integrin's natural ligand to be displaced by RGD (see table 1.1). When describing affinity, an IC_{50} value is generally not the best method, particularly for the describing binding to the $\alpha_v\beta_3$ integrins, which are known to bind to several different ligands (Brooks, 1996). The IC_{50} value is therefore strongly dependent on the particular ligand that is initially bound to the integrin. A summary of some key *in vitro* binding characterizations of RGD-ligands is given in Table 1.1.

Table 1.1 Summary of *in vitro* binding characterizations of RGD-containing ligands targeting the $\alpha_v\beta_3$ integrin

RGD-construct	Publication	Activity assay	Constants reported
Linear RGD-containing peptide	Dechantsreiter et al, 1999	Biotinylated vitronectin in competition with unlabelled RGD-ligands for immobilized $\alpha_v\beta_3$ binding.	$IC_{50}=210$ nM
Cilengitide	Dechantsreiter et al, 1999	Biotinylated vitronectin in competition with unlabelled RGD-ligands for immobilized $\alpha_v\beta_3$ binding.	$IC_{50}=0.58$ nM
RGD-modified antibodies	Schraa et al, 2004	Radiolabelled RGD-antibody in competition with unlabelled RGD ligand for binding to $\alpha_v\beta_3$ -expressing cells	$IC_{50}=150$ nM
PEGylated RGD-imaging agents	Chen et al, 2004a	Radiolabelled echistatin in competition with unlabelled RGD-ligands for binding to immobilized $\alpha_v\beta_3$ integrin	$IC_{50}=30.3$ nM
Octameric and tetrameric RGD-imaging agents	Li et al, 2007	Radiolabelled echistatin in competition with unlabelled RGD-ligands for immobilized $\alpha_v\beta_3$ binding	$IC_{50}=10$ nM for octamer vs. 35 nM for tetramer
RGD-LNs	Janssen et al, 2003	Fluorescent RGD-LNs in competition with non-fluorescent RGD-LNs for binding to $\alpha_v\beta_3$ -expressing cells	No binding constants are reported however, non-specific LNs, are shown to be unable to compete with RGD-LNs for cell binding

From the summary provided in Table 1.1 it can be observed that different conditions for the competition assays are employed between research groups. As a result, the IC_{50} values reported are highly subject to experimental conditions.

The lack of formal binding studies likely arises from the lack of labeled RGD molecules to simplify the conduct of the binding assays. In this thesis, this problem is directly addressed by the synthesis of a well-characterized fluorescently-labeled RGD-ligand. This construct was used to measure equilibrium binding parameters, which describe RGD-binding to the $\alpha_v\beta_3$ -integrin alone and to $\alpha_v\beta_3$ -expressing cells.

Similar difficulties are encountered when measuring the binding of targeted LNs to target cells. A solution to this problem was to incorporate a fluorescent label into the RGD-

lipid before LN formulation. This resulted in the ability to calculate K_d values to describe binding for RGD-targeted LN systems

1.8 Objectives, Evolution and Structure of this Thesis

The original aim of this thesis was to develop well-characterized ILN employing Fab' or scFv fragments of Rituxan for targeting drug-containing ILNs to the CD 20 receptor on B cells to improve the treatment of non-Hodgkin's lymphoma. Such an ILN appeared to represent an interesting opportunity given the synergy observed clinically between Rituxan and non-targeted LNs containing doxorubicin (Zaja, 2006). Given the lack of success over the last 25 years in moving a targeted LN into clinical testing, it was of particular interest was to develop an ILN that was sufficiently well-characterized that it could conceivably gain regulatory approval and move forward into the clinic if the pre-clinical results looked promising. This requires a system where the molecular composition of the targeting ligands is well-defined, where the targeting ligands can be produced in a cost-effective and reproducible manner, where the binding properties of the targeting ligand for the receptor are well-understood, where the number of targeting ligands per LN is well-defined and reproducible and where the ILN as a whole can be made in a straightforward and reproducible manner. Ideally, the targeting ligand employed would also stimulate endocytosis and intracellular delivery of the ILN contents, which would be expected to result in improved potency.

After considerable efforts over two years to develop an ILN targeted with Fab' derived from the mAb, Rituxan, this approach was abandoned. As briefly summarized in

Chapter 2 of this thesis, many difficulties were encountered. These ranged from the relatively trivial, for example the fact that starting reagents such as activated PEG-lipids for coupling to proteins varied significantly in quality between different manufacturers, to the more fundamental, such as the fact that the stoichiometry of attachment of PEG-lipid to Fab' could not be easily controlled and the isolation of molecularly defined Fab'-PEG-lipid targeting ligands at reasonable yield proved impossible. These issues led to the consideration of alternative approaches.

As detailed in this Introduction, peptide-targeting agents such as RGD-based targeting ligands have a number of attractive features. They are small, and can be made to be chemoselective in the sense that only one function on the molecule is available for coupling to a PEG-lipid, for example, leading to a molecularly defined species. The small size also leads to the possibility that the ligand-PEG-lipid will be sufficiently soluble in organic solvent so that it can be incorporated in a quantitative manner into LN at the time that the LN is made. In the case of the RGD-containing ligands, the added attraction is the affinity for tumor vasculature and the resulting potential for the treatment of a variety of solid tumors. It was therefore decided to develop an LN targeting ligand based on Cilengitide®, which is the most advanced of the RGD-based anti-angiogenic agents. However, it was realized that many basic features relating to using this as a targeting ligand were not available. First, as indicated in the preceding Section, the interactions of anti-angiogenic RGD-containing ligands such as Cilengitide® with the $\alpha_v\beta_3$ integrin in cells are largely characterized in terms of IC_{50} values rather than binding parameters such as dissociation constants (K_d). This led to attempts to characterize the binding of Cilengitide® to the isolated $\alpha_v\beta_3$ receptor, which required the synthesis of a fluorescently labeled

analogue of Cilengitide and the identification of a suitable technique for characterizing the ligand-receptor binding properties. I therefore synthesized cRGDfK-488, a fluorescently labeled Cilengitide® analogue and initiated the collaboration with Dr. David Chen to use capillary electrophoresis (CE) to measure, for the first time, the K_d values describing the binding of this analogue with the isolated $\alpha_v\beta_3$ receptor. This work, described in Chapter 3, leads to the conclusion that cRGDfK-488 binds to the isolated $\alpha_v\beta_3$ receptor with micromolar affinity at a 2:1 stoichiometry.

The second basic area that required characterization concerned the binding to the $\alpha_v\beta_3$ receptor in intact cells and the influence of RGD-ligand binding on endocytosis. The literature on the effects of the binding of RGD-containing ligands on endocytosis is ambiguous, with one report suggesting that endocytosis of RGD-peptides is independent of binding to $\alpha_v\beta_3$ integrin (Castel et al., 2001), whereas other reports suggest the opposite (Renigunta et al., 2006). I therefore performed the studies detailed in Chapter 4 characterizing the binding of the cRGDfK-488 ligand to the $\alpha_v\beta_3$ integrin on human umbilical vascular endothelial cells (HUVEC), showing that cRGDfK-488 binds to $\alpha_v\beta_3$ integrins in the membrane again with affinities in the micromolar range and also showing that such binding stimulated endocytosis of the ligand that was dependent on the presence of the $\alpha_v\beta_3$ integrin on the cell surface.

These studies set the stage for achieving one of the original aims of this thesis, namely, the construction of a well-defined ligand-PEG-lipid that could be inserted in a quantitative manner into LN systems. I therefore synthesized cRGDfK-PEG₂-K(MCA)-PEG₂-DSPE, an RGD-PEG-lipid that is fluorescently labeled in order to allow for straightforward estimates of RGD incorporation into LN systems. Further, our construct

contains a defined number of ethylene glycol units in the PEG spacer moiety, resulting in a molecularly well-defined targeting ligand. RGD-PEG-lipids previously constructed are not labeled and contain PEG with a range of molecular weights. These studies are presented in Chapter 5, where it is shown that cRGDfK-PEG₂-K(MCA)-PEG₂-DSPE can be inserted into LN at the time the LN is made, that the resulting ILN systems target to and are endocytosed into HUVEC, and that such systems can be loaded with an anticancer drug such as doxorubicin and can deliver this drug to the interior of these cells.

A substantial amount of time and effort has been spent on the syntheses and *in vitro* studies detailed above, such that this work is now ready for the next phase of study that will involve characterization of the *in vivo* properties of the LN systems constructed. In Chapter 6 some of the issues that will need to be addressed in such studies are discussed.

2 Preliminary Experiments

2.1 Introduction

The studies presented in this brief Chapter produced results that significantly changed the direction of this thesis. These findings concern the difficulties encountered in constructing ILNs using “classical” procedures, which led to the abandonment of attempts to attach either intact antibodies or Fab’ fragments to LNs in order to construct ILNs. In particular, in a series of studies using Fab’ fragments of anti-CD20 antibodies, (Rituxan[®]), it was found the non-chemoselective nature of the coupling between Fab’ fragments and maleimide-PEG-lipids makes it difficult to obtain well-defined compounds. Other limitations also were encountered such as the poor quality of the commercially available maleimide-PEG-lipids and a low yield of synthesis. As a result, it was decided to investigate targeting ligands, such as the RGD peptide, that can be incorporated into ILN in a straightforward and controllable manner.

Rituxan[®] is an approved drug for the treatment of B-cell lymphoma, and is a monoclonal antibody targeted to the CD20 receptor on malignant B-cells (Maloney et al., 1997). It was initially reasoned that by using Rituxan[®] as a targeting ligand, beneficial effects arising from both antibody-mediated and LN-mediated anti-tumor efficacy would be observed. The approach taken to construct ILNs targeted by Rituxan[®] was to isolate the Fab’ fragments from the intact antibody and couple these fragments to maleimide-PEG₂₀₀₀-DSPE in a quantitative manner. The Fab’ fragments were then used rather than intact

antibodies to avoid the potential rapid clearance from the circulation of ILNs that contain the Fc portion of the antibody which is species specific (Harding et al., 1997).

2.2 Methods

2.2.1 Materials

Unless otherwise stated, all reagents were purchased from Aldrich (Milwaukee, WI) and were of reagent grade or higher. All buffers were vacuum degassed, sparged with helium and stored under argon until used. Sodium dodecyl sulphate polyacrylamide gel electrophoresis (SDS-PAGE) separation was performed on 8% non-denaturing polyacrylamide gels and stained with Coomassie blue. Pre-stained molecular weight markers were purchased from Invitrogen (Carlsbad, CA).

2.2.2 Fab' Formation

Fab' fragments were made from commercially available Rituxan[®] (BC Cancer Agency, Vancouver, BC), a chimeric mAb (see Figure 1.2B). The antibody was first digested with immobilized pepsin (Pierce, Rockford, IL) for 8 h, followed by purification on Protein A affinity columns (Pierce, Rockford, IL). The protein was then dialyzed overnight, reduced with a solution of 100 mM Tris base, 65 mM N-mercaptoethylamine (NME) pH 7.5 for 30 min and desalted on PD10 columns (Amersham Biosciences) equilibrated with "PEGylation buffer" (130 mM NaCl, 3 mM KCl, 10.4 mM Na₂PO₄, 5 mM EDTA, 1.7 mM KH₂PO₄ pH 7.0). The resulting product had an apparent molecular weight between 60 and 80 kD, as detected by SDS-PAGE.

2.2.3 Maleimide-PEG₂₀₀₀-DSPE Analysis

The quality of maleimide-PEG-lipids was assessed using a Bruker BiFlex IV matrix-assisted laser desorptive ionization time-of-flight mass spectrometer (MALDI-TOF) with sinnapinic acid used as the matrix. Maleimide-PEG-lipids from Nektar Polymers and Avanti Polar Lipids were compared, resulting in the finding that the Nektar product had significant quality issues and the Avanti product was chosen for use in further experiments.

2.2.4 Fab'-PEG₂₀₀₀-DSPE Conjugation

Conjugation of Fab' fragments (75 μ M) to maleimide-PEG₂₀₀₀-DSPE (herein referred to as Mal-PEG-DSPE) (Avanti Polar Lipids) was carried out over 8 h at room temperature under argon gas, using up to 10 molar equivalents of Mal-PEG-DSPE. The pH was measured once all of the reactants were dissolved and carefully adjusted with pH 8.0 PEGylation buffer. A series of reactions were tested between pH 5-8, and the optimal pH to be employed for subsequent studies was found to be 7.0. The product, Fab'-PEG₂₀₀₀-DSPE typically formed after one hour and was detected by the appearance of a band with greater retardation than the Fab' band by SDS-PAGE.

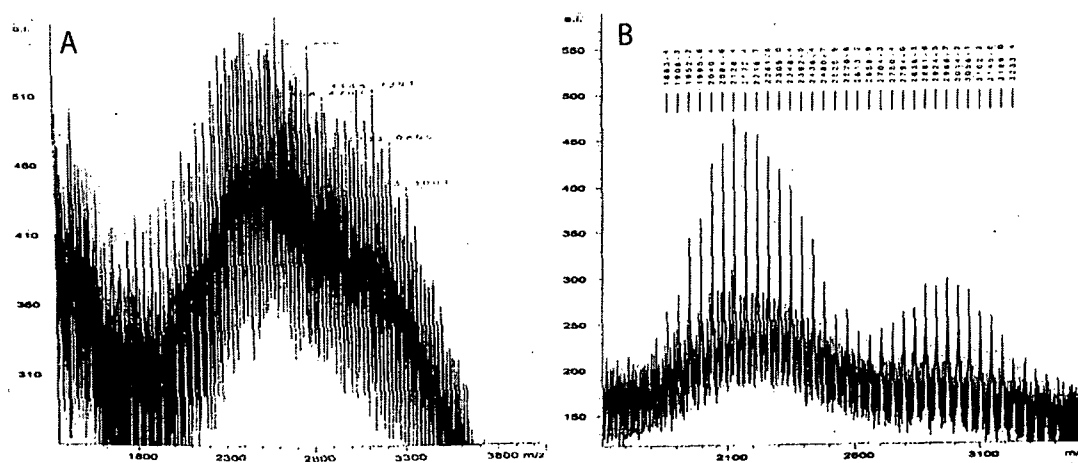
2.2.5 Fab'-PEG₂₀₀₀-DSPE Purification

The reaction mixture was purified by size exclusion chromatography over 40 ml Sephadex Cl-4B hydrated in PEGylation buffer. The Fab'-PEG₂₀₀₀-DSPE product eluted between 7-10 ml and Fab' eluted after 10 ml. Alternatively, ion exchange chromatography was performed using a 1 ml SX Hitrap column on an AKTA fast protein liquid chromatography (FPLC) purification system (GE Healthcare, UK). The PEGylation mixture was first dialyzed overnight against 20 mM H₂PO₄, pH 6.8 (IEX buffer), then 1 mg of the total protein content protein was purified using a gradient of IEX buffer and IEX buffer containing 500 mM NaCl in order to elute the PEGylation mixture over 20 min.

2.3 Results

2.3.1 Quality of Mal-PEG-DSPE

Initial attempts to conjugate Fab' fragments to Mal-PEG-DSPE were unsuccessful, bringing into question the quality of the reagents used. The analysis shown in Figure 2.1 resulted in the choice to use Mal-PEG-DSPE that was obtained from Avanti Polar Lipids for subsequent experiments. As shown in Figure 2.1A, the product supplied by Nektar produced a charge series by mass spectrometry that indicated a poor quality compound, whereas the Avanti product produced a spectrum consistent with a much purer compound. This can be seen in Figure 2.1B where the charge series produced from repeat PEG units is devoid of the contaminating peaks seen in Figure 2.1A. Further analysis by ^1H NMR provided evidence that the maleimide functionality on the Avanti product was stable and accessible for conjugation.



2.3.2 Fab'-Maleimide-PEG-DSPE Conjugation

The overall yield (yield is defined as moles of product produced as a percentage of the moles of the limiting reactant) for the formation of Fab' fragments from the intact antibody was 66%. This yield decreases to less than 30% upon reaction with Mal-PEG-DSPE using the optimized conjugation conditions detailed in the Methods section. Furthermore, a higher yield could not be obtained by increasing the molar equivalents of Mal-PEG-DSPE in the reaction (see Figure 2.2). This yield could also not be improved by adjusting the pH (between 5.5 to 8.0) or by increasing the concentration of the Fab' fragments. The low yield is further decreased to less than 5% overall upon purification by SEC.

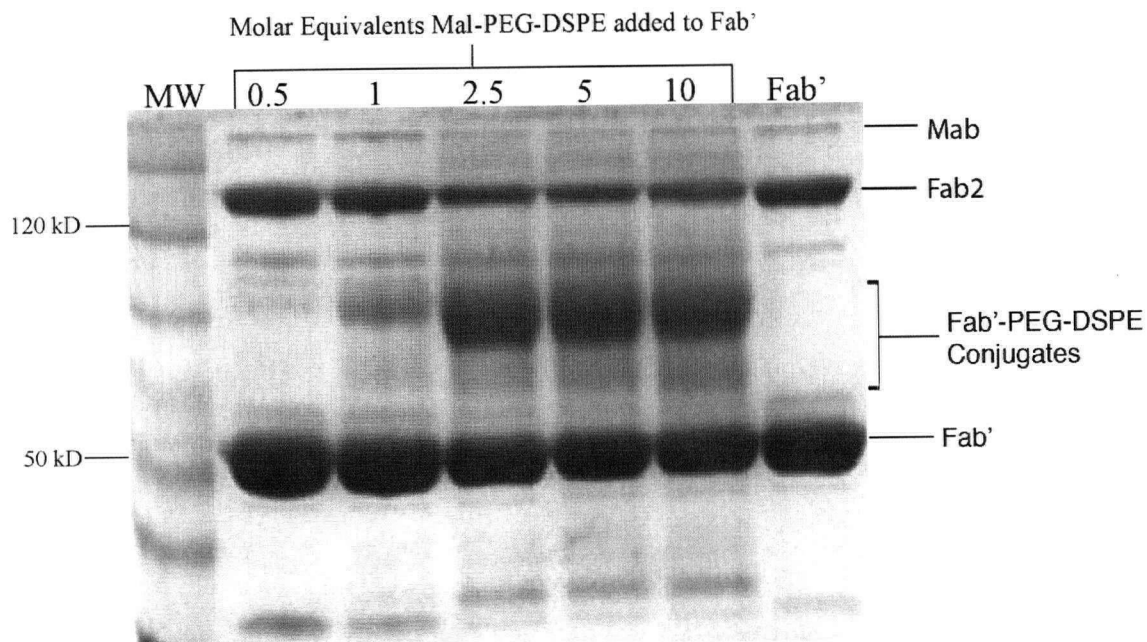


Figure 2.2 Addition of Mal-PEG-DSPE to Fab' to form Fab'-PEG-DSPE

Analysis of the effect of adding increasing amounts of Mal-PEG-DSPE to Fab' fragments in an attempt drive the conjugation reaction to completion. Up to ten molar equivalents of Mal-PEG-DSPE were added to Fab' fragments, and the reaction mixture was separated by SDS-PAGE and stained with Coomassie blue reagent.

2.3.3 Pure Fab'-PEG-DSPE Preparations are Inherently Difficult to Achieve

At least two new bands could be observed upon conjugation of Fab' fragments to Mal-PEG-DSPE. These were interpreted as mono- and di-PEG₂₀₀₀-DSPE substituted Fab' fragments. Some resolution between Fab' fragments and the higher MW conjugates could be obtained by size exclusion chromatography, but the overall yield significantly decreased since the products co-eluted with the unconjugated protein. The elution profile of a typical size exclusion purification is shown in Figure 2.3.

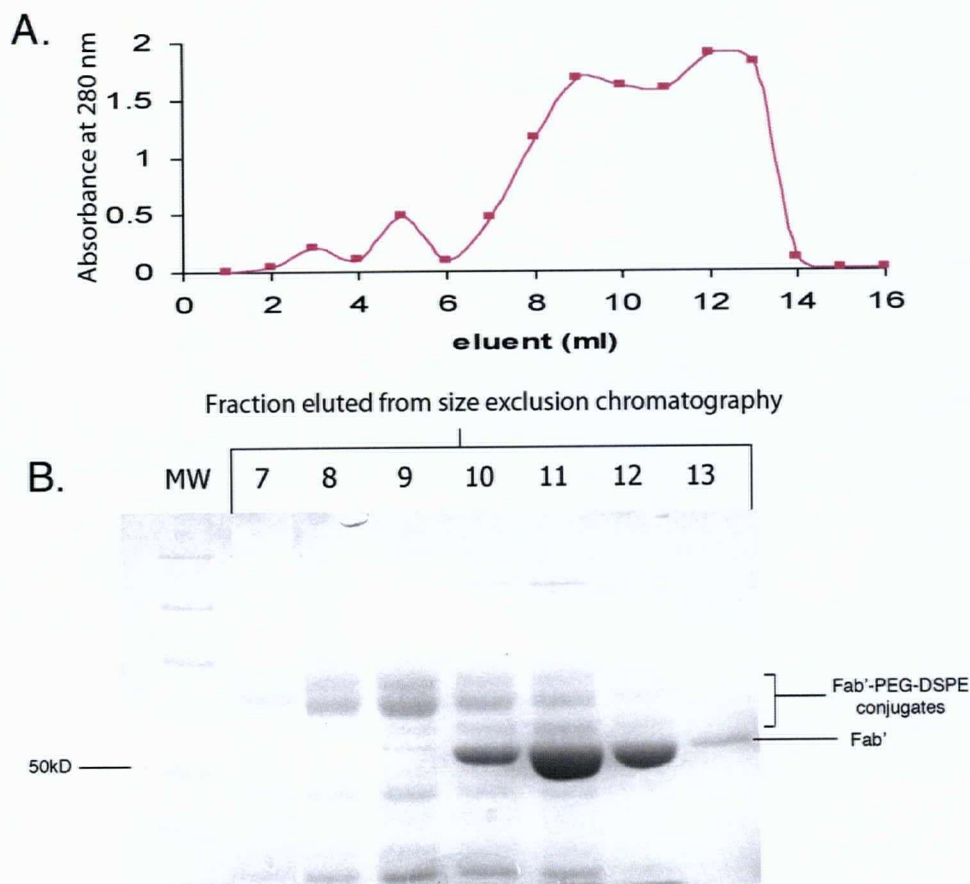


Figure 2.3 Size exclusion purification of Fab'-PEG-DSPE

A) Chromatogram from fractions eluting from a size exclusion column. Fab'-PEG-DSPE conjugates and unreacted Fab' were detected by their relative absorbance at 280 nm. B) SDS PAGE analysis of fractions detected by SDS-PAGE.

Purification to homogeneity of Fab'-PEG-DSPE was also attempted using ion exchange chromatography. This strategy was unsuccessful since the Fab'-PEG-DSPE conjugates eluted before the salt gradient was applied (Figure 2.4). Attempts to adsorb the products to the column using different column matrices or eluting buffers were made without success.

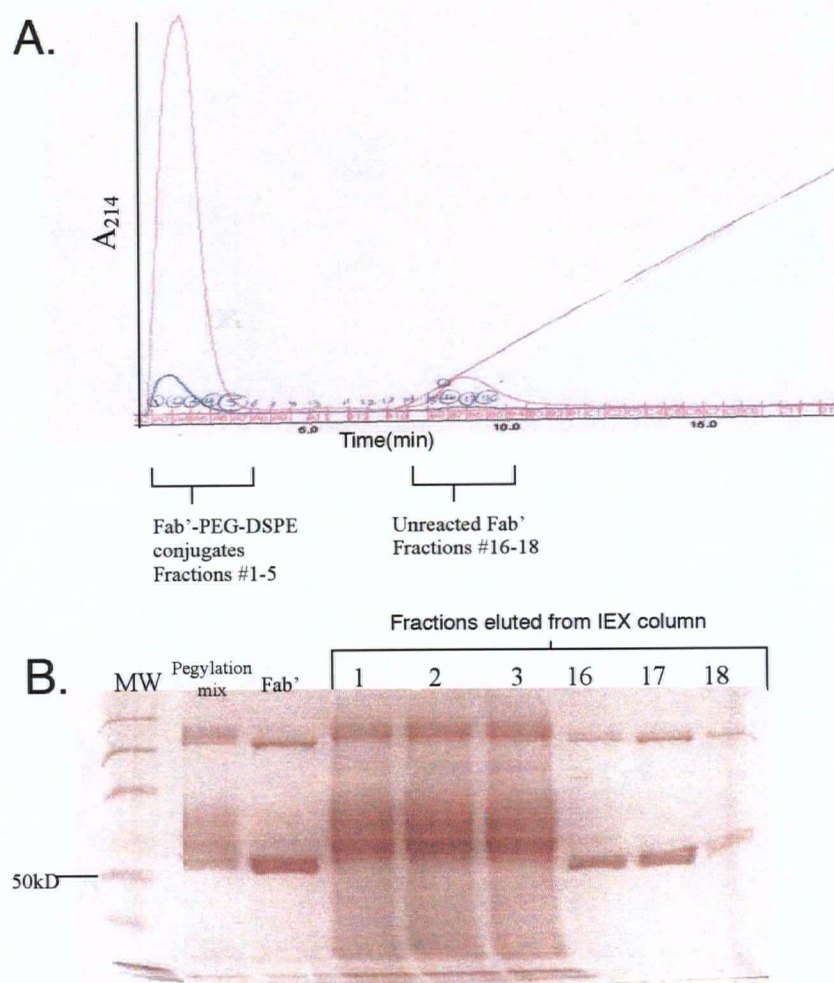


Figure 2.4 Ion-exchange chromatography of Fab'-PEG-DSPE conjugates

A) Ion exchange chromatogram produced from the purification of Fab'-PEG-DSPE conjugates over an SX Hitrap column with absorbance at 214nm detected by an AKTA FPLC. The diagonal line indicates the start of a salt gradient used to elute the compounds from the column. B) Fraction analysis by SDS-PAGE stained with coomassie blue.

2.4 Discussion

Surface coupling, the classic method of introducing a targeting ligand into an LN, does not allow for characterization of the conjugated product before it is introduced into the LN formulation. This is because the maleimide-functionalized lipid is incorporated into the LN before the targeting ligand is subsequently conjugated to the LN surface (see Figure 2.5A).

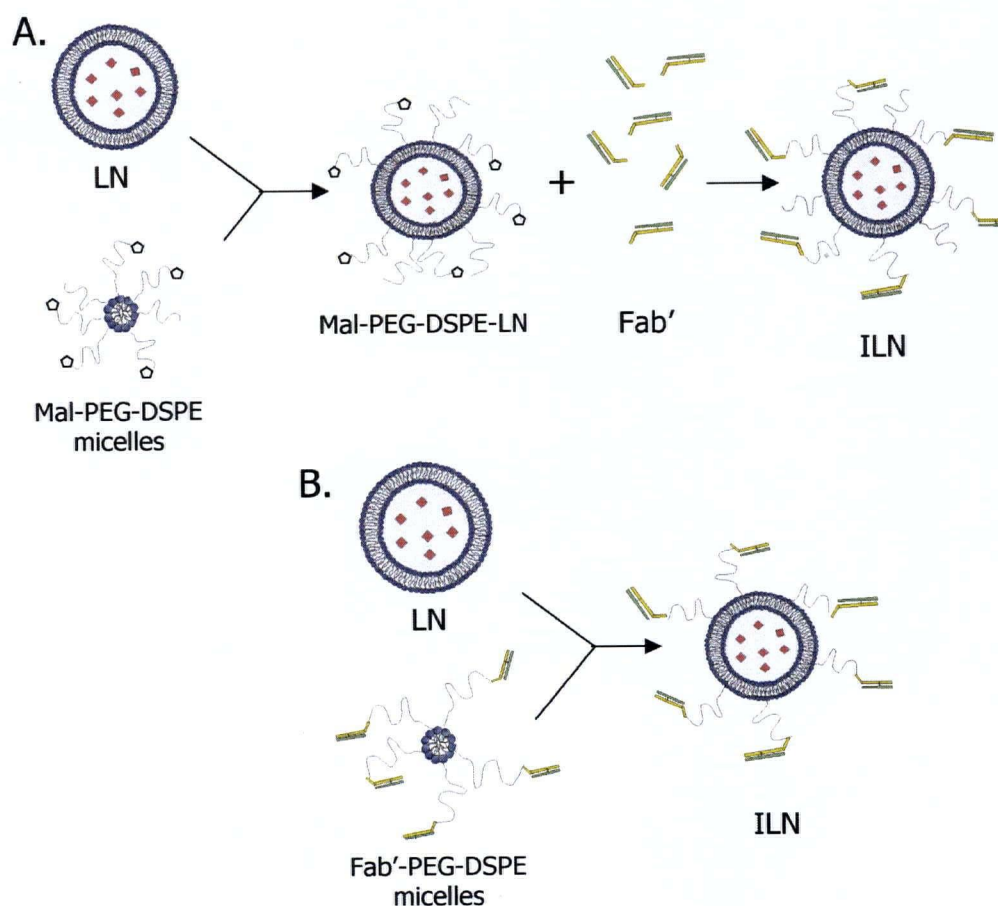


Figure 2.5 Two methods of incorporating targeting ligands for ILN manufacture

A) Surface coupling of antibody (or antibody fragments) to Mal-PEG-DSPE within the LN. The conjugate is formed at the surface of an LN. B) The post-insertion method (Ishida et al., 1999) where the conjugate is formed as a micelle and subsequently incorporated into the LN by co-incubation with pre-formed vesicles.

The post-insertion method, first introduced in 1999 (Ishida et al., 1999), provides the opportunity to analyze the conjugation product. In this method, the targeting ligand is first coupled to the functionalized lipid before it is transferred into an LN (see Figure 2.5B) and has many advantages as indicated in the Introduction.

The observation that there is more than one site for conjugation on the Fab' molecule is not surprising, since other cysteine residues within the variable region of the Fab' fragment are known to exist. This illustrates the inherent difficulty in obtaining a well-defined ILN. This may potentially be overcome by the use of engineered antibody fragments that contain just one cysteine for conjugation. With this type of ligand, Nellis and colleagues have shown that performing the reaction at a relatively low pH (5.7) and limiting the time of the reaction helps to control non-specific conjugation to sites other than the engineered cysteine (Nellis et al., 2005a; Nellis et al., 2005b). In our experience the experimental variables could not be manipulated to control non-specific conjugation to Fab' fragments, indicating the absolute need for a molecule that has a specific site for conjugation. The difficulty encountered here in using ion exchange chromatography to resolve the Fab'-PEG-DSPE conjugates has also been encountered by Nellis and colleagues who found that by using a similar purification strategy, organic solvents, such as 28% aqueous isopropanol, could enable sufficient retention of scFv-PEG₂₀₀₀-DSPE conjugates to an ion exchange chromatography column, which was not possible with aqueous eluting buffers.

The poor conjugation yield and lack of a well-defined product reduce the attractiveness of the Fab'-PEG-DSPE targeting ligand. As an alternate approach to the maleimide functionality, some researchers prefer to use an amine reactive PEG-lipid which

may prove useful given that the resulting urethane bond is of high yield and chemical stability (Torchilin et al., 2001). However, the problem of non-specific conjugation sites remains.

Other functionalities such as a hydrazine-functionalized PEG-DSPEs that are specific for carbohydrates on the Fc terminus of the antibody have been employed for conjugation as an alternative to maleimide-PEG-lipids. Koning and colleagues found that when an antibody was surface coupled to LNs via the hydrazine-PEG-lipid the resulting ILNs promote faster clearance than ILNs with the antibody randomly oriented on the surface by maleimide coupling (Koning et al., 2001). Thus, the true *in vivo* effect of rational ILN design is difficult to predict.

In conclusion, the lack of chemoselectivity (*i.e.* having a defined reaction site) and the very poor overall yield presents difficulties for using proteins such as Fab' fragments to target clinically useful ILNs. A chemoselective ligand that has one site available for conjugation, such as the scFv or small synthetic ligands, seems essential, as does a reasonably efficient method of coupling the targeting ligand to a lipid anchor. For the purpose of this thesis, these findings have led to the abandonment of approaches relying on proteins as targeting ligands.

3 RGD-ligand Synthesis and Binding to the Isolated $\alpha_v\beta_3$ Integrin¹

3.1 Introduction

3.1.1 Targeting Angiogenesis

Angiogenesis refers to the growth of new vasculature from pre-existing blood vessels. Events such as tissue growth, repair and disease (e.g., tumor pathogenesis) produce cytokines and other factors that disrupt the relatively quiescent state of vascular endothelial cells (EC) and cause them to transition to the angiogenic growth state (Boudreau et al., 1997). During this transition, the cell alters the array of integrins that are expressed on the cell surface (Stupack and Cheresch, 2002). During angiogenesis, the integrins function to sense changes in the extra cellular matrix (ECM) as the basal ECM is modified to form what is known as the provisional ECM. The proteins in the provisional ECM are ligands for the integrins that become expressed during angiogenesis (Brooks, 1996).

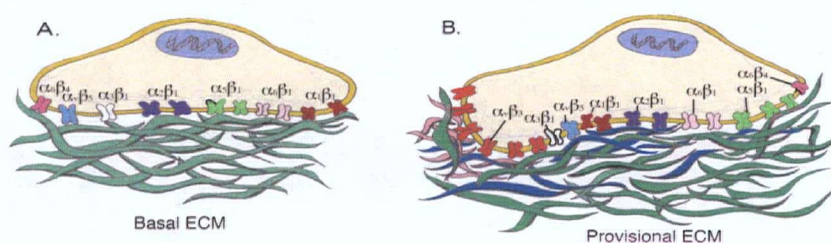


Figure 3.1 The angiogenic transition

A) Quiescent endothelial cells are supported by a basal ECM B) Angiogenic endothelial cells express different integrins that have ligands in the “provisional” ECM. The relative amounts of these integrins change between the different growth states.

¹ A version of the chapter has been submitted for publication

The $\alpha_v\beta_3$ integrins are one of the most interesting of the angiogenic integrins since they are not expressed on quiescent endothelial cells (Brooks et al., 1994a). Furthermore, unlike other EC integrins, the $\alpha_v\beta_3$ integrins do not bind to ligands in the basal ECM (Xu et al., 2001). The contact between ECs and proteins of the provisional ECM functions to mediate EC growth, migration and survival during angiogenesis (Brooks, 1996).

Some of the proteins in the basal ECM contain ligands for the angiogenic integrins that become accessible upon proteolytic cleavage. A well-known example of a proteolytic modulator of the ECM is matrix metalloproteinase 2, which is known to be essential for angiogenic growth and migration of ECs in the case of tumor pathology (Giannelli et al., 1997).

Two main pathways are known to stimulate angiogenesis, both of which are activated by different growth factors. Vascular endothelial growth factor (VEGF) activates one pathway and basic fibroblast growth factor (bFGF) activates the other pathway, which specifically promotes the expression of $\alpha_v\beta_3$ (Friedlander et al., 1995). bFGF is the most powerful mitogen used to stimulate blood vessel growth and has considerable utility in angiogenesis models (Doi et al., 2007; Presta et al., 2005). Cancer, tissue regeneration, and ocular degeneration are some of the compelling reasons why researchers have interest in modulating bFGF/ $\alpha_v\beta_3$ signaling, potentially enabling control over neovascularization. Thus, the interaction of the $\alpha_v\beta_3$ integrin with its natural ligands is an area of considerable research interest.

During angiogenesis, ECs also secrete $\alpha_v\beta_3$ ligands known as matricellular proteins as part of the provisional ECM (Murphy-Ullrich, 2001). The matricellular proteins function to tune the EC response in a rapidly changing environment. Immobilized ligands,

such as those that are anchored into the ECM, promote adhesion whereas soluble or mobilized ligands can antagonize the $\alpha_v\beta_3$ integrins and promote apoptosis (Brassard et al., 1999). This level of control is thought to attenuate the pro-angiogenic momentum once the desired vessel growth has occurred. Secreted matricellular proteins are of particular interest in anti-cancer strategies due to their ability to promote apoptosis of ECs (Murphy-Ullrich, 2001).

Many $\alpha_v\beta_3$ ligands within the provisional ECM interact with the integrin via an RGD sequence, which is usually present on a flexible loop of the protein (see Ruoslahti, 2003 for a personal account of this finding). RGD-containing peptides that mimic the region of the ligand that interacts with the integrin can promote apoptosis by $\alpha_v\beta_3$ antagonism (Buckley et al., 1999). This finding has fueled the pursuit of the RGD sequence as an anti-angiogenesis agent.

Research from Kessler's group has led to the anti-angiogenesis compound, cRGDf-N(Me)V, pursued now with the trade name Cilengitide®. This compound is a promising anti-angiogenesis agent with potency indicated by a low IC_{50} value (0.58 nM) (Dechantsreiter et al., 1999). Moreover, anti-cancer activity in humans has been observed and attributed to $\alpha_v\beta_3$ antagonism of cells that constitute the tumor-associated vasculature (Nabors et al., 2007; Tucker, 2006).

Despite extensive efforts devoted to finding integrin antagonists and the existence of high resolution structural data of the integrin, our understanding of the mechanisms that govern the switch from an inactive to high-affinity active state for integrins is far from complete (Puklin-Faucher et al., 2006).

3.1.2 The CE-FA Method for Measuring Binding to the $\alpha_v\beta_3$ Integrins

Integrins are integral membrane proteins with binding sites on both sides of the membrane that participate actively in the formation of focal adhesion plaques (Petit and Thiery, 2000) and have a high range of intermolecular motion (Xiong et al., 2002). The equilibrium parameters characterizing RGD binding to these receptors remains poorly understood. In this chapter, an equilibrium assay to study the affinity of RGD-containing peptides for the $\alpha_v\beta_3$ integrins is developed.

The development of an equilibrium assay to study such a complex biological system requires a substantial effort. For example, well-characterized, high-purity ligands are essential to distinguish between non-specific effects of contaminating species. Likewise, efforts must be made to conserve the native conformation of the receptor so that the binding process reflects the *in vivo* situation.

A variety of methods have been developed to characterize molecular interactions (Connors, 1987; Harding, 2001). Techniques applied to protein-ligand binding studies in the pharmaceutical and biomedical sciences include equilibrium dialysis, ultrafiltration, ultracentrifugation, gel filtration, calorimetry, microdialysis, spectroscopy, high performance liquid chromatography (HPLC), surface plasmon resonance (SPR), and capillary electrophoresis (CE) (Bertucci and Domenici, 2002; Oravcova et al., 1996; Seville et al., 1990). Due to the relatively short analysis time, low sample consumption ease of automation and high separation efficiency, CE has become a powerful technique for the characterization of protein-ligand interaction.

Reproducible estimates of binding parameters for membrane proteins can be obtained with SPR techniques using an instrument such as Biacore®. One drawback to

SPR methods is that chemical modification of either protein or ligand is required for immobilization to a solid surface. The tethering reaction, usually achieved by amide or thiol conjugation, is non-chemoselective and the tethered species can exist as a number of different conformers. In an effort to obtain further insight into the binding of RGD-peptides to the integrin, we used solubilized $\alpha_v\beta_3$ integrin and measured RGD binding using CE-FA. The following work presents a truly diffusion-controlled process for measuring the equilibrium binding of a therapeutically relevant membrane protein, $\alpha_v\beta_3$ integrin, with a fluorescently labeled ligand, cyclic arginine-glycine-aspartic-acid-d-phenylalanine-lysine (cRGDfK-488) or the control peptide, cyclic arginine-alanine-aspartic-acid-d-phenylalanine-lysine (cRADfK-488). The RAD-containing peptide was chosen as a control, given that substitution of alanine for glycine has been shown to abolish the activity of RGD-peptides towards the $\alpha_v\beta_3$ integrin (Pfaff et al., 1994).

Currently, several CE methods are available to study the equilibrium and kinetic binding properties (Busch et al., 1997c; Galbusera and Chen, 2003; Heegaard et al., 2002; Petrov et al., 2005; Rundlett and Armstrong, 1997; Rundlett and Armstrong, 2001b). These include normal affinity CE (ACE), Hummel-Dreyer method (HD), vacancy affinity CE (VACE), vacancy peak method (VP) and frontal analysis (CE-FA) (Busch et al., 1997a; Busch et al., 1997b; Kraak et al., 1992). The most suitable method can be chosen based on the characteristics of the binding interaction, namely, the speed of the association/dissociation processes, the mobilities of the free species and the complex, each species' ability to absorb UV light or emit laser induced fluorescence, and the availability of the interacting species. In ACE and VACE methods, measurable differences in electrophoretic mobilities between free ligand and the complex are required, and the

measurements are based on the changes in electrophoretic mobility of free protein or ligand due to complex formation (Busch et al., 1997b; Busch et al., 1997c; Rundlett and Armstrong, 2001a; Tanaka and Terabe, 2002). In HD and VP methods, the mobilities of free protein and the complex have to be similar, and the measurements are mainly based on the changes of the free ligand concentration.

The method chosen for use in this study is CE-FA. In CE-FA, a relatively large amount (~ 100 nl) of pre-equilibrated mixture of protein and ligand is injected into the capillary filled with background electrolyte (BGE). The injection of a large volume of sample plug leads to the appearance of plateaus in the observed electropherogram. Partial separation of the binding species can be achieved based on the differences in their mobilities. The compound with a unique mobility in the capillary is separated from the mixture plateau to form another plateau. In the study of protein and ligand interaction, the mobility of the free ligand is usually different from the protein and the protein-ligand complex. The height of the plateau is directly related to the concentration of corresponding species therefore, the binding parameters can be determined by comparing the heights of the plateaus. A schematic of the CE-FA method has been provided in Figure 3.2.

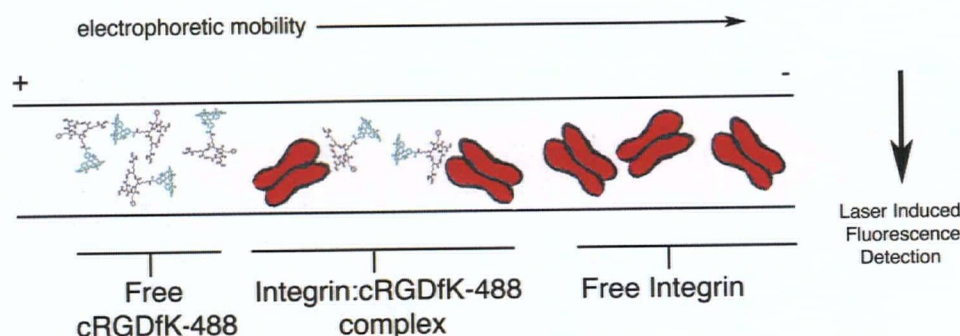


Figure 3.2 Schematic of the Capillary Electrophoresis Frontal Analysis Method

An equilibrated mixture of free cRGDfK-488, cRGDfK-488 bound to $\alpha_v\beta_3$ integrin in a complex and free $\alpha_v\beta_3$ integrin are injected into a capillary containing 20 mM Tris-HCl, pH 7.5, 2 mM $MgCl_2$ and 0.2% Triton X-100. The three components are resolved by differences in their electrophoretic mobility. The amount of the free cRGDfK-488 or the control peptide, cRADfK-488, in complex with the $\alpha_v\beta_3$ integrin is detected by fluorescence.

CE may also provide a unique advantage for the study of membrane proteins, which are inherently difficult to solubilize without disturbing the proteins tertiary structure. It is important for the field of drug discovery that these handling problems are overcome, since the most accessible targets for intravenous drug delivery reside at the surface of a cell.

Different data analysis methods have been utilized for the estimation of binding parameters in CE (Tanaka and Terabe, 2002). With the papers published to date, a complex equilibrium model based on Scatchard analysis has been the most commonly used in CE-FA (Ostergaard and Heegaard, 2003). According to the assumptions used in this approach, binding parameters in cases where the binding stoichiometry is 1:1, and where non-cooperative binding occurs on multiple identical binding sites, can be obtained. However, there are many other cases relevant to biomolecules that do not fit the interaction model described (Bowser and Chen, 1998).

From this application of the CE-FA method, new information about the binding of RGD-containing ligands to the $\alpha_v\beta_3$ integrin is provided. This behavior was characterized by a set of refined equations for determining the parameters of higher order binding. The full details of these equations are shown in Appendix 1 of this thesis.

3.2 Methods

3.2.1 Materials

Unless specified, all reagents were obtained from Aldrich (Milwaukee, WI). Peptides were synthesized using 9-fluorenylmethyloxycarbonyl (Fmoc) protected amino acids and resins obtained from EMD Biosciences (San Diego, CA) and dimethylformamide (DMF) as the main solvent. All solvents, of reagent grade or higher, were from Fisher Scientific (Nepean, ON, Canada).

Reversed phase-high pressure liquid chromatography (RP-HPLC) was performed using gradients of aqueous acetonitrile (aqACN) containing 0.1% trifluoroacetic acid (TFA) on C18 columns purchased from Grace Vydac (Hesperia, CA). Analytical gradients were applied using column no. 218TP5415, (dimensions: 150 mm × 4.6 mm) with a flow rate of 1 ml per min. All peptides were purified on a semi-preparative column: 218TP510 (250mm × 10mm) with a flow rate of 3 ml per min.

3.2.2 Peptide Synthesis, Cyclization and Labeling

The linear sequences: D(t-Bu)fK(Z)R(Pbf)G (The RGD-containing peptide) or D(t-Bu)fK(Z)R(Pbf)A (An RAD-containing peptide) were synthesized by Fmoc based solid phase peptide synthesis. Briefly, peptides were assembled on 0.5 mmoles of 2-chlorotrityl resin using 1.3 molar equivalents (to carboxylic acid) of the following activating agents: O-benzotriazole-N,N,N',N'-tetramethyl-uronium-hexafluoro-phosphate (HBTU) (Advanced Chemtech, Louisville, KY) and N-hydroxybenzotriazole (HOBT) (Advanced Chemtech,

Louisville, KY). Peptides were activated *in situ* with triethylamine (TEA) then coupled to the resin for at least one hour. Fmoc removal steps were performed upon each amino acid addition by soaking the resin in a solution of 20% piperidine in DMF for five min, and repeated once. Between each step, the resin was washed with a constant flow of DMF for at least one min. Linear peptides were cleaved in 0.1% TFA in dichloromethane (DCM) with 2.5% triisopropyl silane (TIS) and H₂O (v/v). The crude peptide was analyzed by RP- HPLC with a linear gradient of 30-90% aqACN over 30 min, (retention time = 16.3 min) and by electrospray mass spectrometry (ESI-MS).

Lyophilized linear peptides were cyclized at 0.5 mM in DMF using benzotriazol-1-yl-oxytripyrrolidinophosphonium hexafluorophosphate (PyBop) and HOBT to produce cR(Pbf)GD(t-Bu)fK(Z) or cR(Pbf)AD(t-Bu)fK(Z). Cyclization yields were typically over 95% and occurred within 30 min, as indicated by RP-HPLC, with a retention time of 19.5 min on the same gradient as the linear peptide and a difference of 18 in the observed MW by ESI-MS. ¹H NMR NOE assignments for all α -amide bonds confirmed a head-to-tail cyclic compound.

The lysine side chain was deprotected by hydrogenation with palladium over a carbon catalyst. The resulting compound (cR(Pbf)GD(t-Bu)fK or cR(Pbf)AD(t-Bu)fK) eluted at 11 min on the same RP-HPLC gradient as the fully protected peptide.

Conjugation of the cyclized RGD peptide to the Alexa Fluor-488 pentafluorophenol ester (Invitrogen, Carlsbad, ON) was performed in DMF, with the pH adjusted to 7.2 with TEA. The products were purified by RP-HPLC with a gradient of 10-85% aqACN over 60 min. The desired compound eluted after 21 min for the Alexa Fluor-488 labeled peptides.

Deprotection of the arginine and aspartic acid side chains was performed using a solution of 95% aqueous TFA and the reaction was subsequently purified by RP-HPLC with a gradient between 0-65% aqACN. Both cRADfK-488 and cRGDfK-488 eluted at 19.5 min. The non-labeled peptide, cRGDfK (employed in Chapter 5), was precipitated into ice-cold diethyl ether, rinsed once, hydrated with distilled water and lyophilized.

All peptides exhibited >95% purity, as determined by capillary electrophoresis (CE). Product identification was validated by ESI-MS as follows: cRGDfK-488 (observed MW 1120.6; calculated MW 1120.1); cRADfK-488 (observed MW 1134.2, calculated MW 1134.3); cRGDfK (observed MW 604.4, calculated MW 603.7).

Peptides were lyophilized, weighed, and a standard curve for peptide quantification was established using the absorbance peak areas from chromatograms collected at 214 nm for peaks eluting between 12 and 13 min on a 0-65% AqACN analytical gradient over 30 min for the Alexa Fluor-488 labeled peptides, 18 min for the TAMRA-labeled peptide and 8 min for the unlabelled peptide. Typically, a 0.5 mM scale synthesis would yield 450 mg of the dry linear peptide. The final yield of the unlabelled peptide was 20 dry mg (overall yield=11%) and the fluorescently labeled peptides was 8 mg (yield= 2%).

3.2.3 Capillary Electrophoresis (CE) Analysis

CE experiments were carried out on a Beckman Coulter ProteomeLab PA800 (Beckman Coulter Inc., Fullerton, CA) instrument with a laser-induced fluorescence (LIF) detector (488 nm excitation and 520 nm emission). Uncoated fused-silica capillaries were used for analysis (70 cm total length, 60 cm length to detector, 50 μm inner diameter, 360 μm outer diameter, for CE-FA: 50 cm total length, 40 cm length to detector, 50 μm inner diameter, 360 μm outer diameter) (Polymicro Technologies, Phoenix, AZ). Prior to use, the capillary was rinsed with 1 M NaOH (30 min), MeOH (30 min), purified water (30 min), and finally the background electrolyte (30 min), and was conditioned overnight. At the beginning of each day, the capillary was rinsed with 1 M NaOH (10 min), followed by MeOH (10 min) and then with water (10 min). A voltage of +10 kV was then applied across the capillary and the fluorescence signals were recorded. The peptide was injected into a capillary filled with the background electrolyte (BGE) under a pressure of 1 psi for 5 s for the analytical runs or 0.5 psi for 30 to 99 s for the frontal analysis experiment and then a voltage of +10 kV was applied when both inlet and outlet vials contained the BGE. The BGE for peptide analysis was phosphate buffered saline (PBS) and for frontal analysis, the BGE was an aqueous solution of 20 mM Tris-HCl, pH 7.5, 150 mM NaCl, 2 mM MgCl_2 , and 0.2% Triton X-100.

3.2.4 Capillary Electrophoresis Frontal Analysis Method

Purified human integrin $\alpha_v\beta_3$ in 20 mM Tris-HCl, 150 mM NaCl, 2 mM MgCl_2 , and 0.2% Triton X-100, pH 7.5, was purchased from Chemicon International (Temecula, CA), catalog #CC1019. The initial concentration was 210 $\mu\text{g/ml}$, and for each experiment, 10 μl was employed.

Purified peptides were re-dissolved in the aforementioned buffer at 36.03 mM, and then diluted to produce saturation isotherms using concentrations between 0-25 μM .

The free ligand concentration ($[L]_{\text{free}}$) was calculated by the peak height on an electrophoregram produced from a sample containing the peptide alone. The amount of binding ($[L]_{\text{bound}}$) was determined by subtracting the amount of the free ligand that remained after reaching equilibrium with the receptor ($[P]_{\text{total}}$). The stoichiometry constant, n , was further determined by the relationship between the amount of the bound ligand and total receptor concentration ($[L]_{\text{bound}} / [P]_{\text{total}}$).

3.3 Results and Discussion

3.3.1 Peptide Synthesis, Labeling and Analysis

The cyclic peptide containing arginine, glycine, aspartic acid, d-phenylalanine, lysine (cRGDfK) was synthesized as indicated in Methods, and was fluorescently labeled to produce cRGDfK-488 (see Figure 3.3). The negative control, cRADfK-488 was similarly synthesized using this scheme.

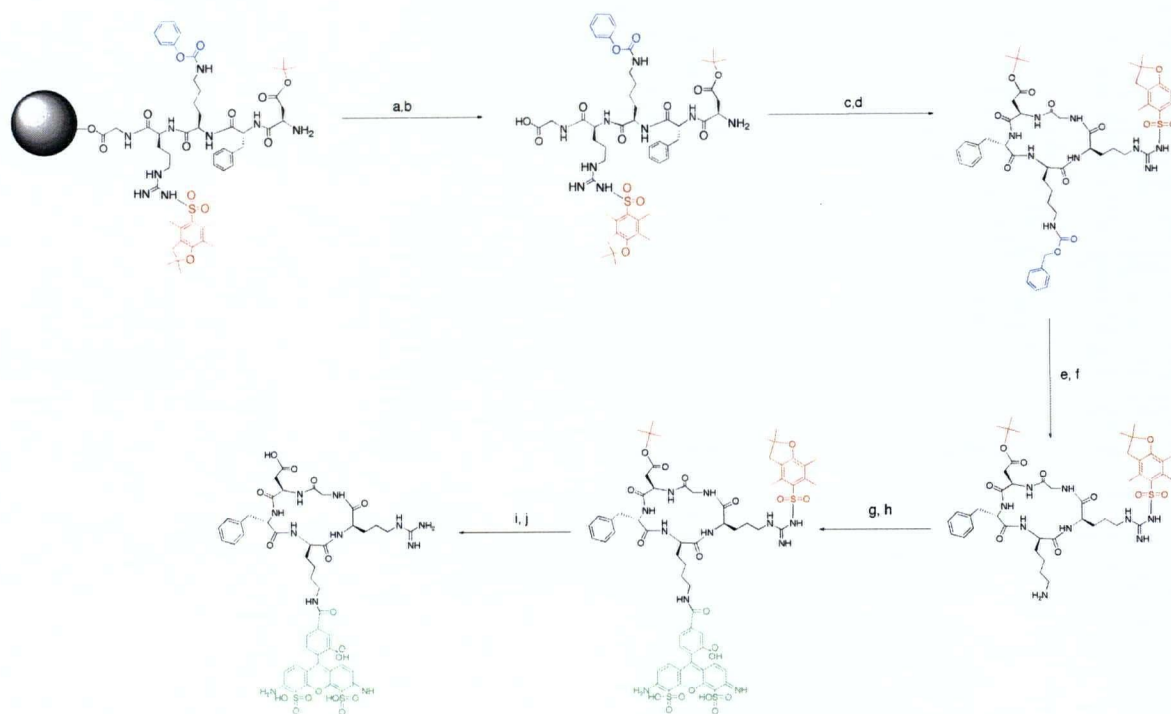


Figure 3.3 Synthesis of fluorescently labeled cRGDfK peptides

Solid phase peptide synthesis (SPPS) generated a linear peptide with protected lysine, aspartic acid and arginine side chains. Selective deprotection of the lysine side chain enabled site-specific conjugation to Alexa Fluor 488™ (in green). a) SPPS b) cleavage c) cyclization d) RP-HPLC e) selective deprotection f) RP-HPLC g) fluorophore conjugation h) RP-HPLC i) Removal of protecting groups j) RP-HPLC

3.3.2 cRGDfK-488 Peptide Purity

Particular attention was paid to achieving the maximum purity of labeled peptides. The water-soluble compound, cRGDfK-488 was inherently difficult to separate from the unreacted fluorophore and additional purification steps were required to ensure good purity values before biological evaluation. Purity could not be assessed using RP-HPLC or TLC, since the fluorophore tends to co-elute with the peptide-conjugated fluorophore.

In order to address this problem, CE proved to be a convenient method for analyzing the purity of the peptide-conjugated fluorochrome. The cRGDfK-488 conjugate was characterized by its electrophoretic mobility, which is determined by the charge to size ratio of the molecule. An electropherogram made by LIF detection best demonstrates the final purity of the cRGDfK-488 conjugate, since the unconjugated fluorophore is the principal contaminating species. An example of the high purity obtained for the fluorescently labeled peptides is shown in Figure 3.4. It should be noted that an equivalent, but less intense, electropherogram is obtained by UV detection at 214nm.

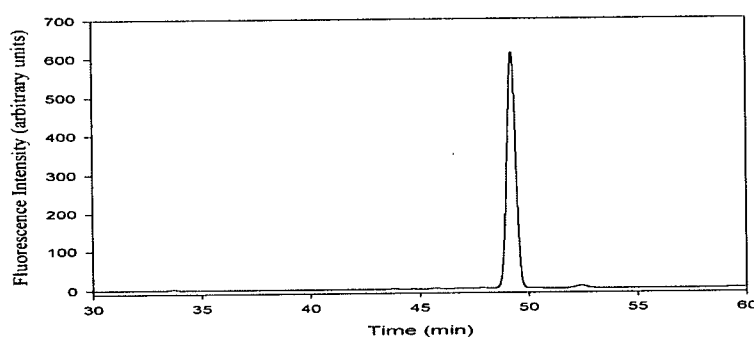


Figure 3.4 Electropherogram demonstrating the purity of cRGDfK-488

The above electropherogram shows the high level of purity (*i.e.* >98%) that was obtained for the peptide ligands employed in this thesis. This level of purity was made possible by additional HPLC purification steps, which were found to be necessary in order to resolve the unconjugated fluorophore.

3.3.3 Binding to Isolated $\alpha_v\beta_3$ Integrin as Measured by the CE-FA Method

Particular attention was given to the design of a binding assay to measure the affinity of the RGD-ligands for the $\alpha_v\beta_3$ integrin. The assay should be non-perturbing to the overall protein structure and require relatively small amounts of the $\alpha_v\beta_3$ integrin, which is available in limited quantities.

Use of the CE-FA method was first validated by a linear relationship that could be obtained for fluorescence signals and peptide concentrations ($r^2 > 0.999$). This calibration curve was used to determine peptide concentrations from fluorescence signals.

A typical sample data point from the CE-FA signal and the resulting electrophoregrams generated from CE-FA experiments is shown in Figure 3.5. It can be observed that as the amount of complex formed in the pre-equilibrated sample, the concentration of free peptide, $[L]_f$, decreases, and the height of the free peptide plateau also decreases compared to the plateau obtained for the sample containing peptide only (dashed curve). The electrophoregrams shown with lower and broader plateaus (solid curve) in the Figure were obtained from the separation of the pre-equilibrated mixture of $\alpha_v\beta_3$ integrin and cRGDfK-488. The CE-FA curve containing a broader plateau have similar plateaus on the right side, generated by the free peptide that is uncomplexed to the $\alpha_v\beta_3$ integrin after equilibrium is reached. The obtained electrophoregram also shows that the complex migrates at nearly the same velocity as the free (unbound) $\alpha_v\beta_3$, but faster than the free peptide.

The amount of cRGDfK-488 or cRADfK-488 that was bound to the receptor ($[L]_{\text{bound}}$) was calculated from these electrophoregrams as detailed in Methods. The $[L]_{\text{bound}}$

per total integrin ($[P]_{\text{total}}$) was then used to generate the binding isotherms presented in Figure 3.6.

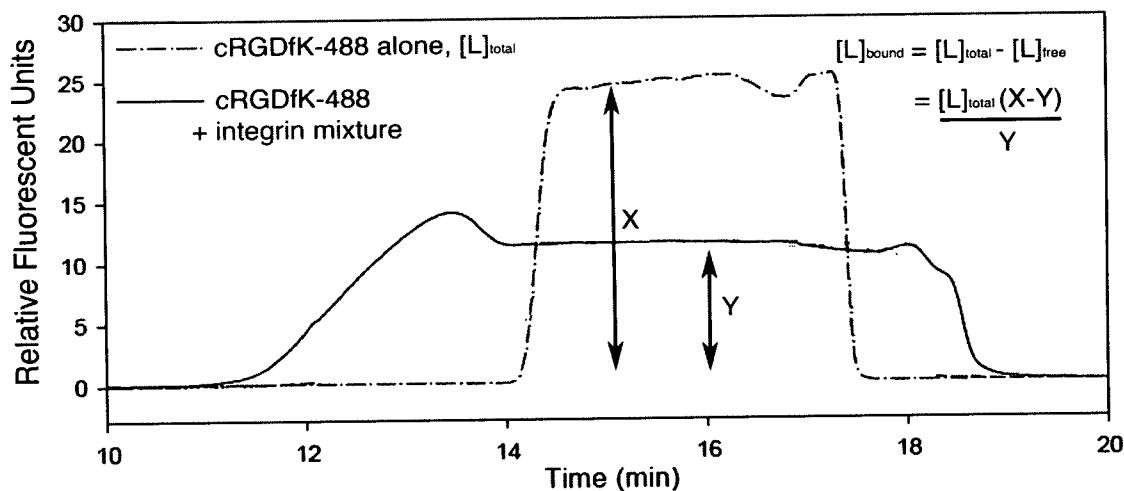


Figure 3.5 Electrophoregrams produced for CE-FA experiments

The above electrophoregram was produced from injection of the pre-equilibrated mixture of $\alpha_v\beta_3$ integrin ($0.295 \mu\text{M}$) and peptide ($2.40 \mu\text{M}$). The difference in the height of the plateau corresponding to free cRGDfK-488 was used to calculate the amount of the peptide that was bound to the $\alpha_v\beta_3$ integrin, and subsequently the equilibrium parameters

The binding isotherms of cRGDfK-488 to the integrin $\alpha_v\beta_3$, and the non-specific binding of cRADfK-488 are shown in Figure 3.6A. Using the specific binding of cRGDfK-488 (total binding minus non-specific, Figure 3.6B), a detailed analysis involving multi-site equilibrium binding revealed the presence of two binding sites for cRGDfK-488 on the integrin having affinities $K_{d1} = 3.18 \times 10^{-6} \text{ M}$ and $K_{d2} = 2.84 \times 10^{-7} \text{ M}$. Full details of this calculation, which was performed by Dr. David Chen and Ms. Ying Sun, may be found in the Appendix.

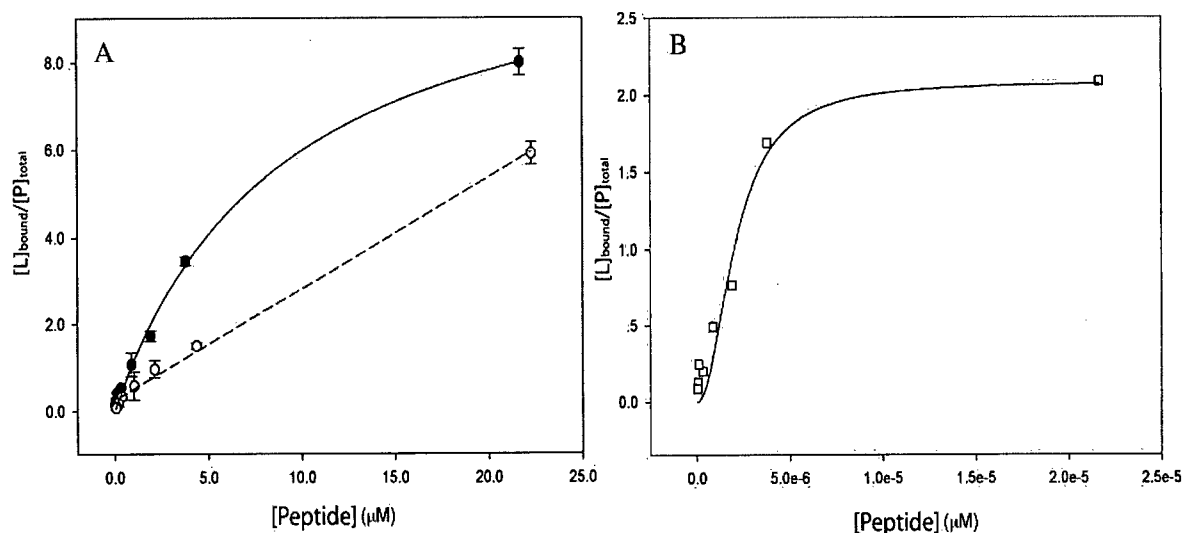


Figure 3.6 cRGDfK-488: $\alpha_v\beta_3$ integrin binding isotherms generated from the CE-FA method

A. Closed circles represent total binding of cRGDfK-488. Open circles represent the non-specific binding of cRADfK-488 to the same amount of $\alpha_v\beta_3$ integrin. B. Specific binding of cRGDfK-488 obtained by subtracting non-specific from total binding. The curve represents a best-fit assuming two binding sites for the cRGDfK-488 on the integrin.

The CE-FA analysis of binding to peptides the isolated $\alpha_v\beta_3$ integrin resulted in three findings. First, the contribution of non-specific binding by cRADfK-488 was similar to that seen for cellular $\alpha_v\beta_3$ (see Chapter 4) indicating that non-specific effects due to partitioning in the lipid bilayer are minimized for the cRGDfK-488 ligand. Second, it was found that a two-site binding model gave the best fit to the data, where the value of K_{d1} is slightly greater than K_{d2} , suggesting that the second binding process is somewhat cooperative to the first binding. The two sites on the $\alpha_v\beta_3$ molecules are saturated gradually as ligand concentration in the sample mixture increases in free solution. It appears that a step-by-step, two-site binding process better describes the experimental data for the interaction of $\alpha_v\beta_3$ integrin and cRGDfK-488.

The third finding revealed by CE-FA is that the binding of cRGDfK-488 to the $\alpha_v\beta_3$ integrin isolate occurs with a 1:2 integrin:RGD stoichiometry. This could be consistent with the proposal by Bednar and colleagues who proposed a two-step binding mechanism for RGD-peptidomimetics with the integrin that is present on activated platelets, GPIIb/IIIa (Bednar et al., 1997). Further, if the stoichiometry of RGD binding is of higher order, it may help to explain why multivalent RGD targeted imaging agents are more effective for binding to their cell target than their monovalent equivalents (Li et al., 2007b; Montet et al., 2006).

This work demonstrates a new approach to deduce important binding characteristics of biomolecules employing one of the simplest CE methods, CE-FA. To understand the binding of membrane proteins with complex biological behavior, non-perturbing analytical methods such as CE-FA may prove to be increasingly useful.

4 Cellular Binding and Endocytosis of RGD-Containing Targeting Ligands²

4.1 Introduction

The $\alpha_v\beta_3$ integrins have become important targets in the development of new anticancer strategies as they are expressed at high levels on the surface of many cancer cells such as gliomas (Gladson and Cheresch, 1991), melanomas (Albelda et al., 1990), ovarian carcinomas (Liapis et al., 1997) as well as tumor-associated endothelial cells (Brooks et al., 1994b). In addition, the $\alpha_v\beta_3$ integrins are involved in angiogenesis (Brooks et al., 1994b), metastasis (Hieken et al., 1996) and resistance to radiotherapy (Albert et al., 2006; R. A. Smith and Giorgio, 2004). The $\alpha_v\beta_3$ integrins on tumor-associated endothelial cells are considered to be particularly important targets given that all tumors require a blood supply for survival (Folkman, 1990).

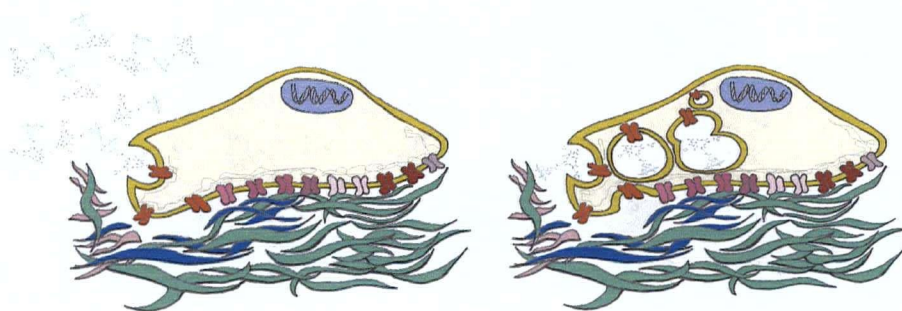


Figure 4.1 Binding and Endocytosis of cRGDfK-488 via the $\alpha_v\beta_3$ integrin

The findings in this Chapter suggest that the enhanced endocytosis of cRGDfK-488 is attributable to the presence of cellular $\alpha_v\beta_3$. Binding plus endocytosis is distinguished from binding alone by incubating the ligand and cells at endocytosis permissive (37°C) or non-permissive temperatures (4°C).

² A version of this chapter has been submitted for publication

The wide variety of natural ligands for the $\alpha_v\beta_3$ integrins (e.g., vitronectin, fibronectin, osteopontin, denatured/proteolysed collagen and the foot and mouth disease virus) bind to the integrin by a conserved RGD tripeptide motif that is usually located on a flexible loop in the protein (Ruoslahti and Pierschbacher, 1987). RGD-containing peptides antagonize the $\alpha_v\beta_3$ integrin have anti-angiogenic activity both *in vitro* (Brassard et al., 1999) and *in vivo* (Storgard et al., 1999), and are thought to mimic structural features at the binding site of the natural integrin ligands.

Furthermore, improved drug delivery has been achieved when the targeting ligand is displayed in a multivalent form, a strategy also used by viruses and antibodies. When radionuclides are conjugated with dimeric (Chen et al., 2005) or (even better) tetrameric (Wu et al., 2005) RGD-containing peptides, localization to the site of a tumor is greatly enhanced. However, because of the complexity of their biology, the response of integrins to even monomeric RGD ligands remains poorly understood (Puklin-Faucher et al., 2006). This applies particularly to basic aspects such as endocytosis following the binding of RGD ligands to integrins, where some reports suggest that binding does not lead to endocytosis (Castel et al., 2001), whereas other reports assume that binding is accompanied by endocytosis (Balasubramanian and Kuppuswamy, 2003).

In the following sections, the ability of the fluorescently labeled peptides described in Chapter 3 to bind to integrins on human umbilical vascular endothelial cells (HUVEC) and subsequently undergo endocytosis has been characterized and compared to the binding and uptake properties of a fluorescently labeled monoclonal antibody, LM609X. It is shown that the RGD ligand exhibited considerably greater uptake following incubation at endocytosis permitting temperatures (37°C) as compared to an endocytosis inhibiting

temperature (4°C). A 7.4-fold increase in uptake of the RGD peptide was observed following a one hour incubation with HUVEC at 37°C, as compared to 4°C. In contrast, only a 1.9 fold increase in cell-associated fluorescence was observed on incubation with LM609X at 37°C as compared to 4°C. Fluorescence microscopy studies provided further evidence supporting rapid endocytosis of the RGD peptide at 37°C as compared to LM609X. These results are discussed with regard to previous work indicating that RGD ligands enter cells by integrin-independent pathways. In addition, it is suggested that this ability of RGD ligands to stimulate endocytosis may be of considerable utility for achieving enhanced intracellular delivery of ligand-associated drugs in anti-angiogenic applications.

4.2 Methods

4.2.1 Materials

Unless otherwise specified, all reagents were obtained from Aldrich (Milwaukee, WI). Peptides were synthesized and characterized as described in Section 3.2. All solvents were obtained from Fisher Scientific (Nepean, ON, Canada) and were of reagent grade or higher.

4.2.2 Cell Culture

HUVEC seed cells, media and supplements were obtained from Cascade Biologics (Portland, OR). M21 and M21L melanoma cell lines (with and without $\alpha_v\beta_3$ expression, respectively were obtained from Dr. D. Cheresh) and were maintained in a 5% CO₂ atmosphere Dubelco's Modified Eagle's Medium supplemented with 10% fetal bovine serum (FBS). Cells were grown to approximately 1.0×10^6 cells per 75 cm² tissue culture flask for HUVEC and 1.8×10^6 cells/flask for melanoma cell lines. At the time of harvest, media was removed and cells were rinsed twice with 10 ml phosphate buffered saline (PBS) with Ca²⁺ and Mg²⁺ (GIBCO product no. 14040). Adhered cells (HUVEC and M21) were harvested manually with a cell scraper to preserve the integrity of the integrins. Once unadhered, cell suspensions were washed, then centrifuged at 1100 rpm for 5 min and resuspended in 5% FBS in PBS (herein referred to as PBS/FBS) to a final volume that yielded 500,000 cells/ml.

4.2.3 Cell Binding

Harvested cells were aliquoted in 200 μ l volumes containing approximately 100,000 cells. Alexa Fluor-labeled peptides or antibodies, dissolved in PBS/FBS before addition to cells. The ligands were then added to cells and the final volume was adjusted to 500 μ l with PBS/FBS. Unbound ligands were removed by rinsing with 5 ml of FACS rinsing buffer (130 mM NaCl, 3 mM KCl, 10.4 mM Na₂PO₄, 1.7 mM KH₂PO₄ pH 7.4) followed by centrifugation at 1100 rpm for 5 min and repeated twice. Unfixed cells were kept on ice and immediately analyzed by flow cytometry on a BD LSR II flow cytometer equipped with an air-cooled argon-ion laser. The instrument was calibrated weekly for fluorescence and light scattering, with 2 μ M Calbrite beads. Light scattering and fluorescence channels were set to a logarithmic scale and 10,000 events were collected per sample. Data was analyzed with Flow Joe (Version 4.5.9, Stanford, CA). Electronic gates were established on unstained live cells based on their ability to exclude the uptake of propidium iodide. The mean fluorescent intensity (MFI) was plotted versus the concentration of peptide and fit to non-linear regression curves using Sigma Plot software from Jandel Scientific (Version 10.1, San Rafael, CA).

4.2.4 Cellular Uptake

Harvested cells were aliquoted in 200 μ l volumes containing approximately 100,000 cells. An antibody saturation curve (Figure 4.2B) for receptor quantitation was made by adding 0-14 nM of the Alexa Fluor 488-labelled antibody that is specific for the $\alpha_v\beta_3$

integrin, LM690X, (Chemicon International, Temecula, CA, USA) to the cells. The Alexa Fluor-labeled peptides, cRADfK-488 and cRGDfK-488 were quantitated by a standard curve produced from the fluorescence emission at 520 nm following excitation at 495 nm. Once accurately prepared, solutions of the peptides were added to cells over a final concentration range of 0-5 μ M. The final volume was adjusted to 500 μ l with PBS/FBS. For kinetic binding experiments (Figures 4.4), the peptides were added at a final concentration of 13.5 μ M. Each data point was prepared in triplicate. Ligands and cells were incubated at either 37°C or 4°C for one hour for equilibrium binding experiments and at either 0, 1, 5, 15, 30, 60 or 90 min incubations for kinetic binding experiments. Unbound ligands were removed by rinsing with 5 ml of FACS rinsing buffer (130 mM NaCl, 3 mM KCl, 10.4 mM Na₂PO₄, 1.7 mM KH₂PO₄) followed by centrifugation at 1100 rpm for 5 min, and repeated twice. Unfixed cells were kept on ice and immediately analyzed by flow cytometry on a BD LSR II flow cytometer as described in Section 3.2.

4.2.5 Receptor Quantitation

The amount of cell-bound antibody (and thus the number of $\alpha_v\beta_3$ integrins) was determined using a Quantum Simply Cellular kit for antigen quantitation (Bang Laboratories, Cat. No.815A, Fishers, IN). The kit contains microspheres with a series of known amounts of IgG antibody binding sites that were used to produce the X-axis of a standard curve. The Y-axis is a measurement of the signal that the labeled antibody, LM609X, emits when bound to the microspheres (see Figure 4.2A). LM609X was added to each series of microspheres in triplicate, and incubated at 4°C for one hour. The actual

amount of antibody used (2 μg) was higher than the manufacturer's recommended value to ensure saturation of the binding sites on the microspheres. After binding, the excess antibody was removed by washing with 5 ml of FACS rinsing buffer, centrifuging at 1500 rpm, and repeated twice. The antibody was added to HUVECs, M21 and M21L over a concentration range between 0-14 nM. The number of $\alpha_v\beta_3$ receptors could then be calculated from the maximum level of fluorescence by using the standard curve shown in Fig. 4.2A (see Results).

To track the internalization of the receptor that resulted from RGD exposure (Figure 4.5), non-labeled cRGDfK was first added to each sample to achieve a final concentration of 7.0 μM . The samples were then incubated for 0, 15, 30, 60 or 90 min, rinsed and stained using 26 nM LM609X at 4°C for one hour, in the presence of 1.5 μM cRGDfK (the unlabelled peptide). Samples were rinsed twice and analyzed by flow cytometry, and statistical analyses were applied using GraphPad InStat Version 3.0. A p-value generated from a Tukey-Kramer multiple comparisons test that was greater than 0.05 was considered significant.

4.2.6 Fluorescence Microscopy

HUVECs were grown to confluence on two, eight-chambered, glass slides (BD, Franklin Lakes, NJ) to confluence. Cells were rinsed three times with PBS/FBS and ligands were added in PBS/FBS with 50 μg of rhodamine-conjugated dextran, MW 10,000 (Molecular Probes, Eugene, OR) as follows: 13.5 μM of cRGDfK-488 or cRADfK-488 (4 μg) for a total volume of 200 μl , 1 μg of LM609X in 200 μl of PBS/FBS and for

comparison, a treatment control, 200 μ l of PBS/FBS. Each slide was incubated at either 4°C or 37°C for 15 min and 1 h. Ligands were removed by washing each slide three times with PBS/FBS then fixed with 3.5% paraformaldehyde in PBS for 15 min. Immediately before imaging, chambers were removed, and the slides were prepared using Vectashield mounting media (Vector Laboratories, Burlingame, CA) containing the blue nuclear stain, 4',6-diamidino-2-phenylindole (DAPI). Cells were visualized on a Zeiss Axiovert 200 fluorescence microscope equipped with a Retiga 2000R camera. Images were captured under a bright field with a 0.3 s exposure time, and in the fluorescent field using three fluorescent filters with the following exposure times: red-3.1 s, green-8.1 s, and blue-0.005 s for each image. Images were compiled using Openlab software (Version 5.0, Improvision, Lexington, MA).

4.3 Results

4.3.1 HUVEC Express 2.63×10^5 Integrins Per Cell

Before characterizing the binding of cRGDfK to $\alpha_v\beta_3$ integrin receptors on HUVECs, it was important to establish that the HUVECs employed express high levels of the $\alpha_v\beta_3$ integrin receptors. The number of receptors was assayed by first incubating the cells with saturating levels of the Alexa Fluor-488-conjugated antibody, LM609X, which is specific for $\alpha_v\beta_3$ integrin. The amount of antibody bound to these cells was quantitated with calibrated microspheres as detailed in Methods. The standard curve obtained for antibody fluorescence as a function of the antibody binding capacity of the microspheres is shown in Figure 4.2A.

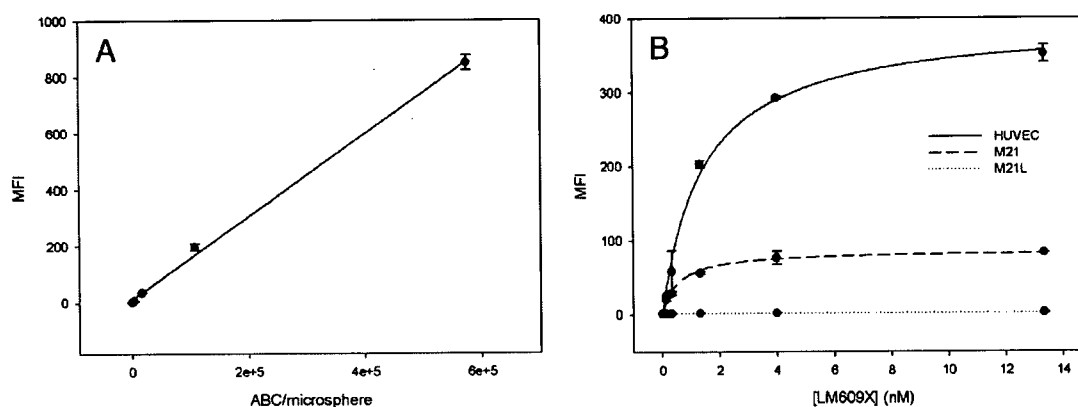


Figure 4.2 Quantitation of the $\alpha_v\beta_3$ receptor on cultured cells

A) Standard curve for antibody-induced-fluorescence (MFI) of calibrated microspheres that have a known antibody binding capacity (ABC). MFI is a measure of the mean fluorescence intensity (arbitrary units) detected by a flow cytometer with $n=3 \pm \text{SD}$. B) Regression curves for saturation of the $\alpha_v\beta_3$ receptor on HUVEC (solid curve) M21 melanoma cells (medium dash) and M21L melanoma cells (dotted), with the antibody LM609X. The maximum number of binding sites (B_{max}) values were used to extrapolate

the average number of receptors for each cell line as indicated in the text \pm the standard error.

The standard curve in Figure 4.2A could be fitted ($r^2=0.998$) by the linear relation:

$$y=11.89 + 0.002x \quad (1)$$

where y is the mean fluorescence intensity (MFI) and x is the total number of antibody binding sites available per microsphere. A plot of the cell-associated fluorescence as a function of antibody concentration for HUVECs, M21 and M21L cell lines is shown in Figure 4.2B. A good fit to this data ($r^2>0.978$) could be achieved using relation (2):

$$y = B_{\max} * x / (K_d + x) \quad (2)$$

Where y is the MFI per cell and x is the antibody concentration (nM), B_{\max} is the maximum MFI per cell (reflecting saturation of all binding sites) and K_d is the antibody-integrin dissociation constant. Using this method, HUVECs were determined to have $2.63 \pm 0.081 \times 10^5$ $\alpha_v\beta_3$ integrins per cell, in reasonable agreement with previous estimates of $4.22 \pm 0.16 \times 10^5$ integrins per HUVEC (R. A. Smith and Giorgio, 2004). The measured K_d value for LM609X binding to HUVEC was 14.4 nM. Similar assays for M21 and M21L cells revealed $56,700 \pm 3500$ and $1,400 \pm 570$ integrins per cell, respectively.

HUVECs were also saturated with cRGDFK-488 and cRADfK-488, demonstrating the total and non-specific binding respectively (Figure 4.3A). A large difference between the total and non-specific binding could be observed for HUVEC cells. Conversely, M21L

cells that do not express the $\alpha_v\beta_3$ integrin, did not show an appreciable difference between the total and non-specific binding curves (Figure 4.3B).

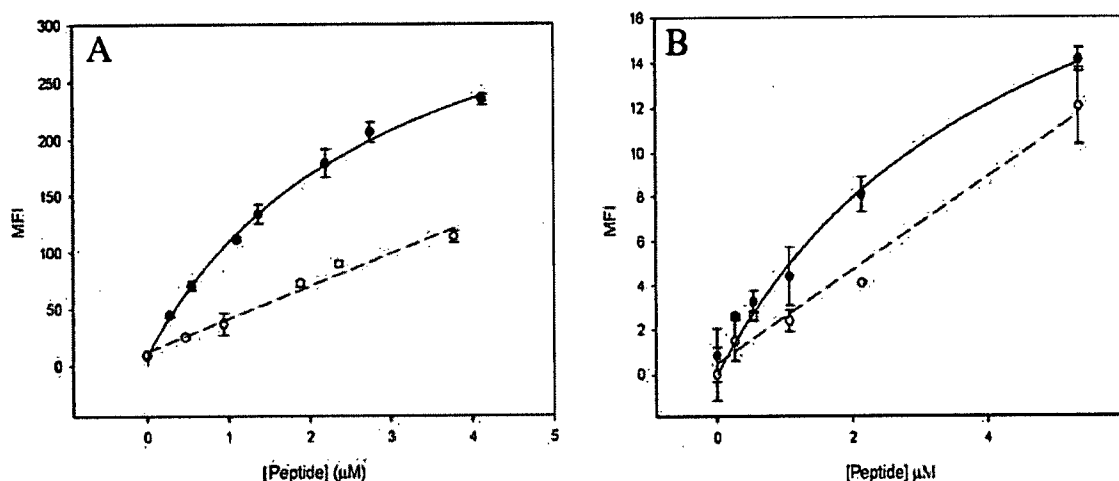


Figure 4.3 Binding of fluorescently labeled peptides to HUVEC or M21L cells

Binding isotherms for the fluorescently labeled RGD and RAD peptides to HUVEC or M21L cells following one hour incubations with the peptide ligands at 37°C. A) Saturation curves characterizing the binding of cRGDfK-488 (closed circles) and cRADfK-488 (open circles) to HUVEC (live cell population) as measured by mean fluorescence intensity following incubation at the peptide concentrations indicated. B) Saturation curves describing the binding of Alexa-Fluor 488 labeled RGD (closed circles) and RAD (open circles) peptides to M21L cells that express low levels of the $\alpha_v\beta_3$ integrin. Measurements were done in triplicate with error bars representing the standard deviation.

4.3.2 cRGDfK-488 Undergoes Extensive Endocytosis Following Binding to HUVEC at 37°C

The cell-based saturation curves presented in the preceding Section reflect the total binding of cRGDfK-488 as assayed after one-hour incubations at 37 °C. The amount of bound ligand includes peptides that are bound to surface $\alpha_v\beta_3$ integrins and peptides that may be subsequently endocytosed. In order to investigate the influence of endocytosis on binding, the association of peptides with HUVEC following one hour incubations at 4°C (a

temperature which inhibits most cellular processes, including endocytosis) or 37°C (endocytosis permitting) was investigated. As shown in Figure 4.4A, a marked difference in the specific (i.e. total minus non-specific) binding of cRGDfK-488 at 4°C and 37°C was observed, corresponding to a 7.6 fold increase in the measured B_{\max} . In contrast, binding of the antibody, LM609X, is only moderately elevated (1.9 fold) when endocytosis is permitted, as shown in Figure 4.4B. Similarly, M21L cells that express low levels of the $\alpha_v\beta_3$ integrin, exhibit a modest 2.8 fold increase in binding at the endocytosis permitting temperature (Figure 4.4C).

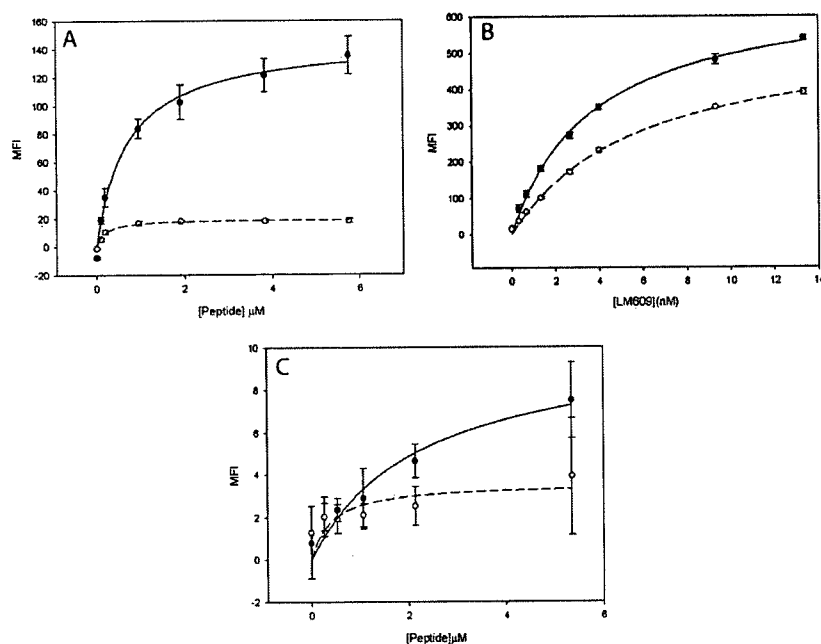


Figure 4.4 Specific Binding and Endocytosis of cRGDfK-488 and LM609 to HUVEC and M21L cells.

Saturation curves describing the binding of RGD peptide and mAb to $\alpha_v\beta_3$ integrins on HUVEC following a one hour incubation at endocytosis enabling (37°C, closed circles) and endocytosis inhibiting (4°C, open circles) temperatures. A) Specific binding (total binding minus non-specific binding, as assayed employing the RAD peptide) of cRGDfK-488 to HUVEC. B) Specific binding of the antibody, LM609X, to HUVEC C) Specific binding of cRGDfK-488 to M21L cells, which express a relatively low amount of the $\alpha_v\beta_3$ receptor. Error bars were calculated from the square root of the sum of squares of the error from non-specific binding and total binding.

Information about the binding constants of cRGDfK-488 may be derived most appropriately from the 4°C curve shown in Figure 4.4A, given that this condition minimizes the effect of endocytosis of the ligand. Fitting the data to Equation (2) resulted in a K_d of $0.20 \mu\text{M} \pm 0.04$ ($r^2 > 0.998$).

The explicit involvement of the RGD sequence in HUVEC binding is further supported by the ability of unlabelled cRGDfK to compete against cRGDfK-488 for binding to HUVEC (Figure 4.5).

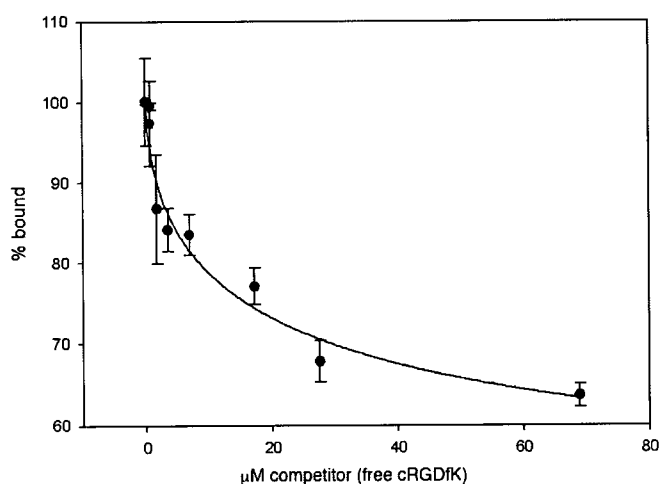


Figure 4.5 Competition of cRGDfK-488:HUVEC binding with free cRGDfK

13.5 μM cRGDfK-488 was added to HUVEC at 37°C in the presence of increasing concentrations of the unlabelled peptide competitor, cRGDfK, incubated for one hour. The y-axis represents amount of cRGDfK-488 bound to HUVEC in the presence of the competitor. A measure of 100% bound is taken from the mean fluorescent intensity observed for cRGDfK-488 binding to HUVECs in the absence of any competitor.

4.3.3 Time Dependent Uptake of cRGDfK-488 by HUVEC

In order to further characterize the increased binding at endocytosis permitting temperatures, a kinetic study of peptide binding to HUVECs at either 4°C or 37°C was performed. The time-dependent binding of cRGDfK-488 and the control peptide (cRADfK-488) to HUVEC over 90 min is illustrated in Figure 4.6. It was found that a reasonable fit to the uptake curves shown in Figure 4.6 could be achieved using the first order equation:

$$y(t)=a(1-e^{-k_{obs}t}) \quad (3)$$

where y is the mean fluorescent intensity of live cells detected on a flow cytometer, a is a constant and t is time, in seconds. At 4°C (Figure 4.6), where endocytosis is inhibited a good fit ($r^2 > 0.969$) could be achieved using Eq. 3 to describe binding of both cRGDfK-488 and cRADfK-488. The rate constant, k_{obs} , associated with this binding was $0.0024 \pm 4.15 \times 10^{-4} [s^{-1}]$ (half life, $t_{1/2} = 288$ s) for cRGDfK-488 and $0.009 \pm 3.84 \times 10^{-4} [s^{-1}]$ ($t_{1/2} = 77$ s) for cRADfK-488. Similarly, a good fit (r^2 values > 0.978) could be achieved for peptide binding at 37°C for both cRGDfK-488 ($k_{obs} = 0.0007 \pm 8.16 \times 10^{-5} [s^{-1}]$, $t_{1/2} = 1004$ s) and cRADfK-488 ($k_{obs} = 0.0004 [s^{-1}]$, $t_{1/2} = 1732$ s). The greater uptake at 37°C associated with slower rate constants could be consistent with endocytosis. In order to evaluate this more definitively, the fluorescence microscopy studies detailed in Section 4.3.5 were undertaken.

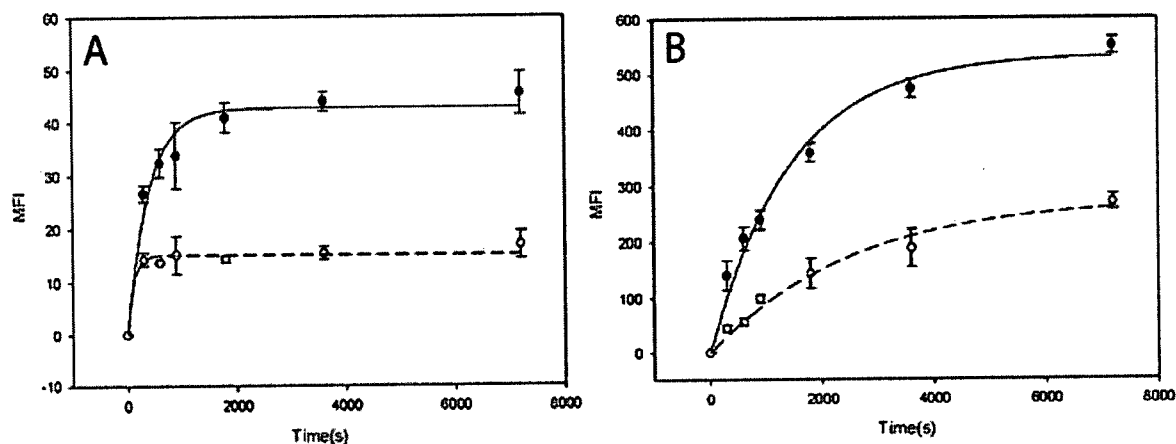


Figure 4.6 Time-dependent uptake of cRGDfK-488 and cRADfK-488 by HUVEC
 13.5 μ M cRGDfK-488 (closed circles) or cRADfK-488 (open circles) were added to HUVEC at A) endocytosis inhibiting (4°C) and B) endocytosis permitting (37°C) temperatures. The HUVECs were incubated in the presence of 13.5 μ M of labeled peptide. The curves represent the best fit of the data to the equation $y(t)=a(1-e^{-k_{\text{obs}}t})$.

4.3.4 $\alpha_v\beta_3$ Expression Decreases Upon RGD Binding.

In an attempt to show more directly that the $\alpha_v\beta_3$ integrin receptor is endocytosed following binding by the unlabelled peptide, cRGDfK, was added at saturating concentrations to HUVEC cells for varying lengths of time at 37°C and the amount of integrin present after these incubations was quantitated by staining with LM609X (Figure 4.7). Although not a significant difference ($p>0.05$), the amount of surface-exposed integrin appeared to decrease by approximately 35% within 30 min, then subsequently increase, supporting the notion that peptide binding to integrin results in endocytosis and internalization of the receptor.

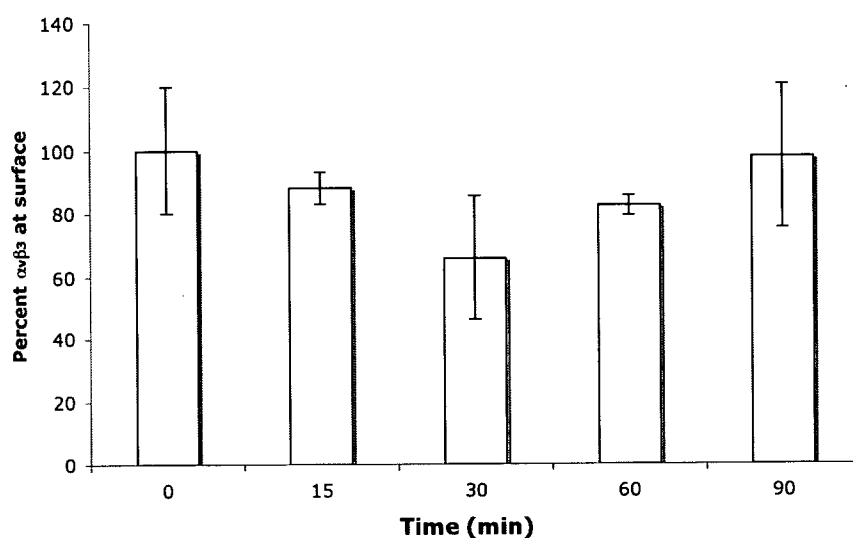


Figure 4.7 $\alpha_v\beta_3$ integrin surface receptor expression after exposure to cRGDfK

Expression of the $\alpha_v\beta_3$ integrin after exposure to cRGDfK as assayed employing the LM609X mAb. HUVEC were incubated with 34 μM of (unlabelled) cRGDfK at 37°C for varying lengths of time and the level of $\alpha_v\beta_3$ was then measured employing saturating amounts of LM609X at 4°C. Error bars represent the standard deviation of measurements performed in triplicate.

4.3.5 Endocytosis as Visualized by Fluorescence Microscopy

In order to directly visualize the ability of HUVECs to endocytose cRGDfK-488 ligands, uptake was followed employing fluorescence microscopy. The appearance of cells following either 15 min or one hour incubations at 37°C are shown in Figure 4.8. As seen for the cells in suspension analyzed by flow-cytometry, the ligand cRGDfK-488 is endocytosed. Co-localization of the green peptide label with the red endocytosis marker (rhodamine-conjugated dextran) commenced as early as 15 min and within one hour, the two labels co-localize within the cell. Internalization of the LM609X antibody was comparatively weak, consistent with the modest increase in B_{max} with temperature observed

for LM609X binding to HUVEC (Figure 4.4B). The cRGDfK-488 peptide induced unique morphological changes (seen best in the bright field images) that are different than those seen for LM609X or cRADfK-488 treated cells. In particular, cells lost their adhesive properties, lifting off the surface. Few cells remained after cRGDfK-488 was removed by the required washing steps.

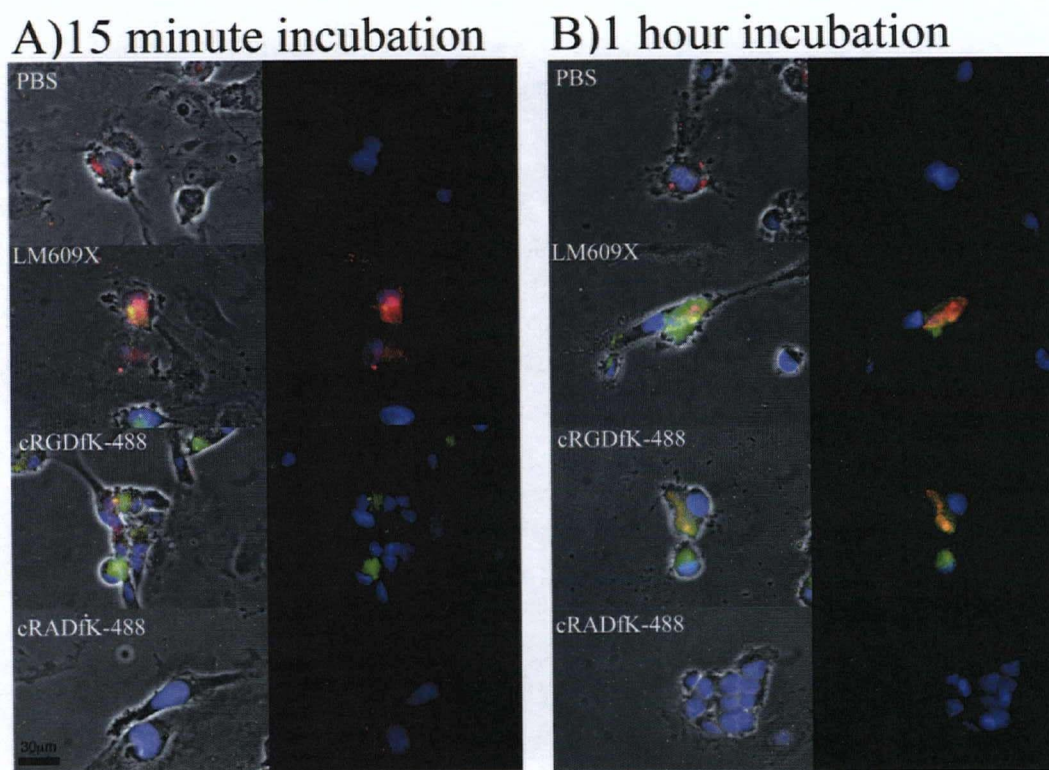


Figure 4.8 Binding at 37°C as seen by fluorescence microscopy

Fluorescence microscopy of HUVEC following incubation with the LM609X mAb, cRGDfK-488 and cRADfK-488 ligands at 37°C. The Alexa Fluor 488 labeled ligands were added together with dextran rhodamine to visualize endocytosis. Fluorescence micrographs obtained A) following a 15 min incubation and B) following a 1 h incubation. The data indicates that cRGDfK-488 co-localizes with endocytosed vesicles while LM609X remains largely located at the surface of the cell. Non-specific binding by cRADfK-488 was not detected.

The same ligand incubations were carried out at 4°C with less overall binding detected for all peptide ligands and most cells remain adhered to the glass slide (Figure 4.9). Binding of the cRGDfK-488 ligand to cells at this temperature was barely detected. Similarly, as shown in Figure 4.4A, binding at 4°C is low compared to the level of could be detected at 37°C.

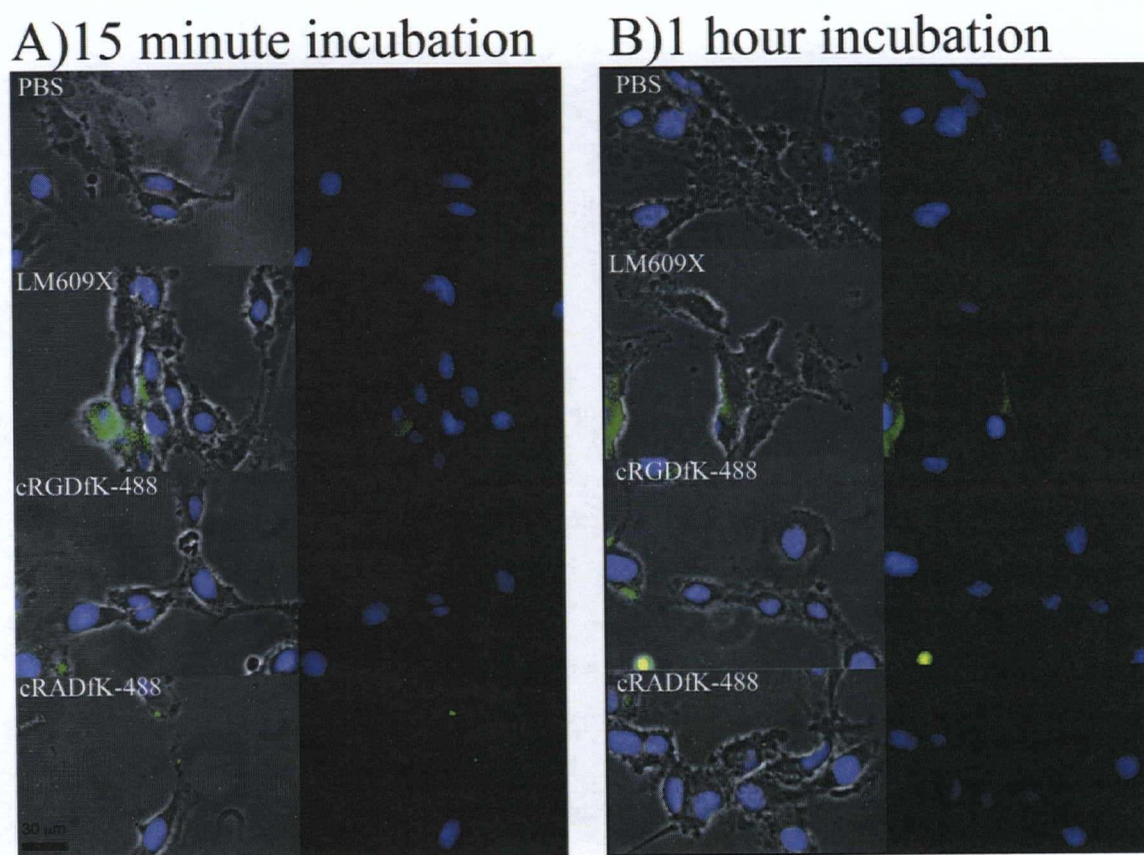


Figure 4.9 Binding at 4°C as seen by fluorescence microscopy

Fluorescence images of HUVEC following incubation with the LM609X mAb, cRGDfK-488 and cRADfK-488 ligands at 4°C. The Alexa Fluor 488 labeled ligands were added together with dextran rhodamine to visualize endocytosis. Fluorescence micrographs obtained A) following a 15 min incubation and B) following a 1 hour incubation.

4.4 Discussion

The major finding of this work is that the cRGDfK-488 peptide binds to $\alpha_v\beta_3$ integrins on HUVECs and stimulates enhanced endocytosis when compared to the LM609X monoclonal antibody or the cRADfK-488 negative control. There are three interesting aspects of this observation. First, it is of interest to compare the ability of the RGD ligand employed here to stimulate endocytosis following binding to the $\alpha_v\beta_3$ integrin with the properties of other RGD ligands as reported by other investigators. The second area concerns the mechanism whereby the peptide ligand could stimulate greater endocytosis than other ligands such as the monoclonal antibody. The final point concerns the potential utility of the cRGDfK-488 peptide as a useful agent to target drugs *in vivo*.

The relation between RGD peptide binding to $\alpha_v\beta_3$ integrins and subsequent uptake into cells has also been studied by other investigators. For melanoma cells, it has been reported that mAb binding to $\alpha_v\beta_3$ integrins results in receptor-mediated endocytosis, whereas cRGDfK is taken up by an integrin-independent pathway (Castel et al., 2001). The conclusion that cRGDfK is taken up by an integrin independent process was indicated by the similar levels of uptake for ^3H -cRGDfK and carboxyfluorescein-labeled cRGDfK for both M21 and M21L cells at both 4°C and 37°C. These results are not in agreement with the results presented here, because little specific binding (and much reduced uptake) of the cRGDfK-488 peptide is observed for the M21L cell line that expresses low levels of receptors. Further, uptake of the cRADfK-488 control peptide, which binds non-specifically to the HUVEC, is considerably reduced compared to the cRGDfK-488 ligand.

It is possible that the high levels of non-specific uptake could have arisen from non-specific binding effects. The M21L cells have only 40 times more receptors as compared

to M21L cells while HUVECs express nearly 200 times more integrin receptors than M21L cells. A second and related point is that the use of ligands with higher non-specific background binding properties can lead to additional difficulties in detecting integrin-specific effects. In the study published by Castel and colleagues, the binding and uptake properties of RAD control ligands were not examined.

Other studies demonstrating enhanced gene delivery of vectors targeted by RGD ligands support a specific receptor-mediated endocytotic process (Renigunta et al., 2006). Specific uptake of RGD-containing ligands is also supported by studies indicating that RGD internalization coincides with the activation of a kinase (S6K1) that is critical for cell growth. This effect is RGD-specific since the negative control (an RGE-containing peptide) is neither internalized nor active in S6K1 phosphorylation (Balasubramanian and Kuppuswamy, 2003).

The next area of discussion concerns the mechanism whereby the cRGDfK-488 ligand could stimulate appreciably higher levels of internalization on binding to the $\alpha_v\beta_3$ integrin as compared to the integrin-specific mAb LM609X. A number of studies suggest that the interactions of RGD ligands with integrins have significantly different features than binding of mAb. The studies presented in Chapter 3 indicate a 1:2 $\alpha_v\beta_3$ integrin:cRGDfK-488 peptide stoichiometry. A two-step process has been proposed for fluorescently labeled RGD-peptides that bind to the main integrin on activated platelets, GPIIb/IIIa. In this study, a rearrangement process was proposed to follow the initial binding event (Bednar et al., 1997). The ratio of $k_{\text{off}}/k_{\text{on}}$ for the first step was observed to be high compared to the second step, indicating that the subsequent rearrangement stabilizes a complex that is less prone to dissociation.

While it is not clear how these different binding characteristics of the RGD ligand to the $\alpha_v\beta_3$ integrin, as compared to the mAb, lead to enhanced endocytosis for the RGD ligand, it is clear that the possibility exists for substantially different conformational and functional consequences for RGD binding as compared to mAb binding. It will be of interest to pursue the correlation between these differences and subsequent endocytotic events.

The utility of RGD-containing peptides for the targeted delivery of associated therapeutics is clearly improved by an enhanced probability of endocytosis (Sapra and Allen, 2002). A related question concerns whether the specific type of RGD peptide influences the levels of endocytosis or whether all RGD ligands have the same endocytotic index. It will be of considerable interest to examine the endocytotic index of multivalent RGD targeting ligands, which demonstrate improved binding to the $\alpha_v\beta_3$ integrins (Montet et al., 2006).

In summary, the results presented here establish that the cRGDfK-488 stimulates enhanced endocytosis in HUVECs as compared to the mAb LM609X, and that the uptake of the RGD ligand proceeds via an endocytotic process that involves specific interactions with the $\alpha_v\beta_3$ integrin. It is anticipated that for RGD-targeted therapeutics the maximum therapeutic benefit will result from the use of targeting ligands that maximize intracellular delivery of associated cargo, pointing out a need to characterize targeting peptides according to their relative ability to stimulate endocytosis in target cells.

5 Targeted Drug Delivery³

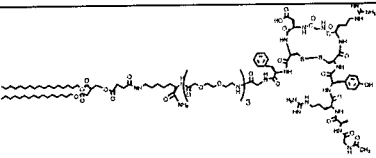
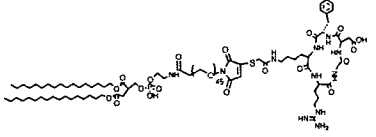
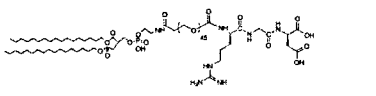
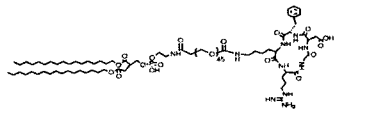
5.1 Introduction

In order for LNs to reach cancer cells, they must extravasate from the blood stream into the tumor. The EPR effect facilitates LN retention at the site of a tumor and targeting ligands with affinity for the tumor-associated vasculature, such as cRGDfK, could help to increase the amount of the drug that is retained at the tumor site. Vascular targeting, as opposed to targeting tumor cells themselves, offers the additional advantage of being a relatively general therapy for the treatment of solid tumors that would not be expected to result in the generation of drug-resistant variants, given that all tumors require neovasculature in order to survive (Folkman, 1990).

Studies on several published RGD-LN formulations have produced contradictory results regarding the effect that a targeting ligand has on the clearance of LN systems from the circulation. In some instances, RGD-LNs had the same circulation lifetimes as non-targeted LNs (Dubey et al., 2004; Xiong et al., 2005) however accelerated clearance has been reported for LN formulations with higher densities of the RGD ligand (Holig et al., 2004). A summary of recent *in vivo* publications describing the behavior of RGD-LNs is provided in Table 5.1. These studies differ in the synthesis and formulation of the RGD-LN employed and the method of incorporating the conjugates into an LN membrane. These differences could account for the differences in their pharmacokinetic properties.

³ A version of this chapter will be submitted for publication

Table 5.1 Summary of targeting lipids used to study RGD-LNs *in vivo*

Targeting lipid	Authors	Method of LN incorporation	Major findings
	Holig et al, 2002	Formulation	1 mole % RGD-LNs are cleared more rapidly than 0.1 mole% RGD-LNs
	Schiffellers et al, 2003	Surface coupling	2.5 mole % RGD-LNs inhibit tumor growth no reported PK properties
	Xiong et al, 2005	Formulation	No difference in clearance between targeted and non-targeted LNs
	Dubey et al, 2004	Formulation	5 mole% RGD-LNs exhibit no difference in their clearance properties as compared to non-targeted LNs

The synthetic route to forming targeted LNs can have an important impact on the ability of the resulting conjugate to be analyzed. For example, a commonly used technique for formulating a peptide into an LN is the maleimide-based, thioether conjugation method which can be done in an aqueous solvent (Schiffellers et al., 2003). RGD-based targeting lipids can be synthesized in an organic solvent, which can lead to a higher yield and a better characterized targeting ligand. Since an aqueous environment is required to maintain the LN's unilamellar structure, organic phase conjugation reactions must be conducted before LN formation and incorporated into the LN before the particle is formed (termed the "formulation" method) or using the post-insertion method (See Figure 5.1).

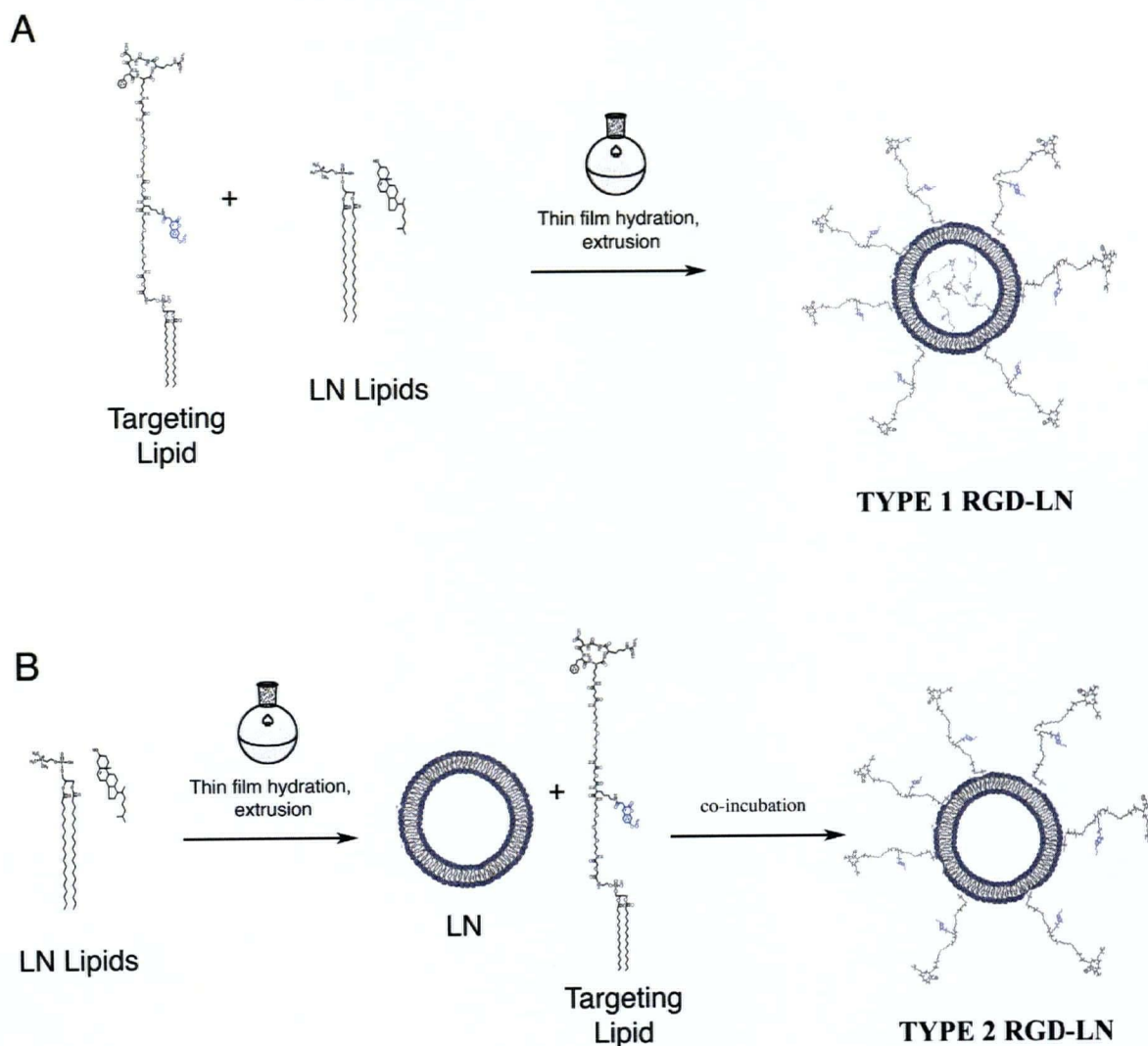


Figure 5.1 Techniques for incorporating an RGD-lipid into an LN

A) The formulation method where RGD-lipid incorporation precedes LN formation resulting in Type 1 RGD-LNs with the RGD ligand exposed at both surfaces of the bilayer

B) The post-insertion method where RGD-lipid incorporation occurs after the LN formation, and the targeting ligand is located in the outer leaflet of the monolayer, resulting in Type 2 RGD-LNs.

Maleimide-based reactions typically tether the peptide by surface coupling, which occurs in an aqueous environment. A major problem with such coupling is that the reagents are highly susceptible to hydrolytic side reactions, and the resulting impurities cannot be subsequently removed from the LN formulation.

In the RGD-LN studies listed in Table 5.1 the purity of the peptide-lipid constructs used is not given. In general, the accurate modification of a peptide with a lipid, which is necessary in order to anchor the peptide in the LN bilayer, is a difficult process. This Chapter is devoted to achieving a well-characterized peptide-lipid conjugate that can be introduced into LN in a quantitative manner at the time that the LN is made. The first part of this work concerns the synthesis of an RGD-based targeting lipid that can be inserted into LN by the formulation method (Figure 5.1A). The second part characterizes the overall properties of the targeted particle including parameters such as size, binding affinity, ability to load and retain drug as well as its ability to facilitate intracellular drug delivery.

5.2 Methods

The following sections describe the synthetic strategies employed for the RGD-lipids shown in Figure 5.2.

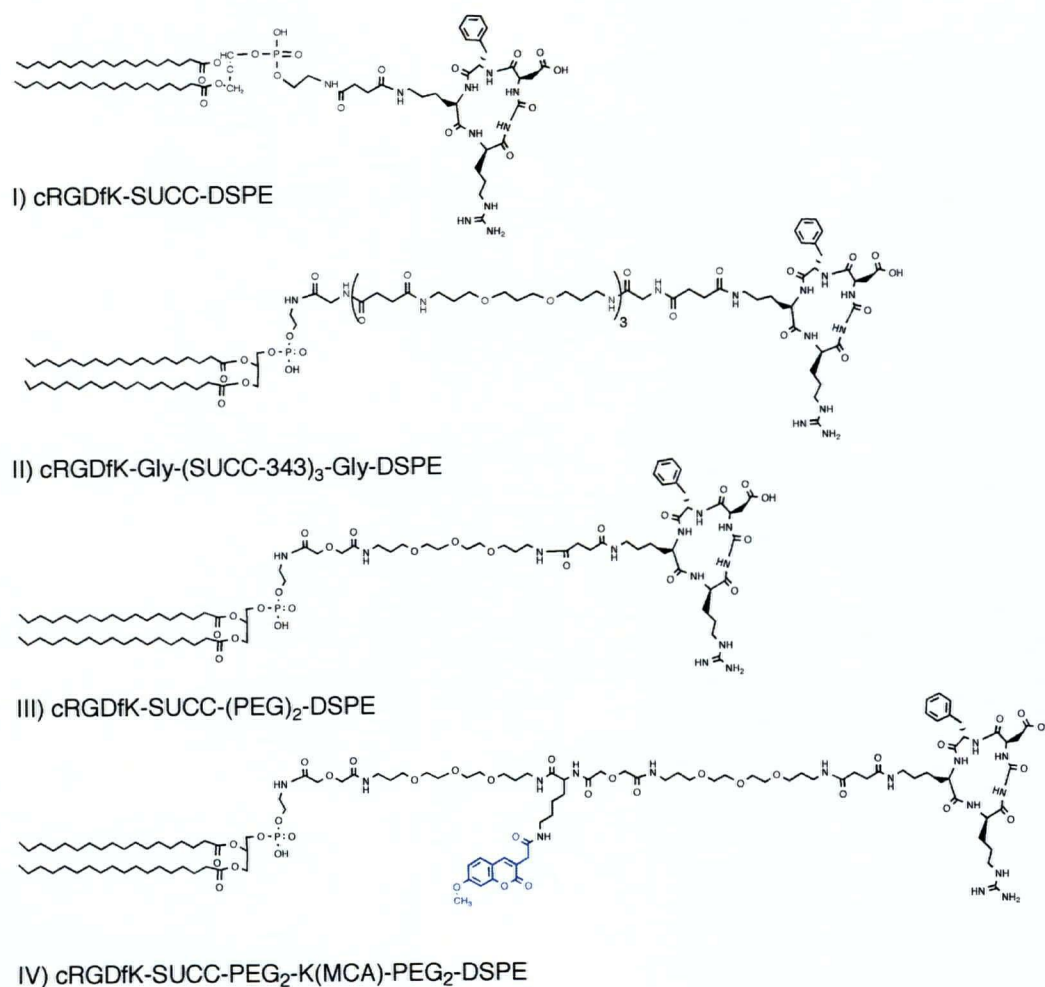


Figure 5.2 RGD-lipids synthesized

Compounds I-IV were synthesized for assessment as LN targeting agents. Compound IV was chosen for further studies, since the fluorescent labeling molecule enabled accurate quantitation and the presence of the PEG spacer reduced aggregation effects noted for compound 1.

Compounds I-III led to the development of compound IV, which was found to be the most appropriate for use in subsequent LN formulation, due to its good analytical and synthetic properties. The synthesis of this lead compound is shown in Figure 5.3.

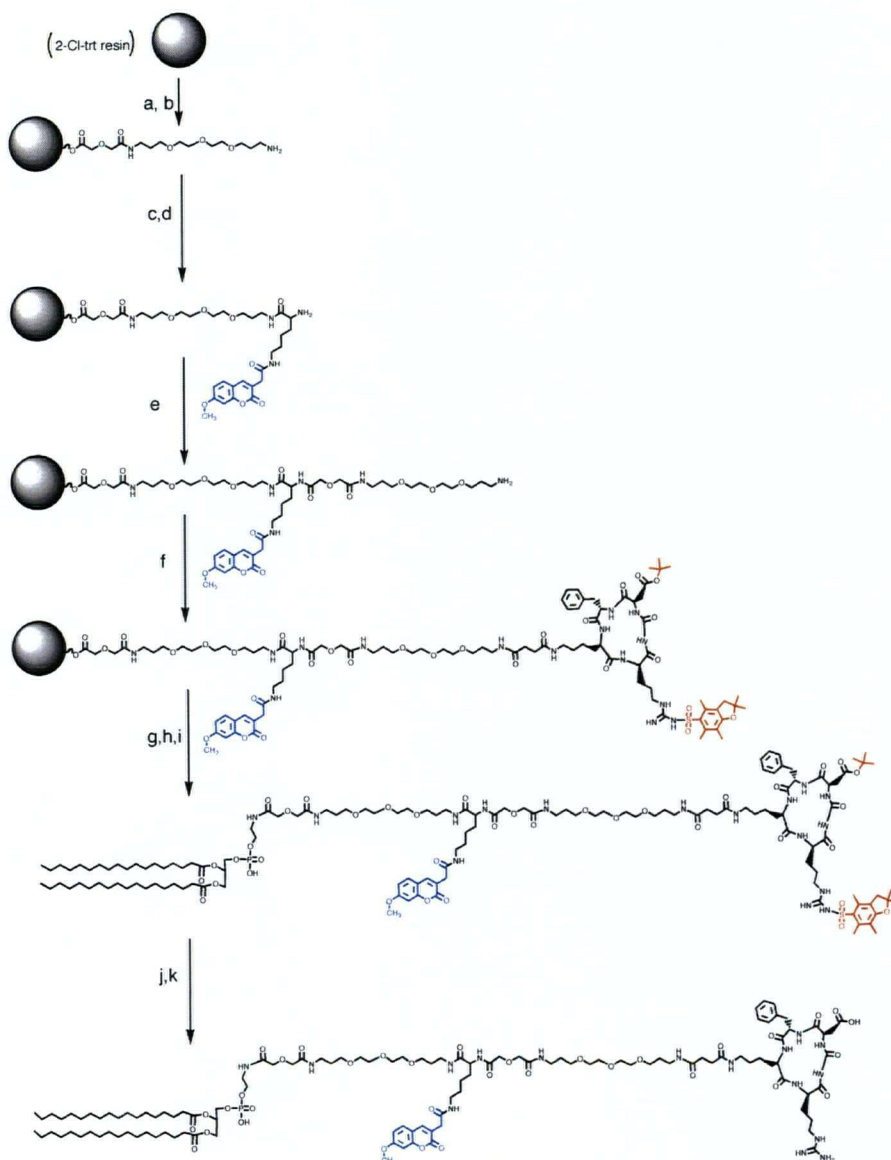


Figure 5.3 Steps in the synthesis of cRGDFK-PEG₂-K(MCA)-PEG₂-DSPE

a) Fmoc-PEG₂-OH, 3 h b) 20% piperidine in DMF c) Fmoc-Lys(MCA)-OH, HBTU/HOBT d) 20% Piperidine in DMF e) Fmoc-PEG₂-OH, PyBop/HOBT, 6 h f) cR(Pbf)GD(tBu)fK-succinic acid, PyBop/HOBT, 12 h. g) 0.1% TFA, 1% TIS, 3.9% H₂O, 95% DCM h) RP-HPLC i) DSPE, PyBOP/HOBT, CHCl₃, 60°C j) Silica gel chromatography k) 95% TFA, 5% DCM, silica gel chromatography.

5.2.1 Materials and Reagents

Unless otherwise specified, all chemicals and solvents were of reagent grade or higher and obtained from the same suppliers as described in Chapter 3. All lipids were purchased from Avanti Polar Lipids (Alabaster, AL). Reversed phase HPLC (RP-HPLC) was performed using gradients of aqueous acetonitrile containing 0.1% trifluoroacetic acid (TFA) (aqACN) applied to C18 columns from Grace Vydac (Hesperia, CA). Analytical gradients were run using column no. 218TP5415 (150 mm X 4.6 mm) with a flow rate of 1 ml per min. Peptides were purified on a preparative scale column no. 218TP1022 (250mm X 22mm) with a flow rate of 10 ml per min.

5.2.2 Peptide Synthesis

The protected cyclic peptide, cR(Pbf)GD(t-Bu)fK(Z), was synthesized as described in Chapter 3. Briefly, the linear peptide was synthesized by the 9-fluorenylmethoxycarbonyl (Fmoc)-strategy solid phase peptide synthesis. Linear peptides were then cyclized in DMF at a final peptide concentration of 0.5 mM, 1.3 molar equivalents (to peptide) of benzotriazol-1-yl-oxytripyrrolidinophosphonium hexafluorophosphate (PyBop) and hydroxybenzotriazole (HOBT), and the pH was adjusted to 7.3 with TEA, with (Advanced Chemtech, Louisville, KY).

The benzyl group on the lysine side chain was removed by hydrogenation using a palladium/carbon catalyst. The amine-functionalized peptide, cR(Pbf)GD(t-Bu)K (100 mM in DMF), was modified with 10 molar equivalents of succinic anhydride to produce cR(Pbf)GD(t-Bu)fK(succ). The reaction mixture was purified with an RP-HPLC gradient

of 10-60% aqACN over one h. A 95% pure product eluting after 40 min was characterized both by ESI-MS ($MW=1011.47 \pm 1$, predicted=1012.18) and by analytical RP-HPLC using a 30-90% aqACN gradient, a product of >95% purity was obtained, with a retention time of 12 min.

5.2.3 cRGDfK-SUCC-DSPE (Compound I) Synthesis

cRGDfK-SUCC-DSPE (i.e. Compound I in Figure 5.2) was the simplest design for an RGD-lipid of the four synthesized. The compound was first made by modifying the lipid, DSPE, with succinic anhydride (Avanti polar lipids Alabaster, AL), as follows: first, DSPE and 10 molar equivalents of succinic anhydride were co-dissolved in $CHCl_3$. The reaction was complete after one hour, and was monitored by disappearance of the free amine from DSPE ($CHCl_3/MeOH$ (7.5/2.5) R_f 0.6). The compound was precipitated into H_2O and lyophilized. The dry carboxylic acid-functionalized lipid was activated with 1.3 molar equivalents of PyBOP/HOBT for 1 min. Two molar equivalents of the peptide with a free amine, cR(Pbf)GD(t-bu)fK, was reacted for 5 h at room temperature. A UV-positive spot with an R_f value of 0.84 TLC corresponded to product formation. The reaction mixture was purified over silica gel and concentrated. The side chain protecting groups from the resulting cR(Pbf)GD(t-bu)fK-succ-DSPE conjugate were removed by methods similar to those used in Chapter 3 to yield the deprotected peptide-lipid conjugate, cRGDfK-succ-DSPE. The final product was precipitated into H_2O and lyophilized (yield 14%).

5.2.4 cRGDfK-(SUCC-343)₃-DSPE (Compound II) Synthesis

The synthesis of cRGDfK-(SUCC-343)₃-DSPE (i.e. compound II in Figure 5.2) was attempted in order to make a relatively inexpensive and analytically defined spacer molecule, which functions to distance the RGD-peptide from the lipid head group, could be used to improve the analytical properties of compound I. The strategy for the SUCC-343 spacer is similar to the solid phase synthesis (SPPS) procedure used to obtain defined length polyamides (Kochendoerfer et al., 2003).

For the SUCC-343 spacer, 1 mmol WANG (NovaBiochem, San Diego, CA) resin was loaded with Fmoc-Gly-OH following activation with 5 molar equivalents of N,N'-diisopropylcarbodiimide, and 0.1 molar equivalents of dimethylaminopyrimidine (DMAP) was added to this solution and coupled to the resin for 2 h. Fmoc removal and amine detection was conducted as described previously. Sixteen molar equivalents (ME) to amine of succinic anhydride, TEA and HOBt were dissolved in DMF and coupled to the resin under N₂ and allowed to react for 30 min. Sixteen ME of carbodiimidazole (CDI) (Sigma-Aldrich, St. Louis, MO) HOBt and TEA were used to activate the resin for 30 mins. Following activation, 16 ME of 4,9 diaxa-1, 12-dodecane, diamine (referred to as 343) was coupled for 1 hr. The succinic anhydride/343 couplings were repeated twice to yield (343-SUCC)₃-Gly-OH. A final Fmoc-Gly coupling was performed using 8 ME of Fmoc-Gly-OH, HOBt, HBTU and TEA and coupled to the resin for 1 h. The WANG resin was cleaved 3x in 10 ml of 25% TFA in DCM for 5 min each. After each cleavage, the resin was rinsed with 10 ml MeOH and 10 ml DCM. The final 30 ml of each cleavage fraction was collected in a small round bottom flask and concentrated to approximately 0.5 ml. The crude cleavage mixture was precipitated into ice-cold diethyl ether. Fifteen ml of

diethyl ether (EMD Biosciences, San Diego, CA) was mixed into the 0.5 ml sample, forming a precipitate. The resulting precipitate was characterized by HPLC and TLC. Subsequent purification by silica gel chromatography, using 100 g of silica powder (SiliCycle, Quebec City, Quebec) was found to be necessary to produce one homogenous UV-positive band in the pooled fraction as detected by TLC ($\text{CHCl}_3/\text{MeOH}$ 7.5/2.5 $R_f=0.74$) and one main peak as by HPLC (gradient 10-85% AqACN/30 min, retention time=13.4 min). The product was hydrated with distilled water and lyophilized to yield solid Fmoc-Gly-(343-succ)₃-Gly-OH an N-terminally protected spacer molecule. The side chain protected peptide was coupled to the spacer by activating the spacer's C-terminal glycine with 1.3 molar equivalents of PyBOP/HOBT and coupling the amine-containing peptide for about 5 h in DMF. The resulting construct was purified by preparative HPLC using a gradient of 10-65% AqACN/60 min eluting after 20 min. The product produced one peak that eluted after 18.8 min. The Fmoc was removed and the purification was repeated, producing a compound with an analytical retention time of 15.5 min. Coupling to SUCC-DSPE was performed as above, and detected by iodine staining. After the final deprotection, (TLC: $\text{CHCl}_3/\text{MeOH}$ (9/1) R_f 0.65) the overall yield was less than 1%.

5.2.5 cR(Pbf)GD(t-Bu)fK-PEG₂-COOH and cR(Pbf)GD(t-Bu)fK-PEG₂-K(MCA)-PEG₂-COOH Synthesis (preceding compounds III and IV, respectively)

It was rationalized that the use of a short PEG-based spacer might likewise improve upon the poor analytical properties of compound I, and the poor synthesis yield observed

for compound II. The peptide-spacer constructs preceding the formation of compounds III and IV were made using a commercially available PEG and a solid phase peptide-spacer coupling strategy (see Figure 5.3). Compound IV evolved from compound III as it became apparent that a fluorescently labeled molecule was required for achieving well characterized RGD-LN systems.

The spacer-peptide conjugates were assembled in a similar manner for compounds III and IV, as follows: 0.112 mmole 2-chlorotrityl resin was loaded with 2.5 molar equivalents of O-(N-Fmoc-3-aminopropyl)-O'-(N-diglycoyl-3-aminopropyl)-diethyleneglycol (Fmoc-NH-PEG₂-COOH) over the course of 3 h, under nitrogen gas with gentle stirring. Fmoc was removed by soaking the resin in a solution of 20% piperidine in DMF for 5 min, and repeated once. Ninhydrin assays were used to monitor the success of SPPS reactions. For compound IV, which contains a fluorescent label, 2.5 molar equivalents of Fmoc-Lys-(MCA)-OH were coupled to the free amine using 1.2 molar equivalents to carboxylic acid of HOBT, HBTU and TEA for one h then subsequently, 5 molar equivalents of the second Fmoc-NH-PEG₂-COOH unit was incorporated over 3 h using 1.2 molar equivalents to carboxylic acid of: PyBOP, HOBT and TEA. In order to monitor the success of each coupling reaction, trial cleavages (performed in a solution of 0.1% TFA in DCM, 2.5% H₂O, 2.5% TIS (v/v)) proved to be more reliable than ninhydrin assays from this point on, presumably due to the shielding effect of PEG. The product (after step d of Figure 5.3) could be detected with a retention time of 21 min on an analytical RP-HPLC gradient from 0-85% aqACN. Successful Fmoc removal resulted in a shift in retention to 14.5 min using the same gradient. 1.2 molar equivalents (to amine) of the cyclic peptide, cR(Pbf)GD(t-Bu)fK(succ) was coupled overnight to the spacers from compound III and IV

under nitrogen gas using 1.2 molar equivalents of PyBop and HOBt and TEA to acid. The products $cR(Pbf)GD(t-Bu)fK-PEG_2-COOH$ and $cR(Pbf)GD(t-Bu)fK-PEG_2-K(MCA)-PEG_2-COOH$ was purified directly by preparative RP-HPLC, (0-85% aqACN) eluting after 36 min (compound III) or 40 min (compound IV).

The dry yield of the peptide-spacer construct was 94 mg for compound III and 80 mg for compound IV. Both products were clearly resolved by TLC (chloroform ($CHCl_3$)/methanol (MeOH), 8.8/2.2), $R_f=0.18$, and were purified to >95% purity as indicated by RP-HPLC (0-85% aqACN).

5.2.6 Synthesis of $cR(Pbf)GD(t-Bu)fK-PEG_2-DSPE$ (Compound III) and $cRGDfK-PEG_2-K(MCA)-PEG_2-DSPE$ (Compound IV)

The peptide spacer-constructs were conjugated with the lipid anchor, DSPE, in a similar manner to form compound III and compound IV. The purified and lyophilized peptide-PEG constructs were dissolved in 2 ml DCM, and activated with 5 molar equivalents of N-hydroxysuccinimide and diisopropylcarbodiimide. The active ester formed within 30 min and 3.5 molar equivalents to acid of distearylphosphatidyl ethanolamine (DSPE) was dissolved in 1 ml $CHCl_3$ at 60°C. The active ester was added to the lipid and 1.2 molar equivalents (to ester) of TEA were added. The reaction occurred within one h at 60°C and the resulting product was purified on 100g of silica gel, mobile phase MeOH/ $CHCl_3$. The product, $cR(Pbf)GD(t-Bu)fK-PEG_2-K(MCA)-PEG_2-DSPE$, eluted between 30-50% methanol in $CHCl_3$ and was identified by TLC ($CHCl_3$ /MeOH 8.8/2.2 R_f 0.74)

The compounds were concentrated and redissolved in 95% aqueous TFA for deprotection of Arg and Asp side chains. The final deprotected products formed within 2 h. TFA was removed by evaporation and precipitated into ice-cold diethyl ether, centrifuged, rinsed with diethyl ether, and centrifuged again. A yield of 40.8 mg of cRGDfK-SUCC-PEG₂(MCA)-PEG₂-DSPE (compound IV) and 22 mg of cRGDfK-SUCC-PEG₂-DSPE (compound III) resulted. ESI-MS values for compound IV were MW 2415.5±1, (predicted MW 2414.89), and for compound III, MW 1751.6±1 (predicted MW 1752.16). Purity was confirmed by TLC detected with iodine and UV (MeOH/EtOH/H₂O/TEA (6/3/1/1) R_f 0.20 for III and 0.25 for IV). Excitation (325 nm) and emission (Max 389 nm) spectra were collected for the construct between 280 and 500 nm using a Varian Cary Eclipse Fluorometer. Since compound IV had the best analytical properties, namely that it could be detected by HPLC and MS methods, and had the highest yield, it was pursued as the lead compound.

5.2.7 cRGDfK-PEG₂-K(MCA)-PEG₂-DSPE Formulation into LNs

Empty RGD-LNs with different RGD content were made by the formulation method shown in Figure 5.1A. Variations in the RGD content were made by increasing the mole % of cRGDfK-PEG₂-K(MCA)-PEG₂-DSPE (Compound IV, herein referred to as the RGD-lipid) in the lipid formulation from which the LN were formed.

In order to detect the LN by a fluorescent signal that could be related back to the concentration of the LN particles, a lipid fluorescently labeled with rhodamine was

included in the formulation. This label could be used to detect the LN concentration whereas the MCA label is used for detection of the RGD-lipid.

The series of RGD-LNs containing different amounts of RGD were formulated as follows: 0.5 mole% RGD-LN was made by incorporating: 54 mole % distearylphosphatidylethanolamine (DSPC) : 45 mole % Cholesterol (Chol) : 0.5 mole% Rhodamine-labeled phosphatidylethanolamine (Rhod:PE) : and 0.5 mole % RGD-lipid (i.e., 54:45:0.5:0.5 mole:mole), 1 mole% RGD-LN (53.5:45:0.5: mole:mole), 2.5 mole% (52:45:0.5:2.5 mole:mole), and 5 mole%: (49.5: 45:0.5:5 mole:mole). Non-targeted LNs were formulated as (54.5:45:0.5:0 mole:mole). Dry lipids were dissolved in CHCl_3 at 60°C. The solvent was removed under a stream of nitrogen gas to form a thin film, and residual solvent was removed by lyophilisation. For empty vesicles, the thin film was hydrated in 100 mM HEPES buffer containing 144 mM NaCl, pH 7.5 (HBS) warmed to 60°C. The resulting multilamellar vesicles were extruded through two polycarbonate filters with a 100 nm pore size ten times employing an Extruder (Northern Lipids, Vancouver, Canada) to form unilamellar LNs. The amount of surface-exposed RGD-lipid per liposome was estimated assuming that one LN contains approximately 148,641 lipids (based on the average diameter of the particle as 116 nm, and the average surface area of a lipid head group as 0.5 nm^2). For this diameter, the proportion of those lipids residing in the outer leaflet is approximately 57% of the total lipid composition.

5.2.8 Post-Insertion of cRGDfK-PEG₂-K(MCA)-PEG₂-DSPE into Pre-Formed LNs

LNs containing 1% RGD were also made by post-insertion of the RGD-lipid into preformed (55:44:0:0 mole:mole) LNs. The procedure, depicted in Figure 5.1B, involved incubating LNs with micelles composed of the RGD lipid at 65°C for 2 h. Incorporation of the RGD-lipid into the LN was measured by emission at 389 nm, following excitation at 325 nm in HBS containing 1% Tween 20, and compared against a standard curve made with known amounts of the RGD-lipid.

The mean diameter of the LNs was characterized by dynamic light scattering (DLS) using a Nicomp 370 particle sizer for size distribution analysis. LNs were further characterized by a phosphate assay using the method of Fiske and Subbarow, and by fluorescence emission at 590 nm, upon excitation at 530 nm.

5.2.9 HPTS Loading

In order to track intracellular delivery of LN contents, the pH sensitive probe, 8-hydroxypyrene-1, 3, 6-trisulfonic acid (HPTS) (Invitrogen, Carlsbad, CA) was loaded into Non-targeted LN and 0.5% RGD-LN (i.e. HPTS-LN (55:45:0:0 mole:mole) and HPTS:RGD-LN (54.5:45:0:0.5 mole:mole)), were formed from lipid dispersed in 10 ml of HBS containing 40 mM HPTS, extruded and dialyzed three times for 12 h against 4 L HBS. The resulting HPTS:LNs were characterized by DLS, phosphorus content and HPTS fluorescence emission at 450 nm following excitation at 395 nm. The contribution from the MCA group of the RGD-lipid was found to be negligible at this wavelength.

5.2.10 Doxorubicin Loading

Doxorubicin was loaded into preformed non targeted LNs and 0.5 % RGD-LNs using the ammonium sulphate method of drug loading (Haran et al., 1993). Briefly, LNs were hydrated in 10 ml of 300 mM ammonium sulfate, extruded and dialyzed twice over 12 h against 150 mM NaCl. Phosphate assays were conducted to determine the amount of doxorubicin required to achieve a drug-to-lipid ratio of 0.2 (mole:mole). Doxorubicin was dissolved in 1 ml of 150 mM NaCl, and the appropriate volume was delivered to each solution of LNs. Doxorubicin and LNs were co-incubated at 55°C for 1 h to load the drug, then the free drug was removed by size exclusion chromatography, with 40 ml Sephadex G50 equilibrated in 150 mM NaCl. Doxorubicin-encapsulated LNs (Dox:LNs) eluted within the first 10 ml fraction and free doxorubicin eluted over the following 15 ml fraction. The resulting particles were sized by DLS, and assayed for phosphate content. The amount of encapsulated material was determined by RP-HPLC, using a standard curve made from the integrated peak area of doxorubicin's 280 nm UV absorbance. Free doxorubicin elutes on a 0-85% aqACN gradient at 15.8 min.

5.2.11 Doxorubicin Leakage Assay

The amount of doxorubicin that was retained in the LNs over time was measured by a doxorubicin leakage assay. Doxorubicin-loaded 0.5% RGD-LN and non-targeted LN (i.e. Dox:RGD-LN and Dox:LN), corresponding to a concentration of 0.25 mM free doxorubicin, were incubated with 30% (v/v) FBS, total volume 1.5 ml, at 37°C over 24 h. During this time, 100 µl was removed in duplicate at 0, 30 min, 1, 2, 5 and 24 h time

points. The sample was applied to a spin column of 750 μ l Sephadex G50, and centrifuged at 100 rpm for 1 min. One ml of 10% Triton X-100 (v/v) in 150 mM NaCl was added to the eluent in order to release the LN-entrapped doxorubicin. Doxorubicin content was subsequently assayed for fluorimetry, using the fluorescent emission of doxorubicin at 590 nm when compared to a standard curve made from free doxorubicin in 10% Triton X-100, 150 mM NaCl.

5.2.12 Cell Culture and LN Binding Assays

HUVEC, M21, and M21L cells were maintained and harvested for binding studies as described in Chapter 4 with minor modifications. Rhodamine-labeled LNs varying in their RGD content (i.e., containing between 0-5 mole% of the targeting lipid) were added to cells to construct binding isotherms (Figure 5.4). LNs were adjusted to have equivalent phosphate content by dilution with HBS, then added to cells at concentrations between 0 and 4 mM (total lipid content). The final volume was adjusted to 500 μ l with PBS/FBS. Cells were incubated with LNs for 1 h at either 4°C or 37°C. After incubation, unbound LNs were removed with 5 ml of FBS/PBS, followed by centrifugation at 1100 rpm for 5 min, repeated twice. Unfixed cells were kept on ice and immediately analyzed by flow cytometry using the same instrument protocol described in Section 4.2.3. The mean fluorescent intensity was plotted versus the concentration of LN. Statistical analyses were conducted using GraphPad InStat, Version 3.0. A Tukey-Kramer multiple comparisons test was used, with n values of 3, representing triplicate data points. P values greater than 0.05 were considered insignificant.

5.2.13 Cellular HPTS Uptake

HPTS-loaded, 0.5% RGD-targeted and non-targeted LNs were added to cells and incubated at 37°C for 0, 5, 15, 30 and 90 min time points. The cells were rinsed and assayed for cell-associated HPTS fluorescence by flow cytometry. At neutral pH, HPTS fluoresces green (excitation at 488 nm and emission at 519 nm). Acidification of the vesicles (pH ~6.5-7) was monitored by detecting blue fluorescent emission at 455 nm following excitation at 405 nm. The contribution of non-targeted HPTS-containing LNs to the observed cellular fluorescence was minimal and this value was subtracted from the fluorescence signals produced by RGD-LNs.

5.2.14 Doxorubicin Uptake into Cells as Determined by Flow Cytometry

The amount of doxorubicin entrapped inside the Dox:LNs was measured quantitatively by HPLC peak area integration and compared to a standard curve as described for the loading of doxorubicin (Section 5.2.10). Eighty μ M of doxorubicin (either encapsulated within the LN or as the free drug) was delivered to each aliquot of M21, M21L or HUVEC cells. The mixture was incubated for 90 min at 37°C then assayed for cell-associated doxorubicin fluorescence by flow cytometry.

5.2.15 LN Uptake into Cells as Observed by Microscopy

HUVEC cells were grown to confluence on four chambered glass slides (BD, Franklin Lakes, NJ). Cells were rinsed three times with PBS/FBS. 0.265 mM of doxorubicin was added for a final volume of 125 μ l. For HPTS uptake, 1.36 mM (total lipid concentration) was added with a final volume of 200 μ l. LNs or free drug were added to the cells, the mixture was incubated at 37°C for 30 min, rinsed 2X with PBS/FBS, the cells were then fixed with 3.5% paraformaldehyde in PBS for 15 min, and rinsed once again with PBS/FBS. Immediately before imaging, chambers were removed and slides were prepared using Vectashield mounting media (Vector Laboratories, Burlingame, USA) containing the blue nuclear stain, 4',6-diamidino-2-phenylindole (DAPI). Images were captured using a Zeiss Axiovert 200 fluorescence microscope equipped with a Retiga 200R camera. Those acquired under a bright field used a 0.3 s exposure time and in the fluorescent field were acquired using three fluorescent filters with the following exposure times: red 3.5 s, green 5.5 s, DAPI 0.5 s.

5.3 Results and Discussion

5.3.1 Synthesis of Targeting Lipids

Of the four RGD-containing targeting ligands synthesized (see Figure 5.3), compound IV had the highest yield and best analytical characteristics. The MCA fluorescent-labeling molecule was also found to be useful during purification steps, since the ability to detect the compound facilitated chromatographic fractionation. Further, detection by the MCA fluorophore in compound IV was found to be essential once the targeting lipid was incorporated into an LN.

A summary of the properties of the synthesized compounds which lead to the selection of compound IV as the lead RGD-lipid can be found in Table 5.2, which relates their production, characterization and LN formulation properties.

Table 5.2 Summary of RGD-lipids synthesized

Compound	Synthesis	Length of spacer(Å) [†]	Purity	Yield [*]	Conclusion
I	Facile, cost effective	12.0	>85% (TLC)	~10mg (14 %)	Poor characterization Induces LN aggregation
II	Difficult	97.5	<50% (TLC)	<1 %	Difficult to analyze Low yield
III	Facile, cost effective	43.0	> 85%	27mg (22%)	Excellent synthesis Difficult to analyze
IV	Facile	75.7	>95%	40.8mg (42%)	Lead candidate for LN formulation

[†]total bond length from phosphate to ε-amine of cRGDFK

^{*}calculated from peptide+spacer to the lipid coupling

RGD-LNs made with compound I did not allow incorporation of RGD-lipid at levels higher than one percent of the total lipid composition. This is because the resulting LNs

produced a non-uniform size distribution with evidence of aggregation. LNs made with less than one mole percent of the targeting lipid could be made without aggregation, however definitive measures of the content in the resulting LN could not be achieved because the RGD-lipid compound was not labeled.

Analytical difficulties were also encountered for compounds II and III, namely that, upon lipid conjugation, they became increasingly difficult to identify by standard methods such as HPLC or TLC. TLC analyses of compounds I-III were based on iodine staining only. The use of a fluorescent label as shown in compound IV enabled accurate analytical characterization. Ionization by ESI-MS was ineffective for compounds I and II. The use of a PEG-based spacer used in compounds III and IV greatly improved ESI-MS ionization, enabling a defined mass to confirm the identity of both compounds. It is also important to note that the PEG-lipid conjugates used in this study differ from commonly used PEG polymers, which are an average molecular weight of PEG repeats. The compounds synthesized here employ homogenous spacers of a defined molecular weight. Table 5.2 also lists the approximate length of the spacer based on the bond distances between the peptide and lipid head group. This estimate does not consider the bending and rotation of the spacer in aqueous solutions, and could be better estimated using an SPR-based technique (Jeppesen et al., 2001) to describe the extension of PEG-spacers in water. Using this method, the length of typical PEG₂₀₀₀ spacers was found to be approximately 200Å.

5.3.2 RGD-LN Characterisation

The RGD-lipid chosen for further studies had good formulation characteristics. When combined with other lipids such as DSPC, cholesterol, and a fluorescently labeled—

PE (Rhodamine-PE), LNs exhibiting a regular Gaussian size distribution with an average diameter of approximately 100 nm could be formed using up to 5 mole % of the RGD-lipid without obvious signs of aggregation. As summarized in Table 5.3, the LN particle size increased slightly, with a moderate increase in the standard deviation, when 2.5 or 5 mole % of the RGD-lipid were included in the formulation. The apparent binding constants (expressed as K_d values) shown in Table 5.3 were calculated from the specific binding at 4°C (data presented in Figure 5.4). It is important to note that the K_d value observed accounts for a sum of several possible cellular processes and has been simplified to describe the binding of RGD-LNs to live HUVEC cells.

Table 5.3 Characterization of RGD-LNs

LN formulation	Number of RGD molecules/LN [‡]	Size (nm)	HUVEC Binding K_d (nM) ^{*†}
Non-targeted	0	102.4 ± 27.3	n/a
0.5% RGD	423	102.2 ± 32.0 nm	2.59 ± 0.58
1% RGD	846	94.2 ± 20.7 nm	1.98 ± 0.35
2.5% RGD	2113	128.9 ± 68.0 nm	0.38 ± 0.07
5 % RGD	4226	117.4 ± 66.0 nm	0.59 ± 0.02

‡ this value was estimated using the assumption that 100% of the RGD-lipid was incorporated into the LN, and that 57% of that value reside on the outer leaflet of the LN lipid bilayer

* error is expressed as ± the standard error of the estimate from non linear regression

† the K_d value is expressed as the concentration of RGD-LN required to achieve half saturation of HUVEC cells and is derived from the data presented in Figure 5.4

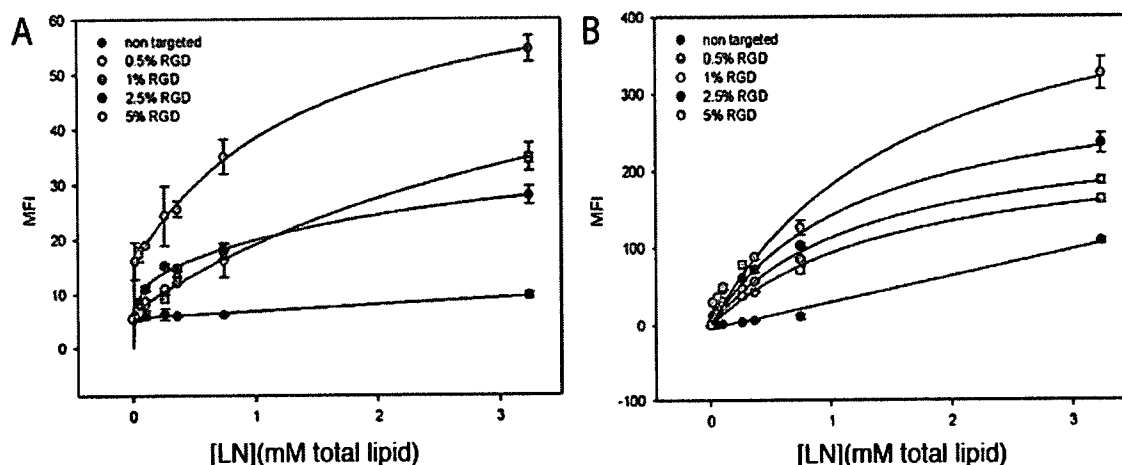


Figure 5.4 RGD-LN binding by HUVECs at 4°C and 37°C

A) Saturation curves describing the binding of LN to HUVEC following a one hour incubation at 4°C. The LNs contain between 0-5 mole percent RGD-lipid. B) The same binding experiment conducted at 37°C.

The apparent K_d values measured from the data presented in Figure 5.4 decrease as the proportion of RGD-lipid is increased to 2.5 mole%. The decrease in observed K_d values as the amount of RGD per LN is increased suggests that the improved binding of the LN can be attributed to the increased RGD valency of the LN. These findings are consistent with results published by Montet and colleagues that reported improved binding for multivalent presentations of the RGD-ligand compared to monovalent (Montet et al., 2006). The minor increase in K_d when the RGD-lipid is incorporated at the 5 mole% level could arise if the RGD-lipid becomes somewhat masked when incorporated at excessive levels. For example, lateral segregation of the RGD-lipid into dimers or larger aggregates may occur. It can also be observed from the data in Figure 5.4A that the B_{max} values observed for the 5 mole% RGD-LNs is higher than the other formulations by 1.7 fold, which could be due to some limited aggregation of the RGD-LNs at these high contents of RGD-lipid.

5.3.3 Methods for Producing RGD-LNs

The post-insertion and formulation methods were compared with regard to their ability to incorporate RGD-lipid into LNs (refer to Figure 5.1 for a schematic of these methods). In order to quantitate the amount of the RGD-lipid that was incorporated into the LN by either method, the fluorescent emission and excitation spectra were obtained for the RGD-lipid (Figure 5.6A). The amount of the targeting ligand within Type 1 and Type 2 RGD-LNs was subsequently measured by fluorometry conducted in the presence of 1% Tween 20 in order to disrupt the LN structure. A linear increase in the fluorescence signal corresponded to increasing amounts of RGD-LNs, therefore, a standard curve was established from known amounts of the RGD-lipid in the presence of non-targeted LNs. The amount of RGD-lipid present in LNs made by the two different techniques was calculated as shown in Figure 5.6B.

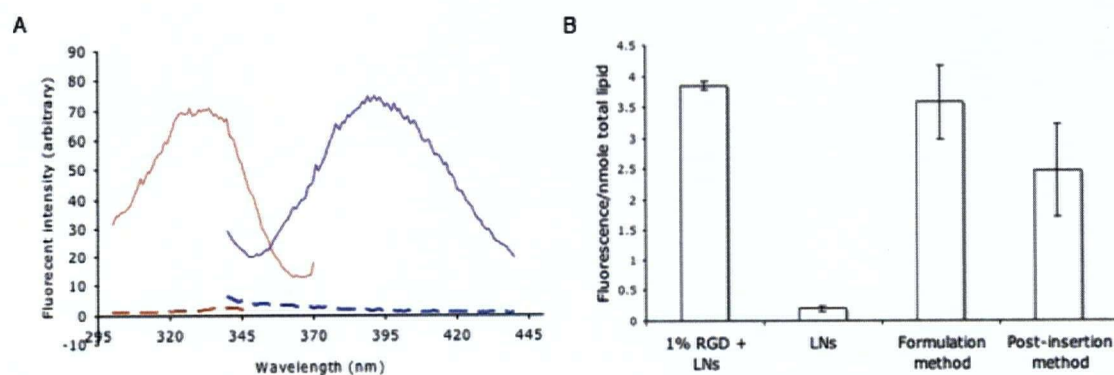


Figure 5.6 Comparison of formulation and post-insertion methods for incorporating RGD-lipids into LNs

A) Excitation (red) and emission (blue) spectra obtained for RGD-LNs with the RGD-lipid embedded in the bilayer. The spectra for non-targeted LNs are shown by dashed lines. B) Fluorescent measurements of the relative amounts of the RGD-lipid in RGD-LNs made by either the formulation method or the post-insertion method. The starting concentration of RGD-lipid (1 mole%) plus non-targeted LNs represents the maximum possible RGD-lipid incorporation that was used before the RGD-lipid was incorporated into an LN.

When compared to the starting material (i.e. RGD-lipid + LN) it was found that the amount of RGD-lipid incorporated into RGD-LNs made via the post-insertion method was slightly reduced ($p < 0.05$). No significant decrease in the amount of RGD-lipid was detected for RGD-LNs made by the formulation method ($p > 0.05$). Because the formulation method was more straightforward and led to effectively complete insertion it was the method of choice in subsequent experiments.

5.3.4 Drug Retention in RGD-Targeted LNs

In some cases, it has been shown that when targeting ligands are incorporated into LNs, the permeability of the LN membrane to the drug may also increase (Ishida et al., 1999; Nallamotheu et al., 2006). For this reason, the release of a commonly used anti-cancer drug, doxorubicin, from LN containing RGD-lipid was investigated.

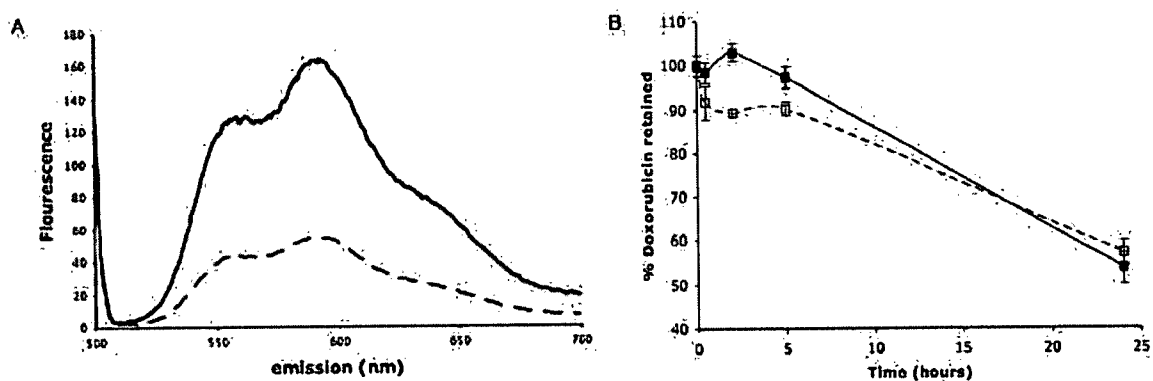


Figure 5.7 Doxorubicin is retained equally well in RGD-LNs and non-targeted LNs

A) Emission spectrum (following excitation at 490 nm) of 1.5 μg of doxorubicin dissolved in water (dashed line) or 10% Triton X-100 (solid line). B) Release of doxorubicin from RGD-LNs made via the formulation method (solid line) and non-targeted LNs (dashed line) over time. Error is given as \pm the standard deviation of three data points from the average doxorubicin emission (590 nm) determined in the presence of 10% Triton X-100.

Doxorubicin was loaded into LN and RGD-LN (containing 1 mole% RGD-lipid) as indicated in Methods and the LN were incubated in aqueous buffer over 24 h. At specified times aliquots were withdrawn, free drug removed by the spin column procedure indicated in Methods and the amount of doxorubicin remaining in the LN, upon release with Triton X-100, was assayed (see Methods). Little difference could be observed between the release of doxorubicin from RGD-LNs or non-targeted LNs (Figure 5.7B) indicating that the RGD-lipid did not significantly ($p>0.05$) enhance the permeability of the LN membrane to doxorubicin over a 24 hour period.

5.3.5 Cellular Uptake and Processing of RGD-LNs.

The internalization and subsequent acidification of an RGD-LN within the cell, was tracked with the pH-sensitive, membrane impermeable probe HPTS. When HPTS is acidified, the emission spectrum shifts to shorter wavelengths. HPTS was loaded into LNs as indicated in Methods and the LNs were added to HUVECs. From the fluorescent microscope images, green fluorescence in punctate cytoplasmic vesicles could be observed within 10 min when delivered by RGD-LNs, but not by non-targeted LNs (Figure 5.8A and B). The signal detected after a 40 min incubation (Figure 5.8D) is more diffuse, suggesting that the fluorophore escapes the endosome at some time between 10 and 40 min following association of the RGD-LN with the HUVEC.

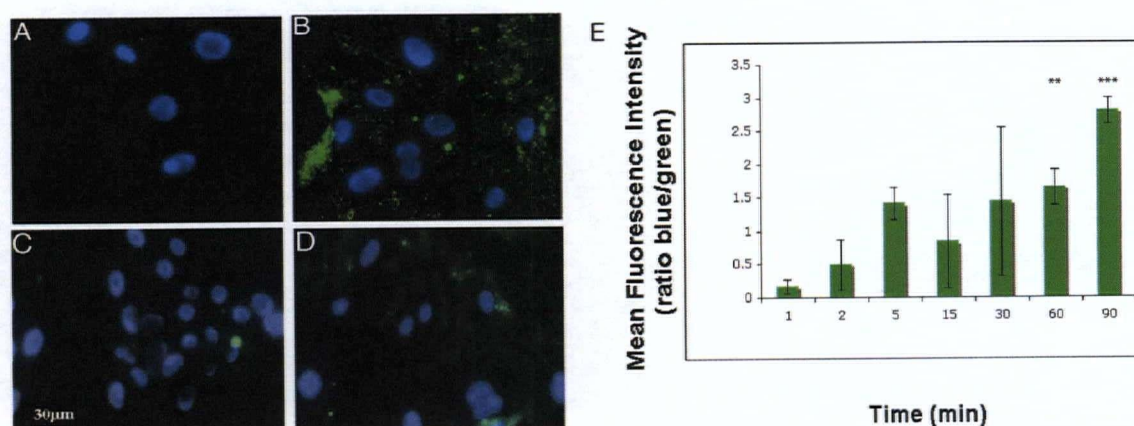


Figure 5.8 RGD-LNs are internalized and acidified by HUVEC

Panels A-D show fluorescent microscopy images demonstrating LN-associated HPTS uptake by HUVEC, while panel E reflects data obtained by flow cytometry which shows that the LN experiences an increasingly acidic environment as reflected by a progressive blue shift in the HPTS fluorescence. LNs loaded with HPTS were co-incubated with HUVEC cells at 37°C. A) Non-targeted LNs, 10 min incubation B) 1% RGD-targeted LNs, 10 min incubation. C) and D) results from a 40 min incubation, with non targeted and RGD-LNs, respectively. E) Ratio of blue fluorescence to green fluorescence for cell-associated HPTS-containing RGD-LNs over time as measured by flow cytometry (see text). Error represents the standard deviation of a series of 3 independent experiments. The significance level compared to the one minute time point is marked as follows: ** indicating $p < 0.01$ and *** indicating $p < 0.001$.

Figure 5.8E indicates the acidification as a function of incubation time using flow cytometric detection of neutral endocytotic environments indicated by green fluorescent cells (excitation at 495 nm, emission at 519 nm) or an acidic environment indicated by blue fluorescent cells (excitation at 405 nm, emission at 455 nm). These results suggest that internalization of the particle commences as early as 5 min, and a significant increase in the relative blue fluorescence is observed after 60 min. From this data it is suggested that, upon binding, the contents within the particle are processed in a manner that coincides with endosomal maturation.

5.3.6 *In vitro* Drug Delivery by RGD-LNs

In section 5.3.3 it was shown that, once entrapped within an LN particle, more than 50% of doxorubicin is retained following incubation at 37°C for 24 h. In this section, it is shown that RGD-LNs can deliver doxorubicin to the cytosol of HUVECs. Fluorescent microscope images comparing the delivery of doxorubicin by LNs versus the free drug are presented in Figure 5.9A-D. As expected for an *in vitro* cellular system with a hydrophobic drug that has affinity for the cell nucleus, the free drug rapidly permeates the plasma membrane and stains nuclear material, thus co-localizing with the nuclear stain, DAPI (Figure 5.9A). Conversely, 1% RGD-LNs deliver doxorubicin to cytoplasmic compartments. Doxorubicin delivered by non-targeted LNs show minimal background staining with uptake levels similar to the saline control.

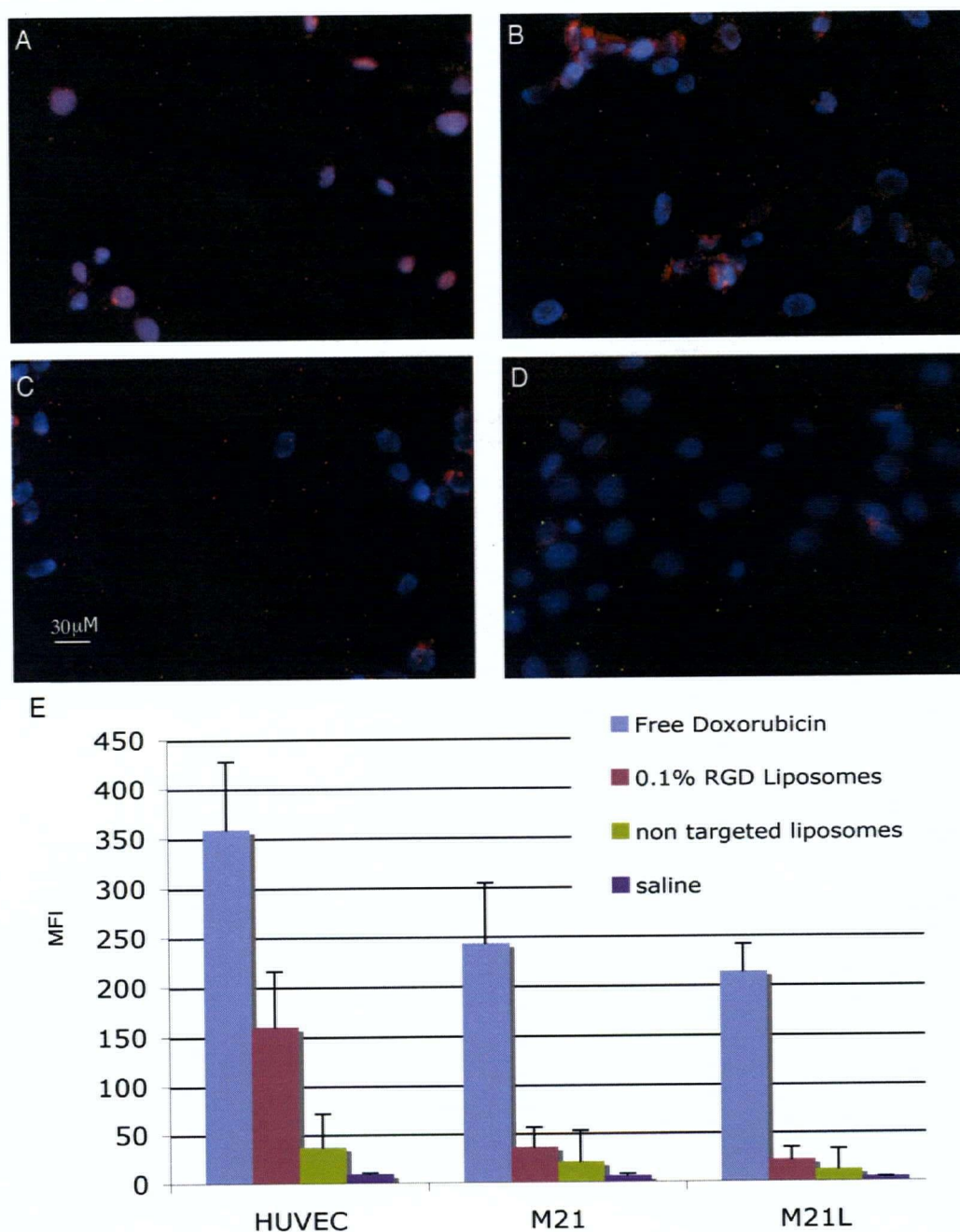


Figure 5.9 Uptake of doxorubicin presented in the free form, in non-targeted LN or RGD-LN by cells expressing various levels of the $\alpha_v\beta_3$ integrin

A-D) Doxorubicin uptake by HUVEC cells as monitored by fluorescence microscopy following a 30 min incubation at 37°C with the same amount of doxorubicin (0.265 mM) delivered to cells either as A) Free drug, B) 1% RGD-LN, C) Non-targeted LN or D) Saline background control. E) Doxorubicin uptake (as measured by flow cytometry) by three different $\alpha_v\beta_3$ -expressing cell lines following addition of 0.08 mM of doxorubicin in either free, RGD-LN or non-targeted LN form to cells and incubation for one hour at 37°C prior to analysis.

The ability of RGD-LNs to deliver doxorubicin to $\alpha_v\beta_3$ -expressing cells is shown in the flow cytometry experiments summarized in Figure 5.9E. It was shown in Chapter 4 that HUVECs express approximately 263,000 $\alpha_v\beta_3$ integrins per cell, whereas M21 and M21L melanoma cells express approximately 56,700 and 1,400 integrins per cell, respectively. RGD-LNs deliver increased amounts of doxorubicin to HUVECs compared to non-targeted LN ($p < 0.05$), and appear to deliver modestly higher amounts to M21 cells over the non-targeted LNs, however this increase is not statistically significant ($p > 0.05$). In contrast, M21L cells that express a relatively low amount of the receptor do not show enhanced uptake of doxorubicin-containing RGD-LN.

5.3.7 Relation to Existing RGD-LN Data

In this section, the results presented in the previous sections are summarized and related to RGD-LNs previously used *in vivo*. The discussion focuses on the four *in vivo* studies on RGD-LNs summarized in Table 5.1. In the present work, it was found that a high synthetic yield and good analytical properties enabled the compound, cRGDfK-PEG₂-K(MCA)-PEG₂-DSPE, to be quantitatively formulated into LNs at the time of manufacture and subsequently used to examine the effects of RGD-targeted LNs *in vitro*. Synthesis of RGD-lipid constructs without the fluorescent label suffered the effects of low overall yield, poor analytical characteristics and inaccurate formulation. Since none of the studies listed in Table 5.1 use a fluorescent label or other means of accurately tracing the incorporation of RGD-lipids into LNs, it is likely that the actual amount of RGD in the formulation is unknown. This uncertainty could explain the different pharmacokinetic effects that were

observed in these studies, namely that some are rapidly cleared from the body and some are not. Furthermore, since quantitative analytical data has not been provided in any of these studies, it is possible that some unreacted or impure material may have been included in their LN formulations. In such case, the mole percent of the RGD-lipid would change, which could potentially affect the clearance of the particle from the circulation.

In the work published by Schifellers *et al*, a Cilengitide® analogue modified with a thioacetyl group for incorporation into pre-formed LNs *via* the surface coupling method was used. The authors assume that all of the peptide is conjugated to a membrane-embedded maleimide-PEG-lipid, but do not address how much RGD-PEG-lipid is actually present in the membrane. Furthermore, although the resulting thioether bond that joins the maleimide-PEG-lipid to the peptide is not stable, and reverses in aqueous environments (Dunphy and Linder, 1998), which may be an issue for production and storage of the drug if it were to progress to the clinic.

Like many other targeted LN formulations, RGD-LNs produced by both Xiong and Dubey *et al*. show equivalent circulation lifetimes to non-targeted LNs, which is different from the studies published by Holig *et al* who claim that LNs containing 0.1 mole % of the RGD-lipid are not rapidly cleared from the circulation, however, LNs with 1 mole% of the RGD-lipid are rapidly cleared. Without knowing the true mole percentage of the targeting lipid in the LN at the time of *i.v.* administration, it is difficult to discuss the effect that the targeted LN has *in vivo*.

The results presented here show that incorporation of the RGD-lipids synthesized here in an LN formulation do not result in the leakage of entrapped doxorubicin. Doxorubicin is an amphiphilic drug that is well-retained in many different LN formulations

(Gabizon et al., 2006), therefore it is perhaps not surprising that a good release profile was achieved using targeted systems.

The experiments with LN containing HPTS demonstrate that $\alpha_v\beta_3$ integrin-expressing cells rapidly internalize RGD-LNs. Using intravital microscopy, Janssen and colleagues have shown that the RGD-targeted imaging agents associate with tumor vasculature within 30 min (Janssen et al., 2003). If LNs can be engineered to bind their target rapidly and become rapidly internalized, without toxic or immunogenic effects, extended circulation lifetimes may not be as important for RGD-LNs as for non-targeted LNs. In a related vein, since the $\alpha_v\beta_3$ integrin target is exposed to the vasculature, it is a highly accessible target for drugs that are administered via the circulatory system. This differs from targets within the tumor tissue, which require extravasation from the bloodstream to enable interactions between LN and the targeted cell.

6 Future Work

6.1 Pharmacokinetics of RGD-LNs

In the previous chapter, the *in vitro* properties of RGD-LNs were investigated. It is expected that these results will lead to the use of these RGD-LNs in animal tumor models. Given that the use of an RGD-targeting entity can promote LN clearance *in vivo*, the pharmacokinetics of these compounds will be of significant concern (Holig et al., 2004). Despite the publication of over 50 *in vivo* efficacy studies of RGD-targeted therapeutics (being either protein, nanoparticulate or small molecule conjugates), little is known about the PK effects of the various RGD motifs *in vivo* (Temming et al., 2005). Perhaps the best PK characterization of RGD-targeted therapeutics has been produced from the use of tumor imaging agents (reviewed in Haubner et al., 2003). In this application, the uptake of RGD-conjugates by the liver or the rapid elimination of the compound by renal filtration will likely affect the quality of the image produced. Efforts to minimize hepatic uptake and maximize the tumor to background signal have included modification of the RGD-peptide-imaging agent with a hydrophilic moiety such as a sugar (Haubner et al., 2001) or PEG chain (Chen et al., 2004c). Nonetheless, the PK behavior of RGD-PEG-imaging agents is not entirely predictable. For example, it has been shown that an ^{125}I -PEG-RGD conjugate is taken up by the liver and cleared more rapidly than the non-pegylated version (Chen et al., 2004c) yet a contradictory effect is observed for ^{64}Cu -RGD conjugates in which pegylation does not significantly affect their hepatic uptake but improves upon their tumor retention (Chen et al., 2004a).

The PK behavior of RGD-LNs is different than imaging agents mainly because of the large difference in the size of the LN particles, which limits renal clearance of the LN systems. However, large particles can also lead to enhanced accumulation by the RES due to opsonization of the particle and subsequent uptake by macrophages. Furthermore, the PK characteristics can be complicated by the fact that cells of the RES express the $\alpha_v\beta_3$ integrin albeit in relatively low amounts (Singh et al., 2001). Thus, it will be important to establish a distinction between non-specific clearance effects and RGD:integrin binding to non-targeted cells. A potential *in vivo* experiment to address this concern might include a receptor quantitation assay such as the one presented in Chapter 4. In this case, the number of $\alpha_v\beta_3$ integrins on cells of the RES that affect the biodistribution of the RGD-LN particles within the body. Flow cytometric analysis of both targeted and non-targeted cells after LN administration may prove useful to aid this understanding.

6.2 Anti-tumor Efficacy of RGD-Targeted Therapeutics

All of the published studies describing the ability of the RGD-motif to target therapeutics to the disease sites report some degree of efficacy leading to the continued interest in the RGD motif for vascular targeting (Temming et al., 2005). The new generation RGD-containing constructs will likely employ multivalent display of the RGD sequence since it is well demonstrated that increased efficacy has been attributed to increasing the valency of the RGD-moiety per agent targeted (Li et al., 2007b; Montet et al., 2006; Wu et al., 2005).

It may also be expected that the treatment of tumors that are resistant to conventional chemotherapy regimes, will benefit from RGD-mediated delivery, since RGD-doxorubicin conjugates can bestow efficacy against the doxorubicin-insensitive C26 colon carcinoma cell line (Schiffelers et al., 2003).

The distinction between anti-tumor efficacy due to direct destruction of tumor cells and efficacy through an anti-angiogenesis mechanism will be an important issue in future efficacy studies. Good evidence has been produced both by Pastorino et al, that shows a synergistic effect of targeting (Pastorino et al., 2006). The finding by Janssen and colleagues that RGD-LNs cluster in the tumor blood vessels while RAD-LNs and non-targeted LNs are extravasated and dispersed in tumor tissue further suggests that this kind of distinction can be made (Janssen et al., 2003).

In Chapter 5, it was established that the RGD-LNs that exhibited the highest level of binding contained 2.5 mole% or greater of the RGD-lipid. Whether these systems will exhibit the best therapeutic properties remains to be determined. As indicated above, it is possible that the presence of high levels of RGD targeting ligands will result in more rapid clearance by the RES, which may effectively reduce the amount of LN that can access the tumor vasculature. Future studies must establish the optimum levels of RGD targeting ligands that are compatible with long circulation lifetimes, enhanced delivery to tumor sites and maximum association with tumor vasculature. In order to be therapeutically advantageous, such systems must clearly exhibit improved efficacy over non-targeted LN formulations that are not bound to and internalized by the target cells.

6.3 Choice of Drug to be Delivered

The drug that is encapsulated within the RGD-targeted LN is also an important variable that will have to be optimized in future studies. As presented in Chapter 5, the incorporation of RGD-lipids in to LN formulations did not significantly change the drug release properties of doxorubicin, which is generally considered not to be a cell-cycle specific drug (Gardner, 2000). Cell-cycle specific drugs such as vinorelbine have been shown to be synergistic with anti-angiogenic agents when administered as a free drug and may be better suited in an LN formulation targeted to tumor neovasculature (Han et al., 2005). In addition, the release rates of cell-cycle specific drugs from within the LN have been optimized for one tumor model and correlated with improved efficacy (Johnston et al., 2006).

Finally, a second variable to be optimized in targeted LNs is the drug-to-lipid ratio, which can dramatically affect the potency of the LN system. This may be important if the density of integrins on target tissue is relatively low, where targeted LN that contains high levels of highly potent drug would be most logically employed. For example, vincristine is a highly potent drug as compared to doxorubicin, as the dose at which maximum efficacy is observed (with reasonable toxicity levels) in mice is approximately 20 mg/kg for doxorubicin as compared to only 2 mg/kg for vincristine. Thus vincristine is approximately ten times more potent than doxorubicin, and it has been calculated that, for LN loaded with vincristine at a drug-to-lipid ratio (wt/wt) of 1, only 5 LN would be required to kill a target cell (Johnston et al., 2006).

Optimization of defined RGD-LNs such as those described in this thesis will likely be achieved by determination of the most appropriate formulation of the drug *in vivo* as well as *in vitro*.

6.4 Bimodal and Multifaceted Chemotherapy Regimes

RGD-LNs may be considered a bimodal chemotherapy regime given that the RGD targeting ligand is anti-angiogenic and that LNs carry a cytotoxic drug. Using bimodal strategies that interfere with different cellular processes may prove to be particularly beneficial in the treatment of drug resistant tumors (Pastorino et al., 2006).

If drug-loaded RGD-LNs were engineered to contain an imaging agent, a chemotherapy regime could include the simultaneous visualization and treatment of a tumor. This scenario is likely, since RGD-based imaging agents have progressed rapidly towards the clinic (Beer et al., 2006). The findings that these agents are non-toxic and can deliver low-dose positron emission to the site of a tumor for example, have resulted in the production of PET images superior to those acquired by non-targeted systems. The design of LN systems that contain radio-labeled or fluorescently labeled agents is relatively straightforward and offers the possibility of directly visualizing the biodistribution of RGD-targeted LN in relation to target tissue.

Overall, it is anticipated that further research and optimization of the nano-design of targeted drug delivery vehicles will lead to advanced chemotherapy regimes with improved therapeutic outcomes for cancer patients.

References

- Adler-Moore, J., 1994. AmBisome targeting to fungal infections. *Bone Marrow Transplant*, 14 Suppl 5: S3-7.
- Albelda, S.M. et al., 1990. Integrin distribution in malignant melanoma: association of the beta 3 subunit with tumor progression. *Cancer Res*, 50(20): 6757-64.
- Albert, J.M. et al., 2006. Integrin alpha v beta 3 antagonist Cilengitide enhances efficacy of radiotherapy in endothelial cell and non-small-cell lung cancer models. *Int J Radiat Oncol Biol Phys*, 65(5): 1536-43.
- Allen, T.M. and Chonn, A., 1987. Large unilamellar liposomes with low uptake into the reticuloendothelial system. *FEBS Lett*, 223(1): 42-6.
- Allen, T.M. and Cullis, P.R., 2004. Drug delivery systems: entering the mainstream. *Science*, 303(5665): 1818-22.
- Allen, T.M. and Everest, J.M., 1983. Effect of liposome size and drug release properties on pharmacokinetics of encapsulated drug in rats. *J Pharmacol Exp Ther*, 226(2): 539-44.
- Allen, T.M. and Martin, F.J., 2004. Advantages of liposomal delivery systems for anthracyclines. *Semin Oncol*, 31(6 Suppl 13): 5-15.
- Allen, T.M., Sapra, P. and Moase, E., 2002. Use of the post-insertion method for the formation of ligand-coupled liposomes. *Cell Mol Biol Lett*, 7(3): 889-94.
- Ambegia, E. et al., 2005. Stabilized plasmid-lipid particles containing PEG-diacylglycerols exhibit extended circulation lifetimes and tumor selective gene expression. *Biochim Biophys Acta*, 1669(2): 155-63.
- Arap, W. et al., 2002. Targeting the prostate for destruction through a vascular address. *Proc Natl Acad Sci U S A*, 99(3): 1527-31.
- Balasubramanian, S. and Kuppuswamy, D., 2003. RGD-containing peptides activate S6K1 through beta3 integrin in adult cardiac muscle cells. *J Biol Chem*, 278(43): 42214-24.
- Bangham, A.D., Standish, M.M. and Watkins, J.C., 1965. Diffusion of univalent ions across the lamellae of swollen phospholipids. *J Mol Biol*, 13(1): 238-52.
- Bednar, B. et al., 1997. Flow Cytometric Measurement of Kinetic and Equilibrium Binding Parameters of Arginine-Glycine-Aspartic Acid Ligands in Binding to Glycoprotein IIb/IIIa on Platelets. *Cytometry*, 28: 58-65.

- Beer, A.J. et al., 2006. Positron emission tomography using [18F]Galacto-RGD identifies the level of integrin $\alpha(v)\beta_3$ expression in man. *Clin Cancer Res*, 12(13): 3942-9.
- Bertucci, C. and Domenici, E., 2002. Reversible and covalent binding of drugs to human serum albumin: Methodological approaches and physiological relevance. *Current Medicinal Chemistry*, 9(15): 1463-1481.
- Boudreau, N., Andrews, C., Srebrow, A., Ravanpay, A. and Cheresch, D.A., 1997. Induction of the angiogenic phenotype by Hox D3. *J Cell Biol*, 139(1): 257-64.
- Bowser, M.T. and Chen, D.D.Y., 1998. Higher order equilibria and their effect on analyte migration behavior in capillary electrophoresis. *Analytical Chemistry*, 70(15): 3261-3270.
- Brassard, D.L. et al., 1999. Integrin $\alpha(v)\beta_3$ -mediated activation of apoptosis. *Exp Cell Res*, 251(1): 33-45.
- Brooks, P.C., 1996. Role of integrins in angiogenesis. *Eur J Cancer*, 32A(14): 2423-9.
- Brooks, P.C., Clark, R.A. and Cheresch, D.A., 1994a. Requirement of vascular integrin $\alpha v \beta_3$ for angiogenesis. *Science*, 264(5158): 569-71.
- Brooks, P.C. et al., 1994c. Integrin $\alpha v \beta_3$ antagonists promote tumor regression by inducing apoptosis of angiogenic blood vessels. *Cell*, 79(7): 1157-64.
- Buckley, C.D. et al., 1999. RGD peptides induce apoptosis by direct caspase-3 activation. *Nature*, 397(6719): 534-9.
- Busch, M.H.A., Boelens, H.F.M., Kraak, J.C. and Poppe, H., 1997a. Vacancy affinity capillary electrophoresis, a new method for measuring association constants. *Journal of Chromatography A*, 775(1-2): 313-326.
- Busch, M.H.A., Carels, L.B., Boelens, H.F.M., Kraak, J.C. and Poppe, H., 1997b. Comparison of five methods for the study of drug-protein binding in affinity capillary electrophoresis. *Journal of Chromatography A*, 777(2): 311-328.
- Busch, M.H.A., Kraak, J.C. and Poppe, H., 1997c. Principles and limitations of methods available for the determination of binding constants with affinity capillary electrophoresis. *Journal of Chromatography A*, 777(2): 329-353.
- Castel, S. et al., 2001. RGD peptides and monoclonal antibodies, antagonists of $\alpha(v)$ -integrin, enter the cells by independent endocytic pathways. *Lab Invest*, 81(12): 1615-26.
- Chen, X. et al., 2004a. Pegylated Arg-Gly-Asp peptide: ^{64}Cu labeling and PET imaging of brain tumor $\alpha v \beta_3$ -integrin expression. *J Nucl Med*, 45(10): 1776-83.

- Chen, X. et al., 2004b. MicroPET imaging of breast cancer alphav-integrin expression with ^{64}Cu -labeled dimeric RGD peptides. *Mol Imaging Biol*, 6(5): 350-9.
- Chen, X., Park, R., Shahinian, A.H., Bading, J.R. and Conti, P.S., 2004c. Pharmacokinetics and tumor retention of ^{125}I -labeled RGD peptide are improved by PEGylation. *Nucl Med Biol*, 31(1): 11-9.
- Chen, X., Plasencia, C., Hou, Y. and Neamati, N., 2005. Synthesis and biological evaluation of dimeric RGD peptide-paclitaxel conjugate as a model for integrin-targeted drug delivery. *J Med Chem*, 48(4): 1098-106.
- Cheresh, D.A., 1987. Human endothelial cells synthesize and express an Arg-Gly-Asp-directed adhesion receptor involved in attachment to fibrinogen and von Willebrand factor. *Proc Natl Acad Sci U S A*, 84(18): 6471-5.
- Cheresh, D.A. et al., 1987. An Arg-Gly-Asp-directed receptor on the surface of human melanoma cells exists in an divalent cation-dependent functional complex with the disialoganglioside GD2. *J Cell Biol*, 105(3): 1163-73.
- Cho, M.J. and Juliano, R., 1996. Macromolecular versus small-molecule therapeutics: drug discovery, development and clinical considerations. *Trends Biotechnol*, 14(5): 153-8.
- Choi, J.S., MacKay, J.A. and Szoka, F.C., Jr., 2003. Low-pH-sensitive PEG-stabilized plasmid-lipid nanoparticles: preparation and characterization. *Bioconjug Chem*, 14(2): 420-9.
- Colton, I.J., Carbeck, J.D., Rao, J. and Whitesides, G.M., 1998. Affinity capillary electrophoresis: A physical-organic tool for studying interactions in biomolecular recognition. *Electrophoresis*, 19(3): 367-382.
- Connors, K.A., 1987. Binding Constant. The Measurement of Molecular Complex Stability. John Wiley & Sons, New York.
- Daugherty, A.L. and Mersny, R.J., 2006. Formulation and delivery issues for monoclonal antibody therapeutics. *Adv Drug Deliv Rev*, 58(5-6): 686-706.
- Dechantsreiter, M.A. et al., 1999. N-Methylated cyclic RGD peptides as highly active and selective $\alpha(\text{V})\beta(3)$ integrin antagonists. *J Med Chem*, 42(16): 3033-40.
- Dhananjaya, K.V. and Antony, A., 1988. Pharmacokinetics and chemotherapeutic efficacy of adriamycin encapsulated in immunoliposomes against avian myeloblastosis virus infection. *J Virol Methods*, 19(2): 121-9.

- Doi, K. et al., 2007. Enhanced angiogenesis by gelatin hydrogels incorporating basic fibroblast growth factor in rabbit model of hind limb ischemia. *Heart Vessels*, 22(2): 104-8.
- Dubey, P.K., Mishra, V., Jain, S., Mahor, S. and Vyas, S.P., 2004. Liposomes modified with cyclic RGD peptide for tumor targeting. *J Drug Target*, 12(5): 257-64.
- Dunphy, J.T. and Linder, M.E., 1998. Signalling functions of protein palmitoylation. *Biochim Biophys Acta*, 1436(1-2): 245-61.
- Fanali, S., 1997. Controlling enantioselectivity in chiral capillary electrophoresis with inclusion-complexation. *Journal of Chromatography A*, 792(1-2): 227-267.
- Fenske, D.B., MacLachlan, I. and Cullis, P.R., 2002. Stabilized plasmid-lipid particles: a systemic gene therapy vector. *Methods Enzymol*, 346: 36-71.
- Folkman, J., 1990. What is the evidence that tumors are angiogenesis dependent? *J Natl Cancer Inst*, 82(1): 4-6.
- Forssen, E.A and Tokes, Z.A., 1981 Use of anionic liposomes for the reduction of chronic doxorubicin-induced cardiotoxicity. *Proc Natl Acad Sci USA* 78(3): 1873-7.
- Friedlander, M. et al., 1995. Definition of two angiogenic pathways by distinct α v integrins. *Science*, 270(5241): 1500-2.
- Friess, H. et al., 2006. A randomized multi-center phase II trial of the angiogenesis inhibitor Cilengitide (EMD 121974) and gemcitabine compared with gemcitabine alone in advanced unresectable pancreatic cancer. *BMC Cancer*, 6: 285.
- Gabizon, A. et al., 1994. Prolonged circulation time and enhanced accumulation in malignant exudates of doxorubicin encapsulated in polyethylene-glycol coated liposomes. *Cancer Res*, 54(4): 987-92.
- Gabizon, A., Goren, D., Fuks, Z., Meshorer, A. and Barenholz, Y., 1985. Superior therapeutic activity of liposome-associated adriamycin in a murine metastatic tumour model. *Br J Cancer*, 51(5): 681-9.
- Gabizon, A.A., Shmeeda, H. and Zalipsky, S., 2006. Pros and cons of the liposome platform in cancer drug targeting. *J Liposome Res*, 16(3): 175-83.
- Gagne, J.F., Desormeaux, A., Perron, S., Tremblay, M.J. and Bergeron, M.G., 2002. Targeted delivery of indinavir to HIV-1 primary reservoirs with immunoliposomes. *Biochim Biophys Acta*, 1558(2): 198-210.
- Galbusera, C. and Chen, D.D.Y., 2003. Molecular interaction in capillary electrophoresis. *Current Opinion in Biotechnology*, 14(1): 126-130.

- Gardner, S.N., 2000. A mechanistic, predictive model of dose-response curves for cell cycle phase-specific and -nonspecific drugs. *Cancer Res*, 60(5): 1417-25.
- Giannelli, G., Falk-Marzillier, J., Schiraldi, O., Stetler-Stevenson, W.G. and Quaranta, V., 1997. Induction of cell migration by matrix metalloprotease-2 cleavage of laminin-5. *Science*, 277(5323): 225-8.
- Gladson, C.L. and Cheresch, D.A., 1991. Glioblastoma expression of vitronectin and the alpha v beta 3 integrin. Adhesion mechanism for transformed glial cells. *J Clin Invest*, 88(6): 1924-32.
- Han, G.Z., Liu, Z.J., Shimoi, K. and Zhu, B.T., 2005. Synergism between the anticancer actions of 2-methoxyestradiol and microtubule-disrupting agents in human breast cancer. *Cancer Res*, 65(2): 387-93.
- Haran, G., Cohen, R., Bar, L.K. and Barenholz, Y., 1993. Transmembrane ammonium sulfate gradients in liposomes produce efficient and stable entrapment of amphipathic weak bases. *Biochim Biophys Acta*, 1151(2): 201-15.
- Harding, J.A., Engbers, C.M., Newman, M.S., Goldstein, N.I. and Zalipsky, S., 1997. Immunogenicity and pharmacokinetic attributes of poly(ethylene glycol)-grafted immunoliposomes. *Biochim Biophys Acta*, 1327(2): 181-92.
- Harding, S.E., Chowdhry, B. Z., 2001. *Protein-Ligand Interactions: Hydrodynamics and Colorimetry*. oxford University Press, oxford.
- Haubner, R. et al., 2001. Glycosylated RGD-containing peptides: tracer for tumor targeting and angiogenesis imaging with improved biokinetics. *J Nucl Med*, 42(2): 326-36.
- Haubner, R.H., Wester, H.J., Weber, W.A. and Schwaiger, M., 2003. Radiotracer-based strategies to image angiogenesis. *Q J Nucl Med*, 47(3): 189-99.
- Heath, T.D., Macher, B.A. and Papahadjopoulos, D., 1981. Covalent attachment of immunoglobulins to liposomes via glycosphingolipids. *Biochim Biophys Acta*, 640(1): 66-81.
- Heegaard, N.H.H., Nissen, M.H. and Chen, D.D.Y., 2002. Applications of on-line weak affinity interactions in free solution capillary electrophoresis. *Electrophoresis*, 23(6): 815-822.
- Hieken, T.J. et al., 1996. Beta3 integrin expression in melanoma predicts subsequent metastasis. *J Surg Res*, 63(1): 169-73.
- Holig, P. et al., 2004. Novel RGD lipopeptides for the targeting of liposomes to integrin-expressing endothelial and melanoma cells. *Protein Eng Des Sel*, 17(5): 433-41.

- Hood, J.D. et al., 2002. Tumor regression by targeted gene delivery to the neovasculature. *Science*, 296(5577): 2404-7.
- Huang, S.K. et al., 1992. Pharmacokinetics and therapeutics of sterically stabilized liposomes in mice bearing C-26 colon carcinoma. *Cancer Res*, 52(24): 6774-81.
- Imai, K. and Takaoka, A., 2006. Comparing antibody and small-molecule therapies for cancer. *Nat Rev Cancer*, 6(9): 714-27.
- Ishida, T., Iden, D.L. and Allen, T.M., 1999. A combinatorial approach to producing sterically stabilized (Stealth) immunoliposomal drugs. *FEBS Lett*, 460(1): 129-33.
- Jain, R.K., 1987. Transport of molecules across tumor vasculature. *Cancer Metastasis Rev*, 6(4): 559-93.
- Janssen, A.P. et al., 2003. Peptide-targeted PEG-liposomes in anti-angiogenic therapy. *Int J Pharm*, 254(1): 55-8.
- Jeffs, L.B. et al., 2005. A scalable, extrusion-free method for efficient liposomal encapsulation of plasmid DNA. *Pharm Res*, 22(3): 362-72.
- Jeppesen, C. et al., 2001. Impact of polymer tether length on multiple ligand-receptor bond formation. *Science*, 293(5529): 465-8.
- Johnston, M.J. et al., 2006. Therapeutically optimized rates of drug release can be achieved by varying the drug-to-lipid ratio in liposomal vincristine formulations. *Biochim Biophys Acta*, 1758(1): 55-64.
- Kale, A.A. and Torchilin, V.P., 2007. Design, synthesis, and characterization of pH-sensitive PEG-PE conjugates for stimuli-sensitive pharmaceutical nanocarriers: the effect of substitutes at the hydrazone linkage on the pH stability of PEG-PE conjugates. *Bioconjug Chem*, 18(2): 363-70.
- Kim, H. et al., 2006. The pharmacokinetics of rituximab following an intravitreal injection. *Exp Eye Res*, 82(5): 760-6.
- Kim, J.W. and Lee, H.S., 2004. Tumor targeting by doxorubicin-RGD-4C peptide conjugate in an orthotopic mouse hepatoma model. *Int J Mol Med*, 14(4): 529-35.
- Klibanov, A.L., Maruyama, K., Torchilin, V.P. and Huang, L., 1990. Amphipathic polyethyleneglycols effectively prolong the circulation time of liposomes. *FEBS Lett*, 268(1): 235-7.
- Kochendoerfer, G.G. et al., 2003. Design and chemical synthesis of a homogeneous polymer-modified erythropoiesis protein. *Science*, 299(5608): 884-7.

- Kohler, G. and Milstein, C., 1975. Continuous cultures of fused cells secreting antibody of predefined specificity. *Nature*, 256(5517): 495-7.
- Koning, G.A. et al., 2001. Pharmacokinetics of differently designed immunoliposome formulations in rats with or without hepatic colon cancer metastases. *Pharm Res*, 18(9): 1291-8.
- Kraak, J.C., Busch, S. and Poppe, H., 1992. Study of Protein Drug-Binding Using Capillary Zone Electrophoresis. *Journal of Chromatography*, 608(1-2): 257-264.
- Lee, S.M. et al., 2007. Targeting bladder tumor cells in vivo and in the urine with a peptide identified by phage display. *Mol Cancer Res*, 5(1): 11-9.
- Leserman, L. D., Machy, P., Barbet, J., 1981. Cell-specific drug transfer from liposomes bearing monoclonal antibodies. *Nature* 293(5829):226-8
- Li, W., Huang, Z., MacKay, J.A., Grube, S. and Szoka, F.C., Jr., 2005. Low-pH-sensitive poly(ethylene glycol) (PEG)-stabilized plasmid nanolipoparticles: effects of PEG chain length, lipid composition and assembly conditions on gene delivery. *J Gene Med*, 7(1): 67-79.
- Li, Z.B. et al., 2007. ⁶⁴Cu-Labeled Tetrameric and Octameric RGD Peptides for Small-Animal PET of Tumor $\alpha_v\beta_3$ Integrin Expression. *J Nucl Med*, 48(7): 1162-71.
- Liapis, H., Adler, L.M., Wick, M.R. and Rader, J.S., 1997. Expression of $\alpha_v\beta_3$ integrin is less frequent in ovarian epithelial tumors of low malignant potential in contrast to ovarian carcinomas. *Hum Pathol*, 28(4): 443-9.
- Livnah, O. et al., 1996. Functional mimicry of a protein hormone by a peptide agonist: the EPO receptor complex at 2.8 Å. *Science*, 273(5274): 464-71.
- Maeda, H., Wu, J., Sawa, T., Matsumura, Y. and Hori, K., 2000. Tumor vascular permeability and the EPR effect in macromolecular therapeutics: a review. *J Control Release*, 65(1-2): 271-84.
- Maloney D. G., Grillo-López A. J., White C. A., Bodkin D., Schilder R. J, Neidhart J. A., Janakiraman N., Foon K. A., Liles T. M., Dallaire B. K., Wey K., Royston I., Davis T., Levy R. (1997) IDEC-C2B8 (Rituximab) anti-CD20 monoclonal antibody therapy in patients with relapsed low-grade non-Hodgkin's lymphoma. *Blood* 90(6):2188-95.
- Martino, R. et al., 2002. Cyclophosphamide, pegylated liposomal doxorubicin (Caelyx), vincristine and prednisone (CCOP) in elderly patients with diffuse large B-cell lymphoma: results from a prospective phase II study. *Haematologica*, 87(8): 822-7.

- Maruyama, K., Takahashi, N., Tagawa, T., Nagaike, K. and Iwatsuru, M., 1997. Immunoliposomes bearing polyethyleneglycol-coupled Fab' fragment show prolonged circulation time and high extravasation into targeted solid tumors in vivo. *FEBS Lett*, 413(1): 177-80.
- Matsumura, Y. et al., 2004. Phase I and pharmacokinetic study of MCC-465, a doxorubicin (DXR) encapsulated in PEG immunoliposome, in patients with metastatic stomach cancer. *Ann Oncol*, 15(3): 517-25.
- Maurer, N., Fenske, D.B. and Cullis, P.R., 2001. Developments in liposomal drug delivery systems. *Expert Opin Biol Ther*, 1(6): 923-47.
- Mayer, L.D., Bally, M.B., Hope, M.J. and Cullis, P.R., 1985. Uptake of antineoplastic agents into large unilamellar vesicles in response to a membrane potential. *Biochim Biophys Acta*, 816(2): 294-302.
- Mayer, L.D., Hope, M.J. and Cullis, P.R., 1986. Vesicles of variable sizes produced by a rapid extrusion procedure. *Biochim Biophys Acta*, 858(1): 161-8.
- Mehta, R., Lopez-Berestein, G., Hopfer, R., Mills, K. and Juliano, R.L., 1984. Liposomal amphotericin B is toxic to fungal cells but not to mammalian cells. *Biochim Biophys Acta*, 770(2): 230-4.
- Montet, X., Funovics, M., Montet-Abou, K., Weissleder, R. and Josephson, L., 2006. Multivalent effects of RGD peptides obtained by nanoparticle display. *J Med Chem*, 49(20): 6087-93.
- Moreira, J.N., Ishida, T., Gaspar, R. and Allen, T.M., 2002. Use of the post-insertion technique to insert peptide ligands into pre-formed stealth liposomes with retention of binding activity and cytotoxicity. *Pharm Res*, 19(3): 265-9.
- Muggia, F. and Hamilton, A., 2001. Phase III data on Caelyx in ovarian cancer. *Eur J Cancer*, 37 Suppl 9: S15-8.
- Mui, B., Raney, S.G., Semple, S.C. and Hope, M.J., 2001. Immune stimulation by a CpG-containing oligodeoxynucleotide is enhanced when encapsulated and delivered in lipid particles. *J Pharmacol Exp Ther*, 298(3): 1185-92.
- Murphy-Ullrich, J.E., 2001. The de-adhesive activity of matricellular proteins: is intermediate cell adhesion an adaptive state? *J Clin Invest*, 107(7): 785-90.
- Nabors, L.B. et al., 2007. Phase I and correlative biology study of cilengitide in patients with recurrent malignant glioma. *J Clin Oncol*, 25(13): 1651-7.

- Nallamothe, R. et al., 2006. A targeted liposome delivery system for combretastatin A4: formulation optimization through drug loading and in vitro release studies. *PDA J Pharm Sci Technol*, 60(3): 144-55.
- Nayeem, M.S. and Khan, R.H., 2006. Recombinant antibodies in cancer therapy. *Curr Protein Pept Sci*, 7(2): 165-70.
- Nellis, D.F. et al., 2005a. Preclinical manufacture of an anti-HER2 scFv-PEG-DSPE, liposome-inserting conjugate. 1. Gram-scale production and purification. *Biotechnol Prog*, 21(1): 205-20.
- Nellis, D.F. et al., 2005b. Preclinical manufacture of anti-HER2 liposome-inserting, scFv-PEG-lipid conjugate. 2. Conjugate micelle identity, purity, stability, and potency analysis. *Biotechnol Prog*, 21(1): 221-32.
- Northfelt, D.W. et al., 1996. Doxorubicin encapsulated in liposomes containing surface-bound polyethylene glycol: pharmacokinetics, tumor localization, and safety in patients with AIDS-related Kaposi's sarcoma. *J Clin Pharmacol*, 36(1): 55-63.
- Olson, F., Hunt, C.A., Szoka, F.C., Vail, W.J. and Papahadjopoulos, D., 1979. Preparation of liposomes of defined size distribution by extrusion through polycarbonate membranes. *Biochim Biophys Acta*, 557(1): 9-23.
- Olson, F., Mayhew, E., Maslow, D., Rustum, Y. and Szoka, F., 1982. Characterization, toxicity and therapeutic efficacy of adriamycin encapsulated in liposomes. *Eur J Cancer Clin Oncol*, 18(2): 167-76.
- Oravcova, J., Bohs, B. and Lindner, W., 1996. Drug-protein binding studies - New trends in analytical and experimental methodology. *Journal of Chromatography B-Biomedical Applications*, 677(1): 1-28.
- Ostergaard, J. and Heegaard, N.H.H., 2003. Capillary electrophoresis frontal analysis: Principles and applications for the study of drug-plasma protein binding. *Electrophoresis*, 24(17): 2903-2913.
- Padlan, E.A., 1991. A possible procedure for reducing the immunogenicity of antibody variable domains while preserving their ligand-binding properties. *Mol Immunol*, 28(4-5): 489-98.
- Papahadjopoulos, D. et al., 1991. Sterically stabilized liposomes: improvements in pharmacokinetics and antitumor therapeutic efficacy. *Proc Natl Acad Sci U S A*, 88(24): 11460-4.
- Park, J.W. et al., 2002. Anti-HER2 immunoliposomes: enhanced efficacy attributable to targeted delivery. *Clin Cancer Res*, 8(4): 1172-81.

- Pasqualini, R. et al., 2000. Aminopeptidase N is a receptor for tumor-homing peptides and a target for inhibiting angiogenesis. *Cancer Res*, 60(3): 722-7.
- Pasqualini, R. and Ruoslahti, E., 1996. Organ targeting in vivo using phage display peptide libraries. *Nature*, 380(6572): 364-6.
- Pastorino, F. et al., 2006. Targeting liposomal chemotherapy via both tumor cell-specific and tumor vasculature-specific ligands potentiates therapeutic efficacy. *Cancer Res*, 66(20): 10073-82.
- Pastorino, F. et al., 2004. Targeted delivery of oncogene-selective antisense oligonucleotides in neuroectodermal tumors: therapeutic implications. *Ann N Y Acad Sci*, 1028: 90-103.
- Petit, V. and Thiery, J.P., 2000. Focal adhesions: structure and dynamics. *Biol Cell*, 92(7): 477-94.
- Petrov, A., Okhonin, V., Berezovski, M. and Krylov, S.N., 2005. Kinetic capillary electrophoresis (KCE): A conceptual platform for kinetic homogeneous affinity methods. *Journal of the American Chemical Society*, 127(48): 17104-17110.
- Pierschbacher, M.D. and Ruoslahti, E., 1984. Cell attachment activity of fibronectin can be duplicated by small synthetic fragments of the molecule. *Nature*, 309(5963): 30-3.
- Presta, M. et al., 2005. Fibroblast growth factor/fibroblast growth factor receptor system in angiogenesis. *Cytokine Growth Factor Rev*, 16(2): 159-78.
- Puklin-Faucher, E., Gao, M., Schulten, K. and Vogel, V., 2006. How the headpiece hinge angle is opened: New insights into the dynamics of integrin activation. *J Cell Biol*, 175(2): 349-60.
- R. A. Smith and Giorgio, T.D., 2004. Quantitation and Kinetics of CD51 Surface Receptor Expression: Implications for Targeted Delivery. *Annals of Biomedical Engineering*, 32(5): 635-644.
- Renigunta, A. et al., 2006. DNA transfer into human lung cells is improved with Tat-RGD peptide by caveoli-mediated endocytosis. *Bioconjug Chem*, 17(2): 327-34.
- Rundlett, K.L. and Armstrong, D.W., 2001a. Methods for the determination of binding constants by capillary electrophoresis. *Electrophoresis*, 22(7): 1419-1427.
- Ruoslahti, E., 2000. Targeting tumor vasculature with homing peptides from phage display. *Semin Cancer Biol*, 10(6): 435-42.
- Ruoslahti, E., 2003. The RGD story: a personal account. *Matrix Biol*, 22(6): 459-65.

- Ruoslahti, E. and Pierschbacher, M.D., 1987. New perspectives in cell adhesion: RGD and integrins. *Science*, 238(4826): 491-7.
- Safra, T. et al., 2000. Pegylated liposomal doxorubicin (doxil): reduced clinical cardiotoxicity in patients reaching or exceeding cumulative doses of 500 mg/m². *Ann Oncol*, 11(8): 1029-33.
- Sapra, P. and Allen, T.M., 2002. Internalizing antibodies are necessary for improved therapeutic efficacy of antibody-targeted liposomal drugs. *Cancer Res*, 62(24): 7190-4.
- Sapra, P. and Allen, T.M., 2003. Ligand-targeted liposomal anticancer drugs. *Prog Lipid Res*, 42(5): 439-62.
- Scatchard, G., Ann, N. Y., 1949. *Acad. Sci.*, 51(660).
- Schiffelers, R.M. et al., 2003. Anti-tumor efficacy of tumor vasculature-targeted liposomal doxorubicin. *J Control Release*, 91(1-2): 115-22.
- Schraa, A.J. et al., 2002. Targeting of RGD-modified proteins to tumor vasculature: a pharmacokinetic and cellular distribution study. *Int J Cancer*, 102(5): 469-75.
- Sebille, B., Zini, R., Madjar, C.V., Thuaud, N. and Tillement, J.P., 1990. Separation Procedures Used to Reveal and Follow Drug Protein-Binding. *Journal of Chromatography-Biomedical Applications*, 531: 51-77.
- Segal, A.W., Gregoriadis, G., and Black, C.D., 1975. Liposomes as vehicles for the local release of drugs. *Clin Sci Mol Med*. 49(2):99-106.
- Singh, B., Rawlings, N. and Kaur, A., 2001. Expression of integrin $\alpha v \beta 3$ in pig, dog and cattle. *Histol Histopathol*, 16(4): 1037-46.
- Stephens, S., Emtage, S., Vetterlein, O., Chaplin, L., Bebbington, C., Nesbitt, A., Sopwith, M., Athwal, D., Novak, C., Bodmer, M., 1995. Comprehensive pharmacokinetics of a humanized antibody and analysis of residual anti-idiotypic responses. *Immunology* 85(4):668-74.
- Storgard, C.M. et al., 1999. Decreased angiogenesis and arthritic disease in rabbits treated with an $\alpha v \beta 3$ antagonist. *J Clin Invest*, 103(1): 47-54.
- Stupack, D.G. and Cheresch, D.A., 2002. ECM remodeling regulates angiogenesis: endothelial integrins look for new ligands. *Sci STKE*, 2002(119): PE7.
- Szoka, F. et al., 1980. Preparation of unilamellar liposomes of intermediate size (0.1-0.2 μ m) by a combination of reverse phase evaporation and extrusion through polycarbonate membranes. *Biochim Biophys Acta*, 601(3): 559-71.

- Tanaka, Y. and Terabe, S., 2002. Estimation of binding constants by capillary electrophoresis. *Journal of Chromatography B-Analytical Technologies in the Biomedical and Life Sciences*, 768(1): 81-92.
- Temming, K., Schiffelers, R.M., Molema, G. and Kok, R.J., 2005. RGD-based strategies for selective delivery of therapeutics and imaging agents to the tumour vasculature. *Drug Resist Updat*, 8(6): 381-402.
- Torchilin, V.P., 1985. Liposomes as targetable drug carriers. *Crit Rev Ther Drug Carrier Syst*, 2(1): 65-115.
- Torchilin, V.P. et al., 2001. p-Nitrophenylcarbonyl-PEG-PE-liposomes: fast and simple attachment of specific ligands, including monoclonal antibodies, to distal ends of PEG chains via p-nitrophenylcarbonyl groups. *Biochim Biophys Acta*, 1511(2): 397-411.
- Tucker, G.C., 2006. Integrins: molecular targets in cancer therapy. *Curr Oncol Rep*, 8(2): 96-103.
- Watt, P., 2006 Screening for drugs from the natural repertoire of biodiverse protein folds. *Nature Biotechnology* 24(2):177-183
- Winterhalter, M., and Lasic, D. D., 1993. Liposomes stability and formulation: experimental parameters and theories on the size distribution. *Chem Phys Lipids*. 64(1-3):35-43
- Wu, Y. et al., 2005. microPET imaging of glioma integrin $\alpha_v\beta_3$ expression using (64)Cu-labeled tetrameric RGD peptide. *J Nucl Med*, 46(10): 1707-18.
- Xiong, J.P. et al., 2002. Crystal structure of the extracellular segment of integrin $\alpha_v\beta_3$ in complex with an Arg-Gly-Asp ligand. *Science*, 296(5565): 151-5.
- Xiong, X.B. et al., 2005. Intracellular delivery of doxorubicin with RGD-modified sterically stabilized liposomes for an improved antitumor efficacy: in vitro and in vivo. *J Pharm Sci*, 94(8): 1782-93.
- Xu, J. et al., 2001. Proteolytic exposure of a cryptic site within collagen type IV is required for angiogenesis and tumor growth in vivo. *J Cell Biol*, 154(5): 1069-79.
- Zhang, L., Hoffman, J.A. and Ruoslahti, E., 2005. Molecular profiling of heart endothelial cells. *Circulation*, 112(11): 1601-11.
- Zimmermann, T.S. et al., 2006. RNAi-mediated gene silencing in non-human primates. *Nature*, 441(7089): 111-4.

Zaja F., Tomadini, V., Zaccaria, A., Lenoci, M., Battista, M., Molinari, A., L., Fabbri, A., Battista, R., Cabras, M., G., Gallamini, A., Fanini, R., 2006. CHOP-rituximab with pegylated liposomal doxorubicin for the treatment of elderly patients with diffuse large B-cell lymphoma. *Leukemia Lymphoma* 47(10): 2174-2180.

APPENDIX

Theory for multi-site equilibrium calculations

Currently the most often used approach to determining the binding characteristics for interactions with higher order stoichiometry is to evaluate the changes of a physical parameter of the system with a Scatchard Plot.(Connors, 1987) For a Scatchard Plot to provide meaningful information, certain conditions have to be satisfied. The ligand should have only one active site, and the multiple binding sites on the protein should be identical, distinguishable, and independent. However, in practice, these conditions may not be easily met. Specific binding events often differ from non-specific bindings, and the binding of the first ligand often affects the second binding, favorably or adversely, depending on the function of the protein. To properly address these properties, the following equations are derived and used to process the data used in this work.

As the binding of the species (protein-ligand) occurs with a 1:1 stoichiometry, the equilibrium is given by:

(1)

$$K_b = \frac{[PL]}{[P][L]} \quad (2)$$

where $[P]$, $[L]$ and $[PL]$ are the concentrations of the protein, the ligand and the protein-ligand complex, respectively. The binding constant, K_b , is given by Eq 2. The fraction of the proteins bound, $f_{b,P}$, is an important factor that can be used to determine the affinity between the protein and the ligand:

$$f_{b,P} = \frac{[P]_b}{[P]_t} = \frac{[PL]}{[P]_f + [PL]} \quad (3)$$

The subscripts b , f , and t denote bound, free, and total concentrations of corresponding species in the solution, respectively. In CE-FA, the injected sample plug contains pre-equilibrated proteins and ligands. The total concentration of protein present in the sample mixture, $[P]_t$, is kept constant, and the total ligand concentration, $[L]_t$, is varied in each CE process. As species start to migrate through the capillary under a high voltage, the free ligands are partially separated from the proteins and the protein-ligand complexes. As shown in Figure 1A, the free ligand concentration can be calculated by using a common calibration curve, obtained by injecting samples containing only the ligand. The calculated $[L]_f$ can be used to estimate the binding parameters. In CE-FA, $[P]_b$ is always hard to measure because the mobilities of free protein and protein-ligand complex are often very close. Therefore, the average number of ligand molecules bound per protein molecule, I , is introduced as $[L]_b/[P]_t$ base on the relation of $[P]_b$ and $[L]_b$ in different interaction stoichiometries. For a 1:1 binding, I is defined as

$$I = \frac{[L]_b}{[P]_t} = \frac{[PL]}{[P]_f + [PL]} = \frac{K_b[L]_f}{1 + K_b[L]_f} \quad (4)$$

With a plot of $[L]_b/[P]_t$ vs. $[L]_f$, the binding constant, K_b , can be determined by a non-linear curve fit.

Higher Order Binding Processes

Specific binding of small molecules to macromolecules, such as enzymes and other proteins, poly-nucleic acids, and synthetic polymers, is an important area that often requires consideration of multiple binding sites (Scatchard, 1949). Scatchard plot (I vs. $[L]_f$) have been used to process data obtained in several CE methods, such as CE-FA, HD, and VP (Colton et al., 1998; Fanali, 1997; Rundlett and Armstrong, 2001a).

Because the assumptions used in the Scatchard method are often not valid for biological molecules, a more general model should be developed. For a 1:2 interaction, Eq 1 and Eq 2 can be used to describe the first step binding, with K_{b1} , replacing K_b as the binding constant. The following steps can be expressed as the following:

(5)

$$K_{b2} = \frac{[PL_2]}{[PL][L]_f} \quad (6)$$

and

(7)

$$K_{bn} = \frac{[PL_n]}{[PL_{n-1}][L]_f} \quad (8)$$

The overall binding constant, K , is generally calculated as the product of binding constants of each step:

$$K = \prod_{n=1}^N K_{bn} = K_{b1} \cdot K_{b2} \cdots K_{bn} = \frac{[PL_n]}{[P]_f [L]_f^n} \quad (9)$$

In this study, we will focus on the specific interaction with a small number of binding sites (i.e., $n = 2$ and/or 3), which is common for binding of macromolecules in real biological systems. For a protein-ligand binding with 1:2 or 1:3 stoichiometry, inserting $[PL]$, $[PL_2]$ and $[PL_3]$ into Eq 9, the I value for 1:2 binding is obtained from:

$$I = \frac{[L]_b}{[P]_t} = \frac{[PL] + 2[PL_2]}{[P]_f + [PL] + [PL_2]} = \frac{K_{b1}[L]_f + 2K_{b1}K_{b2}[L]_f^2}{1 + K_{b1}[L]_f + K_{b1}K_{b2}[L]_f^2} \quad (10)$$

and the I value for 1:3 binding is obtained from:

$$I = \frac{[L]_b}{[P]_t} = \frac{[PL] + 2[PL_2] + 3[PL_3]}{[P]_f + [PL] + [PL_2] + [PL_3]} \quad (11)$$

$$= \frac{K_{b1}[L]_f + 2K_{b1}K_{b2}[L]_f^2 + 3K_{b1}K_{b2}K_{b3}[L]_f^3}{1 + K_{b1}[L]_f + K_{b1}K_{b2}[L]_f^2 + K_{b1}K_{b2}K_{b3}[L]_f^3}$$

For the case of multiple types of binding sites, the overall I can be defined as:

$$I_t = \sum_{i=1}^m I_i \quad (12)$$

Most commonly, i is 1 or 2 as reported in the literature. If non-specific binding also exists, I is the sum of $I_{specific}$ and $I_{non-specific}$, and Eq 4, 10 and 11 still describe the specific binding process, if the non-specific binding can be account for. Thus, the appropriate isotherm describing higher order equilibrium for each type of sites is generalized:

$$I = \frac{\sum_{n=1}^N nK_n[L]_f^n}{1 + \sum_{n=1}^N K_n[L]_f^n} \quad (13)$$

Most of the parameters in Eq 13 are defined earlier, except for N , which is the maximum number of binding sites available on each protein molecule. The individual binding constant for each step, K_{bn} , can be determined by plotting $[L]_b/[P]_t$ vs. the free ligand concentration, $[L]_f$, and the number of binding sites can be determined by fitting the experimental results with the n th order equation, such as Eq 10, 11 and 13. It should be noted that the unit of the binding constant obtained from Scatchard Plots is always in M^{-1} , forcing all multiple bindings to a pseudo 1:1 stoichiometry. The overall binding constant obtained by Eq 4, 10 and 11 have units of M^{-1} , M^{-2} , or M^{-3} , depending on the overall stoichiometry. Strictly speaking the binding constants are unitless. The units are used in this work only to follow the conventions practiced in most current literature.

There are also cases where the concentration of ligand present in the BGE is much greater than that of protein in BGE ($[L]_t \gg [P]_t$), in which case the binding sites on the protein molecules are saturated, and the concentration of the unsaturated species ($[PL]$, $[PL_2], \dots, [PL_{n-1}]$) are negligible. Eq 13 can be simplified in these situations as the following:

$$I = \frac{nK_n[L]_f^n}{1 + K_n[L]_f^n} \quad (14)$$

Due to the similarities of the CE techniques, these equations can be also applied to Hummel-Dreyer (HD) and vacancy peak (VP) methods for the determination of binding parameters in either cooperative or non-cooperative multiple-site protein-ligand interactions (Busch et al., 1997b).